Predicting cycling risk at intersections with natural cycling data for speed-controlled e-bikes

Daniël Landré

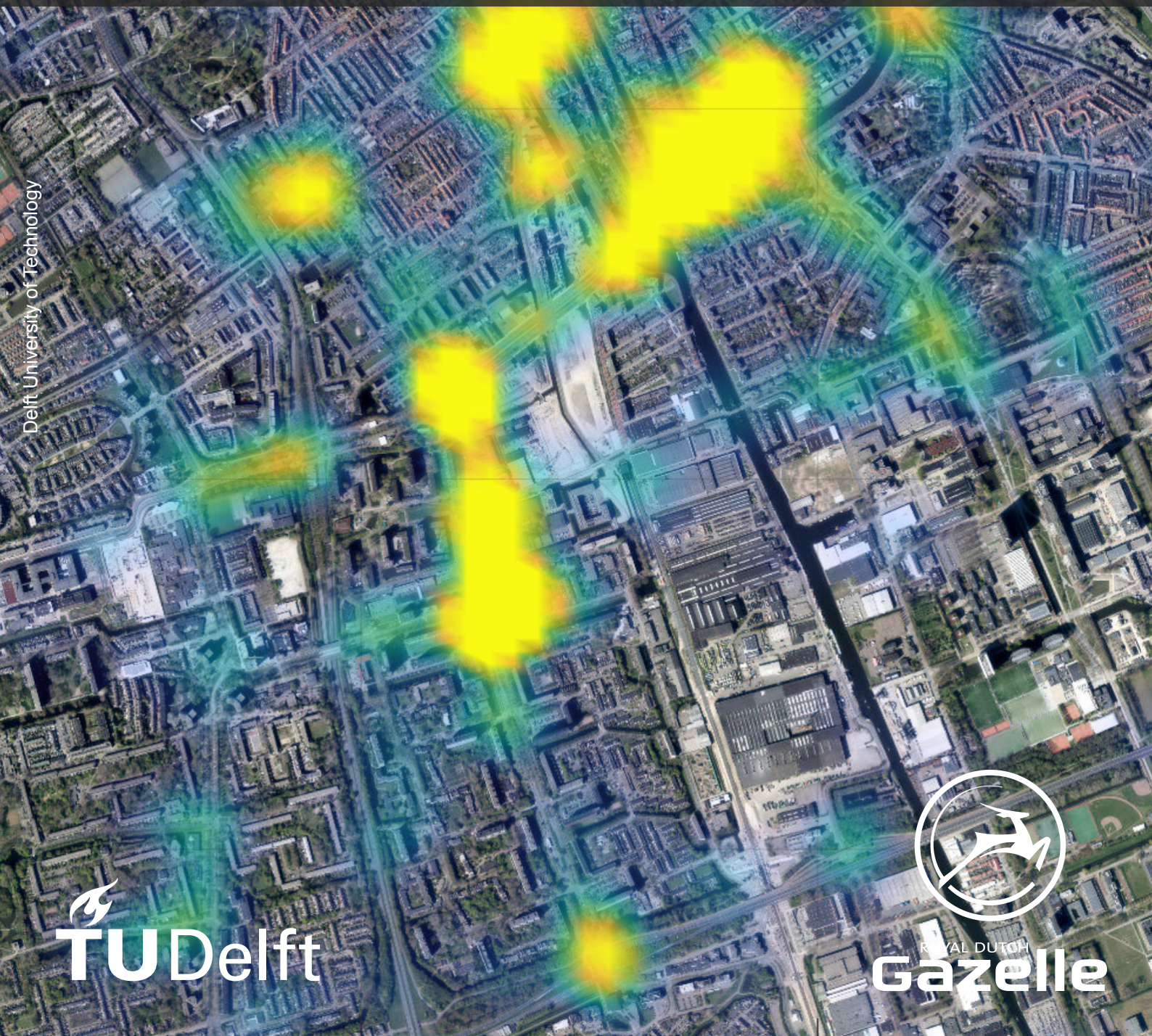

Delft University of Technology

TU Delft

ROYAL DUTCH Gazelle

Predicting cycling risk at intersections with natural cycling data for speed-controlled e-bikes

by

Daniël Landré

to obtain the degree of Master of Science
at the Delft University of Technology,
to be defended publicly on Friday, September 16, 2022 at 10:00 AM.

Student number:	4346831	
Project duration:	March 7, 2022 – September 16, 2022	
Thesis committee:	Dr. J. K. Moore,	TU Delft, Chair, Daily supervisor
	Dr. V. L. Knoop,	TU Delft
	Dr. L. Marchal Crespo,	TU Delft
	Ing. B. Oor MBA,	Koninklijke Gazelle N.V.

This thesis is confidential and cannot be made public until September 16, 2024.

Style: TU Delft Report Style, with modifications by Daan Zwaneveld

An electronic version of this thesis is available at `http://repository.tudelft.nl/`.

TU Delft

Preface

“Don’t learn safety by accident.”

I am delighted to present you, the reader, with my thesis document. This document is the result of a research project that spans almost a full year of my master’s degree. This research project is the first project where I truly feel that the research approach and results are the fruits of my own input and hard work. The initial project proposal was very open-ended, which fortunately gave me a lot of directions to choose for the research project.

With the excellent guidance of my daily supervisor Jason Moore, a direction for the research project was chosen and the work could begin. The setup of the GNSS sensor proved to be more difficult than anticipated, but luckily I was able to work together with fellow lab member Leila Alizadehsaravi on the setup. I slowly began to realise that doing research is a marathon and not a sprint, as it could be difficult at times to keep a good overview of the work that had to be done. Fortunately, the biweekly lab meetings, lab lunches, and weekly meetings with Jason kept me motivated and disciplined.

And then, as all things go, the research project came to a conclusion. Finishing this document feels almost anticlimatic, as most research opens doors for further research. I am very happy with the results of this work and it feels bittersweet to end the research project. I hope this document inspires you in your own research. I would like to thank my supervisors, Jason Moore, Bart Oor, Victor Knoop and Laura Marchal Crespo for their involvement in the project. I also thank the other Bicycle Lab members for their quality discussions and comradery, and I would also like to thank everyone who helped me collect data during my experiment. Finally, I would like to thank you for opening this document and reading my thesis. Happy reading!

Daniël Landré
Delft, September 2022

Abstract

The rapid adoption of e-bikes as an alternative mode of transportation to automobiles gives rise to new methods of safety regulations for cyclists. Modern e-bikes feature Internet of Things (IoT) modules capable of collecting and sending cycling data that can be used for traffic safety analysis. This study explores the potential of using cycling data to detect dangerous intersections and then implement local low-speed areas using geofencing.

A natural cycling experiment with 10 participants is conducted, where data is collected similar to the capabilities of e-bike IoT modules (GNSS, power and IMU data) and participants are asked to cycle through Delft, The Netherlands. The data is combined with a traffic accident dataset from the Dutch government, where intersections with accidents are labelled dangerous. The cycling data is separated into separate intersection approaches, based on positional data. Metrics based on power and cadence data show the most significant statistical difference (p-values <0.02) and the largest effect size (Cohen's d >0.80) at dangerous intersections. A binary classification model is trained on the dataset, which can correctly predict whether an intersection is dangerous or safe with an accuracy of 68,2%, a specificity of 50,0%, and a sensitivity of 24,2%. This prediction is based on the metrics of a single intersection approach.

To investigate the viability of using geofencing to implement low-speed areas at designated dangerous intersections, a simulation is carried out to determine the minimum size of a geofence that effectively slows down e-bike cyclists. The minimal effective geofence size to limit a cyclist's speed at an intersection is determined by simulating cyclists approaching a geofence for several geofence perimeters, incline levels, and wind speeds. The e-bike's motor stops supporting when the geofence is entered and the cyclist is cycling above a target speed. The minimal effective geofence size ranges from 50 to 300 + m and depends on the target speed, wind speed, and road incline.

This study shows that cycling data can be used to identify dangerous intersections. Enforcing a slower speed on intersections with local geofencing is not feasible, as the geofences have to be extremely large, showing a lot of overlap on other intersections in cities due to high intersection density. Future work can be done on the intersection risk estimation method and the feasibility of speed-limiting geofences that employ active braking.

Contents

List of Figures

List of Tables

1

Introduction

1.1. Surge in e-bike usage

Modern bicycle traffic is going through a transformation with the rapid adoption of e-bikes. E-bikes (also called electric bikes or pedal-assisted bicycles) have been commercially available since 1992. In the Netherlands, the e-bike has seen a sharp increase in sales figures over the past 15 years. The e-bike has been the dominant type of bicycle in recent sales figures (see Figure 1.1) and is likely to remain this way. Although conventional bicycles still outnumber e-bikes, it could be possible that e-bikes may slowly replace conventional bicycles over time, especially since cyclists are unlikely to switch to conventional bikes after purchasing an electronic bike [1],[2]. Early adopters of e-bikes were primarily people of older age (>60) [3], but the recent growth in sales can also be attributed to younger people buying an e-bike for their commute.

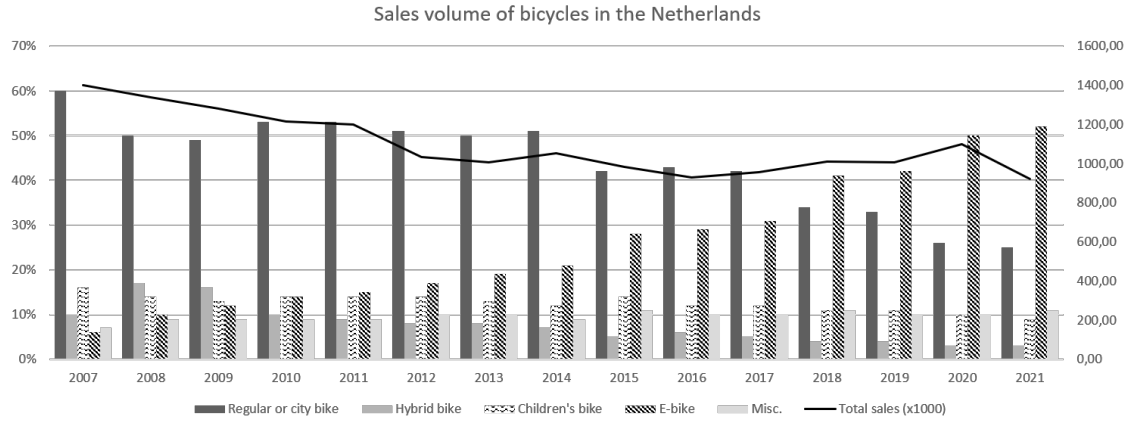

Figure 1.1: Bicycle sales in the Netherlands, visualised from BOVAG data [4]. The bars show the percentage of sales attributed to that type of bicycles. The line shows the total sales of all bicycles combined. E-bike sale numbers have dominated the market since 2018 and continue to increase in proportion to regular/city bicycles, showing that bicycle traffic composition is shifting towards e-bikes.

E-bikes have advantages over regular bicycles, allowing users to travel at higher speeds and motivating users to choose to travel by e-bike instead of by car or other means of travel. For example, working-age people more frequently choose the e-bike over the car for their commute, compared to regular bicycles [5]. Also, e-bikes facilitate mobility for older people, allowing them to enjoy recreational cycling trips that they would not be able to make on a regular bicycle.

1.2. The role of the e-bike in cycling safety

Improving traffic safety is always a topic of discussion in government decisions. Protecting vulnerable road users (VRU) is an important goal in this discussion. In the Netherlands, the number of traffic deaths as a whole has decreased significantly (see Figure 1.2). However, there is no similar reduction in the number of cyclist deaths.

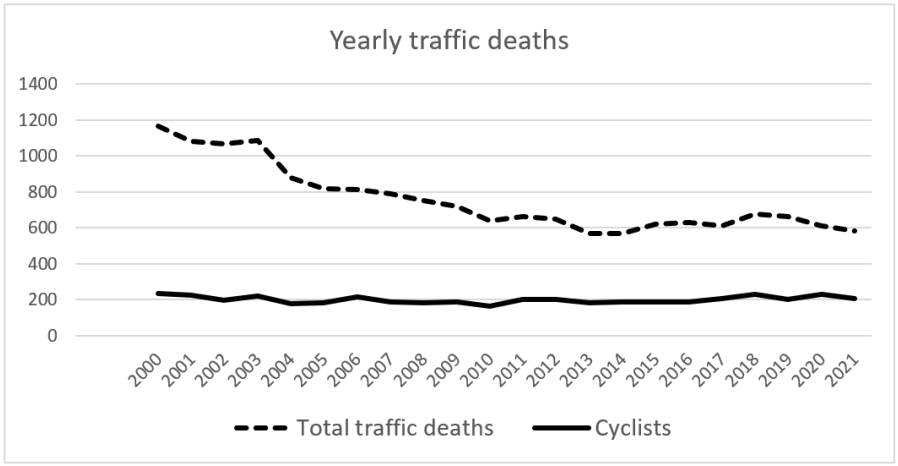

Figure 1.2: Yearly fatal traffic accidents in the Netherlands, visualised from CBS data [6]. Note the decline of overall traffic deaths (until around 2013) due to reduction of fatal car accidents. Unfortunately, there is no similar noticeable change in fatal cycling accidents.

This raises the question of what the role of the increased use of e-bikes is in these numbers. The common opinion is that they are considered more dangerous in traffic than regular bicycles [7]. It is not clear whether e-bikes have higher accident rates than regular bicycles. However, it has been observed that cyclists tend to have more serious accidents on e-bikes compared to regular bicycles [8]. In fact, detailed accident and traffic death statistics in the Netherlands are consistent with this assumption (see Figure 1.3). It can be seen that the participation of e-bikes in traffic accidents is increasing. However, the proportion of e-bike vs regular bicycle fatal cycling accidents is much higher than the proportion of e-bike vs regular bicycle involvement in all traffic accidents (including nonfatal accidents).

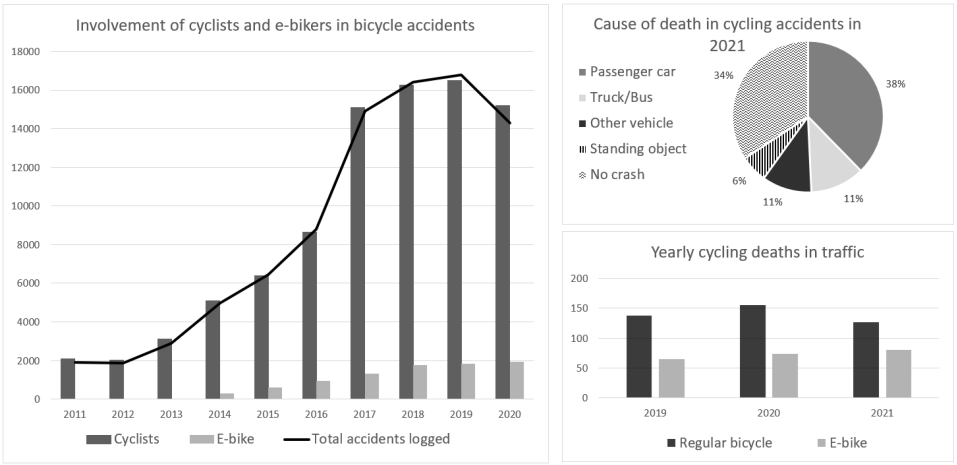

Figure 1.3: Statistics of cycling accidents in the Netherlands. a) Total amount of accidents logged by local police departments, including non-fatal accidents, visualised from Rijkswaterstaat data [9]. b) Cause of death in a cycling accident, visualised from CBS data [6]. c) Yearly cycling deaths for regular bicycles and e-bikes, visualised from CBS data [6]. Note that the e-bike numbers in figures a and c are likely to be underestimated, since these figures stem from police reports. If the police could not figure out whether the bicycle was an e-bike or regular bicycle, it was logged as a regular bicycle.

1.3. Cyclist speed and cyclist-car crash risk

Natural cycling studies have shown that cyclists on e-bikes travel at higher speeds [10],[11], which is true for all age groups [12]. E-bikes also tend to travel at higher speeds in traffic conflicts [13]. The higher average speed of e-bikes could be one of the factors that causes the over-representation of e-bikes in cycling deaths. Figure 1.3 shows that accidents with other road users (e.g., two-sided accidents) account for 60% of all fatal cycling accidents. One could assume that a higher cycling speed could result in a higher two-sided accident rate or higher two-sided accident severity.

Measuring gap acceptance is a way to quantify the risks a traffic participant takes in traffic. It is mostly used to quantify the minimum space a car driver needs when merging into traffic, but it can also be used to explain crossing behaviour at intersections. The ”gap” in this situation can be defined as the time between the arrival times of two vehicles at a potential conflict point (the point where their projected paths meet); see Figure 1.4. A study shows that higher cycling speeds could result in more car-cyclist accidents by testing gap acceptance for car-cyclist interactions at intersections [14]. In this study, the crossing behaviour of the car driver is investigated by facing the driver with an approaching cyclist at an intersection (see Figure 1.5).

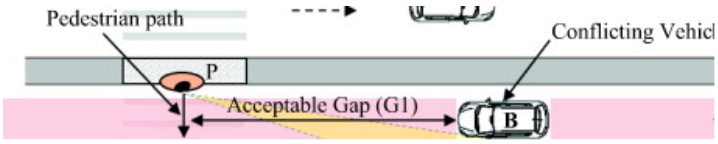

Figure 1.4: Gap acceptance for a pedestrian crossing a street, [15]. The pedestrian decides whether they consider it safe enough to cross the street by estimating the gap time between the arrival time of the car at the crossing and their own arrival time at the crossing. The acceptable gap (G1) is the lowest gap time that the pedestrian considers safe enough to cross the street.

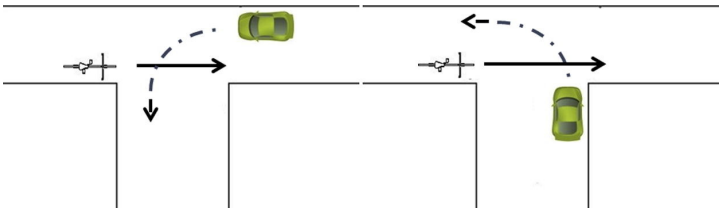

Figure 1.5: Experimental setup for the gap acceptance experiment, a) cyclist from the front, b) cyclist approaching from the side (cyclist has the right of way), [14]. The driver of the car is asked to press the gas pedal at the last moment they consider it safe to cross the intersection in front of the cyclist.

The results of the study are two-fold (see Figure 1.6). First, higher cycling speeds are shown to result in smaller gaps accepted by a car driver. Second, it is also shown that e-bikes lower the accepted gap time by the car driver compared to regular bicycles (the authors argue that this could be caused by the lower pedaling frequency, resulting in an underestimation of the speed of the e-bike cyclist by the car driver).

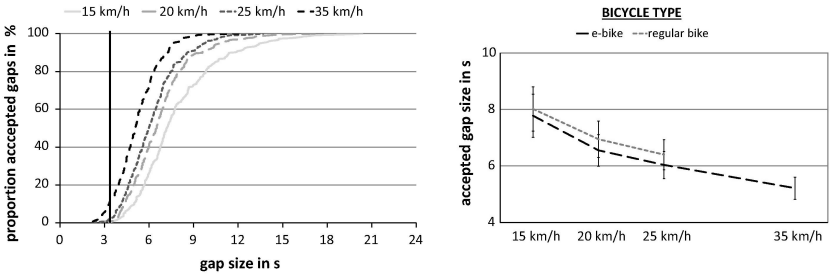

Figure 1.6: Results of the gap acceptance experiment. a) Accepted gap time (not corrected for turning manoeuvre time; manoeuvre time is the black line in the graph = 3.4 seconds) vs cyclist speed, b) Accepted gap time vs cyclist bicycle time, [14].

Similar results were also found in a natural cycling study, where the authors noted that bicycle-car

conflicts occur more frequently at intersections. Furthermore, the authors found that e-bikes were more frequently involved in traffic conflicts with cars compared to traditional bicycles. The study came to the following conclusion: ”Because e-bikes resemble traditional bicycles, but are frequently ridden faster, not only do drivers have less time to notice them, they may also underestimate their speed. Both these possibilities may explain the higher number of conflicts with motorised vehicles experienced by e-bikes.” [16], thus agreeing with the findings of the gap-acceptance study. Therefore, the results of these studies support the theory that a higher cycling speed could result in a higher number of traffic conflicts or accidents of e-bikes with cars.

1.4. Room for innovation

Proposed by Royal Dutch Gazelle, this thesis project will investigate the viability of a speed limiter for e-bikes, with the aim of increasing overall traffic safety and decreasing accident rates. Modern e-bikes come equipped with Internet of Things (IoT) modules that can communicate over the Internet. These modules contain sensors such as Global Navigation Satellite System (GNSS) sensors, gyroscopes, and accelerometers and therefore provide opportunities for technological innovations that are not possible with regular bicycles. Data collected from IoT modules on e-bikes could open up new ways to optimise safety for e-bikes.

This thesis project will focus on one approach to increase safety for e-bikes, which is to investigate the idea of a speed limiter based on GNSS data. This speed limiter should limit the speed of the e-bike in designated dangerous areas, in order to potentially decrease the severity of injuries associated with accidents and decrease accident rates simultaneously. Since modern e-bikes are capable of being equipped with IoT modules, the speed of e-bikes could be reduced at specific locations by using geofencing to intervene with the motor assistance settings. Compared to geolocations, which refer to a single latitude and longitude coordinate, geofences instead refer to a boundary around a geolocation. Using the geolocation of a device, a device can detect whether it is inside or outside a geofence. A visualisation of the concept of a geofence can be seen in Figure 1.7.

Figure 1.7: An example of the practical implementation of a geofence. The geofence could correspond to a low-speed e-bike area, where the cyclist will not be assisted by the motor of the e-bike, for example.

Current applications of geofences vary widely. For example, Amazon Alexa uses geofencing for individual routines, allowing users to receive weather notifications when they leave the house or letting the system turn on the lights when the user arrives home. Another example can be found in bicycle or e-scooter sharing services, where the vehicle can only be locked if the vehicle resides inside a certain area. A more relevant example can be seen in Ford’s speed limiter software, where they are trying to enforce certain speed limits in specific areas on their all-electric E-transit vans [17]. This study will investigate whether it is viable and effective to rely on geofencing to reduce the speed of e-bike cyclists at dangerous locations. Using geofencing to reduce the speed of cyclists at dangerous locations does beg the question; how do you identify dangerous cycling locations?

There are multiple methods (see Figure 1.8) that can be used to quantify cyclist accident risk at certain locations. Some models, such as the bike compatibility index [18] or the bike stress level [19]

try to design a Level of Service (LOS) score by evaluating several parameters such as bicycle lane width, car speed limit, etc. These LOS scores are based primarily on the characteristics of the road and the built environment. The main disadvantage of methods that rely solely on this type of data is that they rely on perceived safety from surveys (which does not necessarily correlate with actual safety) or on a drawn-up model (which also does not necessarily correlate with accident rates).

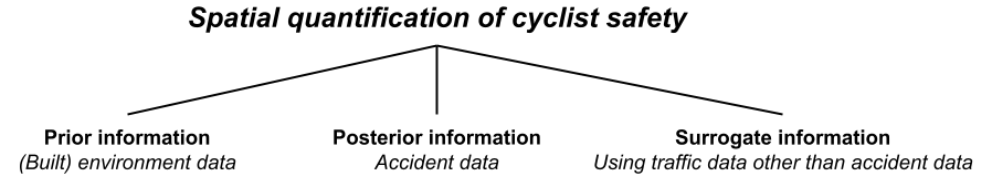

Figure 1.8: Different methods to quantify safety for cyclists at certain locations. The methods focus either on prior data (built environment, road characteristics, etc.), posterior data (traffic accidents), or surrogate data (data measured from traffic behaviour, excluding accident data).

Other models base their risk scores on accident data, which can be seen as posterior information. This means that the proposed models will use outcome information (e.g., accident databases) to determine the characteristics of dangerous locations. The models can focus on relating spatial features (such as traffic volume or specific infrastructure features) to accident frequency. For example, the first model of this type related the frequency of cyclist accidents at intersections to traffic volume [20]. The second type of posterior models does not look at the correlation of spatial features to accident frequency, but instead merely seeks to identify accident hot spots by looking at the spatial distribution of accidents. For example, Machado et al., (2015) focused on identifying dangerous locations in Rome by employing a kernel density estimation (KDE) analysis on the locations of accidents of vulnerable road users (VRU).

A model based on prior information may seem to be the go-to method to identify dangerous cycling areas. Such a model would not need data from accident databases or traffic data and could instead immediately give a safety estimation based on features of the built environment. However, these methods are based either on perceived safety (which does not necessarily correlate with actual safety) or on a drawn-up LOS model (which also does not necessarily correlate with accident rates). Posterior methods do not have this interpretation problem and instead directly show their correlation to accident rates. Therefore, the safety estimations of such methods are more relevant for the purposes of this study. However, the drawback of these methods is that they require access to accident databases, which might underreport accidents or might be too sparse to make an accurate estimation. Furthermore, using a safety estimation method based on accident data for a design aimed at reducing bicycle accidents would reduce the amount of future accident data, resulting in a decrease in the effectiveness of the spatial safety estimation method.

The most ideal spatial safety estimation method for a speed-controlled e-bike lies in the middle of the two aforementioned methods. These so-called surrogate models try to correlate accident data with other traffic data. For example, Strauss et al., (2017) [22] constructed a univariate surrogate safety estimation model, comparing cycling accident rates at intersections with cycling deceleration rates at those intersections, gathered from naturalistic cycling data (see Figure 1.9). They noted that locations with a high amount of dangerous cyclist decelerations had a high correlation rate with accident data. Using such a method would allow one to estimate cycling safety at locations where limited accident data is available by collecting and analysing cycling data. This study expands upon the approach of using a surrogate measure to estimate cyclist safety. Data collected by IoT modules on modern e-bikes could be used as a surrogate measure for spatial estimation of cyclist safety. Ideally, this results in a safety estimation method that the bicycle manufacturer or the government can use to locate dangerous cycling locations. Furthermore, this study will also investigate whether it is feasible to limit the speed of e-bike cyclists at these dangerous locations by using geofencing. In addition, geofencing for speed-pedelecs will also be investigated.

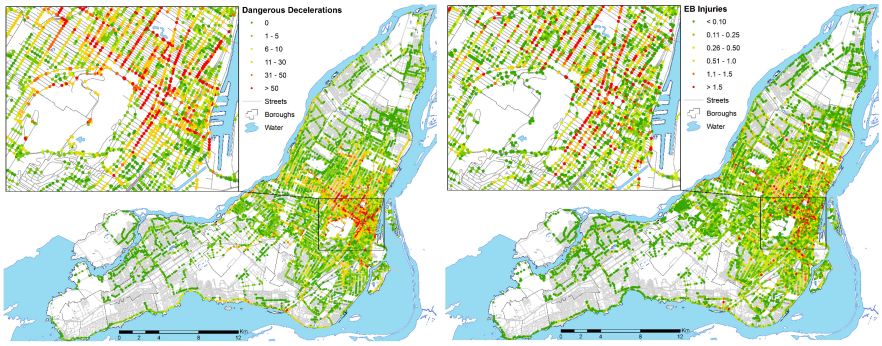

Figure 1.9: Map of; a) Dangerous cyclist deceleration rates in Montreal, b) Cyclist injuries in Montreal. A correlation between locations with high accident rates and high volume of dangerous decelerations can be seen, [22]

1.5. Research approach

This study will investigate whether it is possible to identify dangerous cycling locations with data that can be collected from e-bike IoT modules. Furthermore, this study will investigate whether geofencing is an effective tool for an e-bike speed limiter to ensure that cyclists cycle at a safer and lower speed at these dangerous locations. Although most of this study will focus on regular e-bikes, geofencing for speed-pedelecs will also be investigated, since geofencing could also be employed on these bicycles. This study will limit its focus to intersections, since most car-cyclist interactions and most fatal two-sided cyclist accidents occur at intersections [23],[24],[25].

These goals are summarised in the following main research question:

- **Can e-bike cycling data be utilised to identify dangerous intersections and enforce low-speed areas for e-bike cyclists?**

In order to provide more clarity, the main research question will be split into two sub-questions:

- **Is there a significant correlation in certain metrics of bicycle data at accident-prone intersections and can this be used to detect dangerous intersections?**
- **What is the smallest area of a geofence that still effectively enforces a low speed on an e-bike cyclist?**

1.6. Thesis outline

This study will follow the following structure. Chapter 2 clarifies the methods and experiments carried out to answer the first research sub-question. The results and discussion for that particular topic are also included in that chapter. Chapter 3 follows an identical structure but instead focusses on answering the second research sub-question. Chapter 4 draws conclusions based on the results of the previous chapters.

2

Estimating intersection cycling risk with cycling data

2.1. Methods

In order to answer the question posed by the first research sub-question (see 1.5), two datasets had to be gathered. First, a detailed traffic accident dataset was required to identify which intersections are prone to cyclist accidents. It was vital that this dataset contained accident data at the level of individual intersections (summarised accident statistics at a city-wide level would not be detailed enough). Second, a data set was to be collected that contained cycling data. At a minimum, this dataset had to contain GNSS traces of cyclists (to link the cycling data to specific intersections). Ideally, this dataset would contain all the relevant data IoT modules of modern e-bikes are able to collect (IMU data, power data, and GNSS data).

2.1.1. Cyclist accident dataset

The traffic accident dataset was downloaded from the Rijkswaterstaat agency of the Dutch Ministry of Infrastructure and Water Management [9]. This dataset contains detailed data on all traffic accidents that the Dutch police reported from 1 January 2011 to 31 December 2020 and contains information on the digital road network, which is a representation of the Dutch road network in geolocations. Traffic accident reports are linked to the digital road network, which means that each accident entry can be traced back to a precise location on the digital road network. The digital road network is divided into geolocations representing intersections, road parts (locations between intersections), and hecto points on highways (markers placed every 100 meters on highways); a representation of these geolocations can be seen in Figure 2.1.

All reported traffic accidents are linked to an intersection, or to a road part. If the accident occurred on a road with hecto points, the accident is linked to the closest hecto point. Each accident entry contains information on the parties involved, the type of vehicle of those parties, the date of the accident, the circumstances at the time of the accident, and the manoeuvres made by the parties involved prior to the accident. Unfortunately, detailed information about the outcome of the accident (level of injury or amount of material damage) is not attached to the public dataset, due to Dutch privacy legislation. However, since traffic accidents are only registered when the police were involved after the fact, these accidents can be considered serious accidents, as it should be safe to assume that the police are only contacted in the case of serious material damage or injury. Since this dataset contains information on the exact location of every intersection and traffic accident, it meets the requirements of the desired data set of traffic accidents.

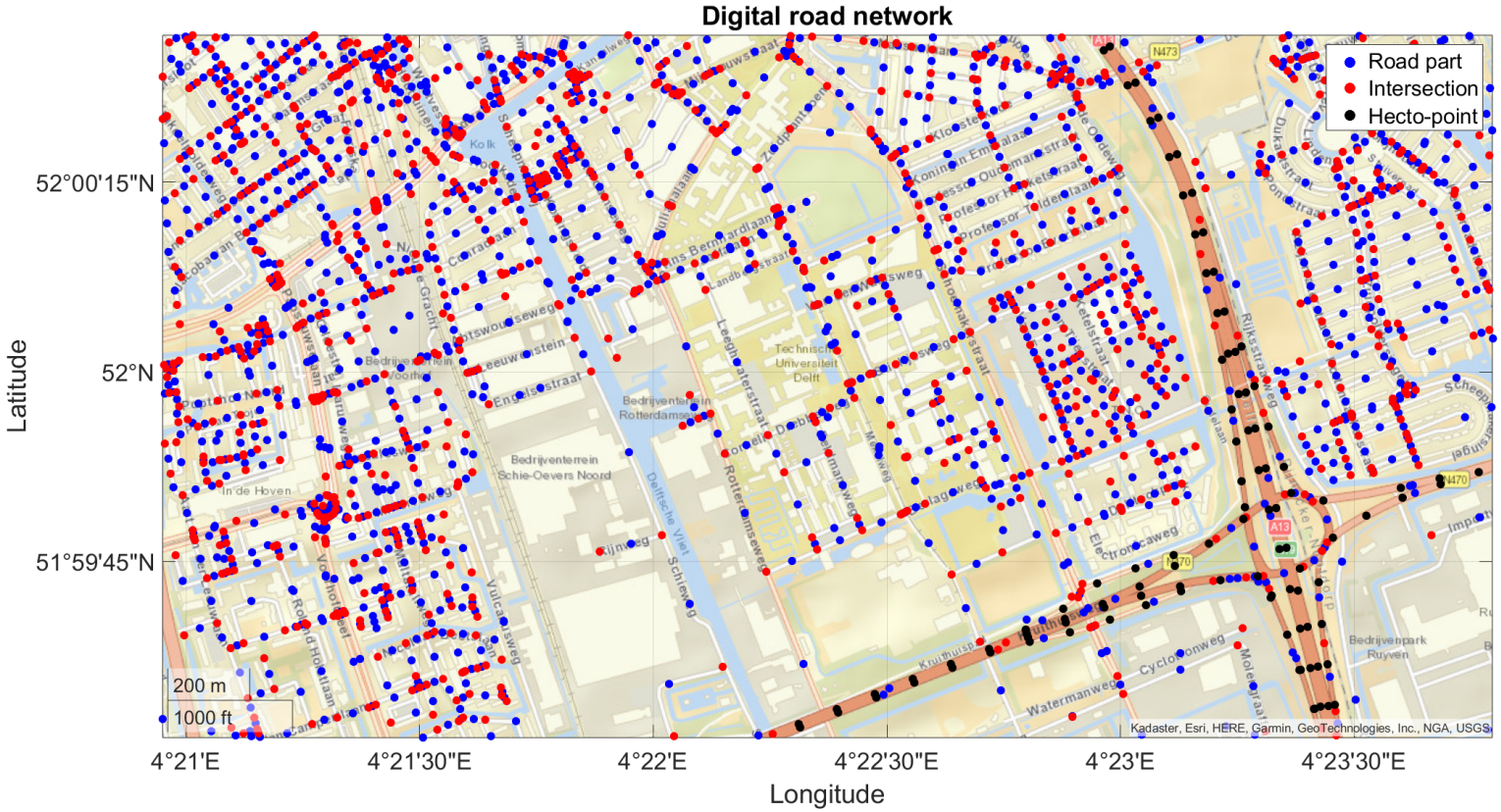

Figure 2.1: Geolocations of the digital road network in Delft. The digital road network consists of geolocations for road parts (blue), intersections (red), and hecto points (black).

2.1.2. Natural cycling experiment

Obtaining a complete and detailed cycling dataset proved to be a difficult task. Using an existing dataset was not feasible, as the datasets were either not in the Netherlands, had too little relevant data, or were not open access. This led to the decision to generate original data with a natural cycling experiment. A great advantage of this approach is that the sensor setup of the experiment can be tailored toward collecting data that is similar to the data collection capabilities of modern IoT modules carried by e-bikes. The experiment should be tailored as much as possible to collect cycling data similar to how cyclists cycle during their daily lives. The equipment used during the experiment can be seen in Figure 2.2.

(a) The e-bike (Gazelle Grenoble C8 HMS prototype e-bike) used during the natural cycling experiment, along with the attached sensors. The backpack contains the evaluation board of the GNSS antenna.

(b) A phone (Nokia 3.4) is placed under the saddle. The phone records accelerometer and gyroscope data.

(c) Front rack carrying the GNSS antenna of the Piksi Multi GNSS module. The evaluation board (along with the USB logging device and power supply) is placed in the backpack, which is connected to the antenna with a wire running along the bicycle frame.

(d) The regular pedals have been replaced by power meter pedals (Favero Assioma DUO). The power data is logged with a cycling app on the phone during the experiment.

Figure 2.2: Equipment setup of the natural cycling experiment.

The bicycle used is a Gazelle Grenoble C8 HMS prototype e-bike. The IMU sensor of the phone collects accelerometer and gyroscope data at a frequency of 100 Hz. The GNSS antenna records positional data at a frequency of 10 Hz, with a positional accuracy of 1,2 m and a velocity accuracy of 0.10 m. The power pedals measure the power output and cadence of the cyclist at a frequency of 1 Hz, and the application that is used to collect the power data also records the GNSS position by using the GNSS antenna on the phone at a rate of 1 Hz and a positional accuracy of 3.5-4 m. The GNSS antenna provides positional data with much greater accuracy and frequency than the IoT modules on e-bikes, whereas the positional data of the phone is more similar to the data logged by the IoT modules. The two reasons to include the GNSS antenna in this experiment are to improve the quality of the data gathered during this experiment (since a large cycling dataset could not be obtained) and to see whether it is necessary to log positional data at a high frequency to see some correlation between cycling data and dangerous intersections, or whether it also suffices to log data at a lower frequency and lower accuracy.

Five women and five men aged 20 to 30 years were asked to participate in the experiment and were recruited through personal contacts. The experimental protocol and the consent process were approved by the HREC board of the TU Delft prior to the execution of the experiments. The ethics proposal, the informed consent form and a rough outline of the protocol of this experiment can be found in Appendix A, B and C. The weight of the participants was recorded and the participants were asked how experienced they were riding an e-bike and a conventional bicycle on a scale of 1 to 5. The weights were recorded to allow for acceleration analysis based on the measured acceleration and relative wind speed; however, this analysis was not pursued further in this study. The participants were asked about their cycling experience to ensure that they were comfortable and experienced enough to ride an e-bike unsupervised through traffic. This information about the participants can be found in Table 2.1.

Table 2.1: Participant details

Gender	Weight	Regular bicycle experience (1-5)	E-bike experience (1-5)
Five females	73.8 ± 5.3 kg	5 ± 0	3 ± 0.9
Five males	77.2 ± 10.3 kg	5 ± 0	4 ± 0.9

The experiment took place between 17:00 and 18:00 on working days from late July to early August. These conditions simulate young adults cycling during their commute. Furthermore, these conditions ensure that some variables can be assumed to be the same between experiments. By ensuring that the gender distribution in the subject population is equal, it can be assumed that gender bias should not play a significant role during data analysis. By ensuring that the experiment takes place at the same time on working days, it can be assumed that the amount of traffic on the road should be similar for every participant. Participants are asked to cycle according to how they would cycle in their daily life and are asked to wear the lightweight backpack that contains the GNSS antenna evaluation board on their back during the experiment. The e-bike will be set to a specific assistance level for all participants (the assistance level is set to ”Normal”, selected from a range of Off/Eco/Norm/High assistance levels).

The experiment consists of two phases. First, participants are instructed to cycle to a random destination in Delft; they can choose this location themselves or ask the researcher to pick a random destination for them. All participants were familiar with cycling in Delft, but a navigation system on the handlebars showed the route to the destination if they got lost. The participant is instructed to return to the starting location of the experiment after reaching the random destination. The experiment then progresses to the second phase, where participants are instructed to cycle two predetermined routes (these can be seen in Figure 2.3b and Figure 2.3c), each time returning to the starting location of the experiment. These routes consist of a good spread of intersections with accidents and intersections without accidents. Figure 2.4 gives a visual presentation of the spread of traffic accidents at the site of the experiment. Each route, including the random route, takes between 10-15 minutes for a round trip. This results in 40-45 minutes of cycling data per participant on average.

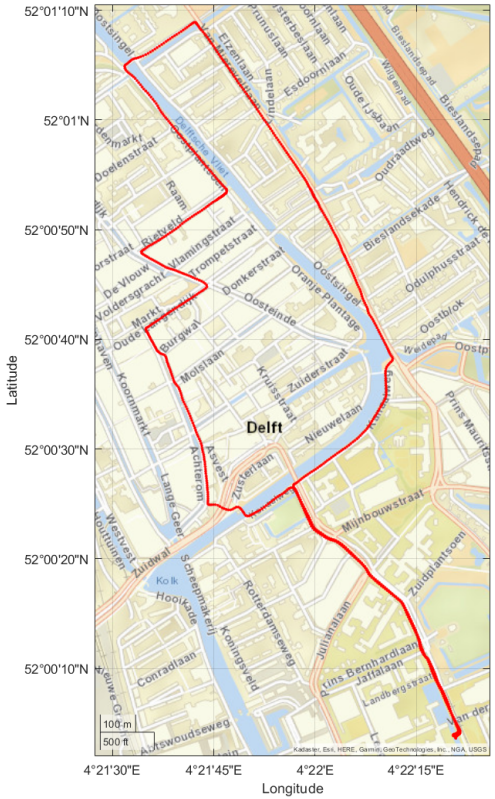

(a) Route with a random destination. The participant opted to cycle towards the Plantagebrug in Delft and constructed their own route.

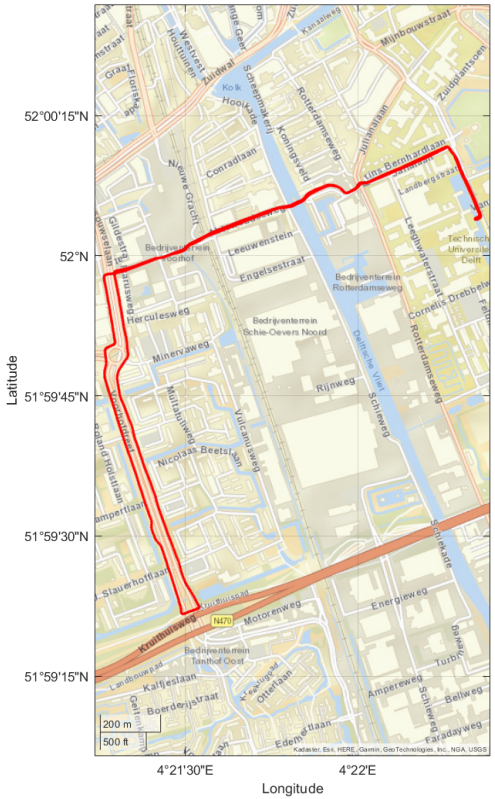

(b) Predetermined route 1, containing intersections with a lot of car-cyclist interactions

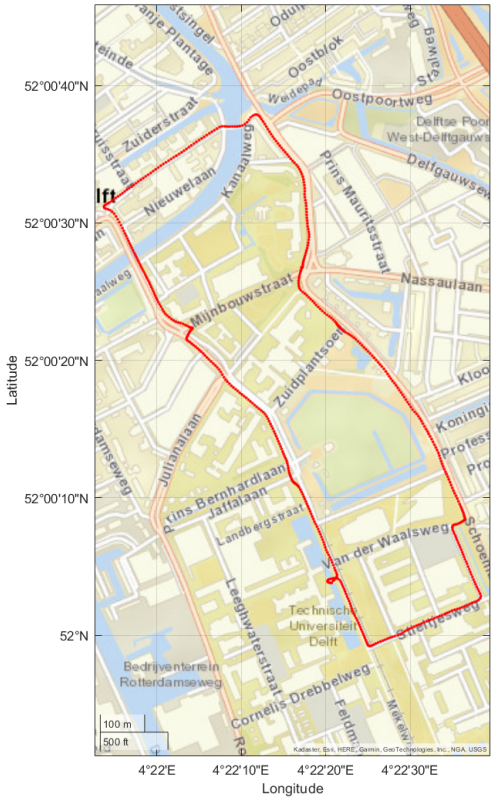

(c) Predetermined route 2, containing intersections with fewer car-cyclist interactions, but relatively more cyclist-cyclist interactions.

Figure 2.3: Cycling routes of Participant 2 during the experiment.

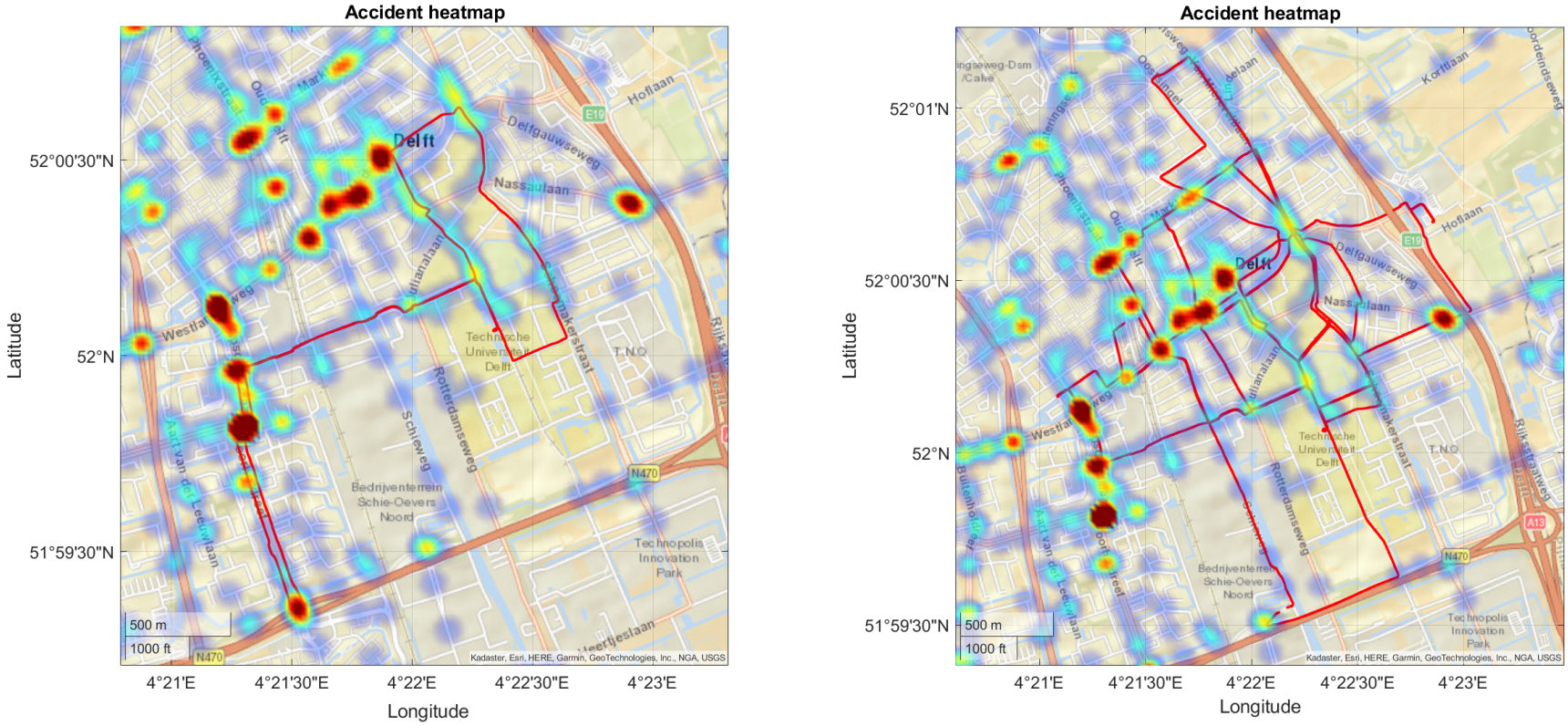

(a) Predetermined cycling routes.

(b) Random cycling routes of all participants combined.

Figure 2.4: Predetermined and random cycling routes projected on a heat map of all cycling accidents. It can be seen that the random routes are more spread out than the predetermined routes. The heat map shows the density of cycling accidents, with each pixel of the heat map showing the amount of accidents within 100 m of that pixel. Red areas show a high density of cycling accidents, blue areas show a low density of cycling accidents.

2.1.3. Data analysis

Traffic accident dataset analysis

The traffic accident dataset had to be filtered and post-processed for analysis. In particular, the dataset had to be filtered so as to only include accidents in which cyclists were involved, and the geolocations had to be transformed from x-, y-coordinates to latitude and longitude coordinates to connect the GNSS traces of cyclists to intersections. A detailed overview of the post-processing process can be seen in Figure 2.5.

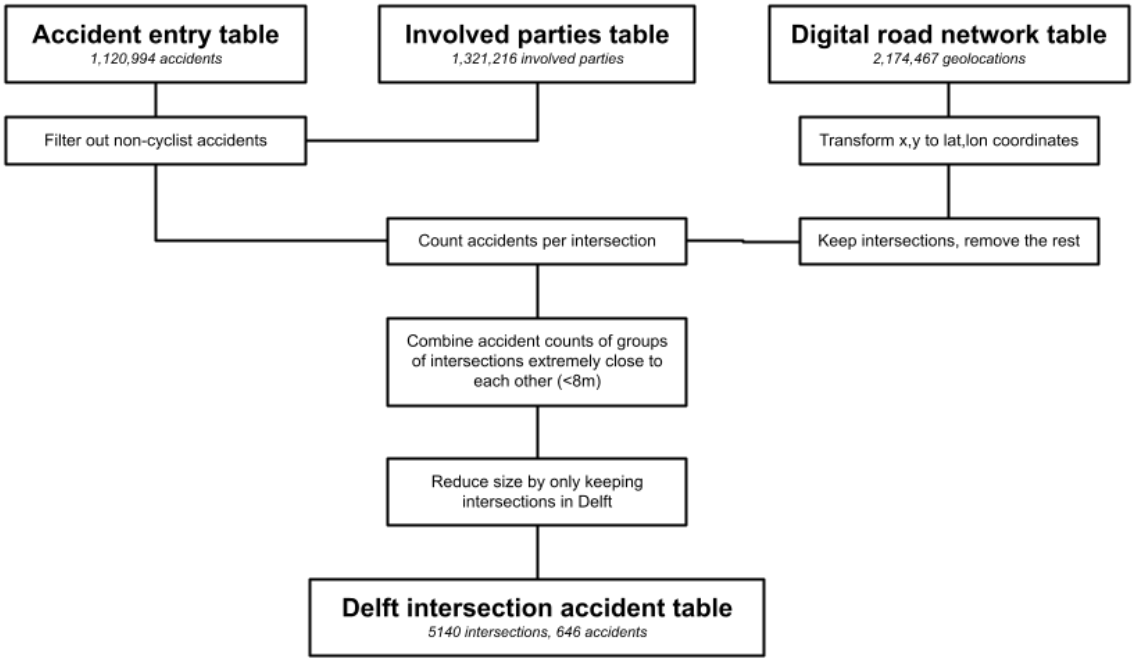

Figure 2.5: An overview of how the traffic accident dataset has been post-processed.

After filtering out accidents in which cyclists were not involved and transformation of the coordinates of the digital road network, an additional processing step was needed. Since some intersection geolocations are extremely close to each other (which is sometimes caused by old geolocation entries that are still left in the database, other times by unknown reasons), it is difficult to link the GNSS traces of cyclists to one of these specific geolocations; see Figures 2.6a and 2.6b for examples. These figures show that a single intersection in the real world sometimes has multiple geolocation entries in the digital road network. Having multiple geolocation entries at one actual intersection becomes an issue if accidents are linked to these geolocations. When there are multiple geolocations at one intersection and one of the geolocations has no accidents associated with it, but the other has, a GNSS trace of a cyclist crossing through that intersection could either be assigned to a safe intersection or a dangerous intersection. This problem is further complicated by the fact that GNSS traces (and intersection geolocations as well) carry some positional inaccuracy.

To ensure that individual intersections with multiple geolocations in their proximity (such as the intersection in Figure 2.6b) show consistent accident counts when linked with GPS traces of cyclists, geolocations close to each other (within 8 m) had their accident counts combined during the analysis. This process is shown in Figures 2.6c and 2.6d. After this step is completed, intersections that are not roughly within Delft are removed from the dataset, in order to decrease future performance demand.

(a) Two geolocation entries in the digital road network for one actual intersection. One geolocation has accidents linked to it (black cross), but the other geolocation (red dot) has no accidents associated with it. If a cyclist would cross this intersection, the cyclist GNSS trace could be linked to either one of these geolocations since they are extremely close together. To make sure that the analysis shows consistent results, the accidents counts of both locations are combined.

(b) Similar situation as Figure 2.6a, but this time with other intersections close by. The middle intersection has two geolocation entries, one with accidents (black cross), the other (red dot) with none. Again, the accident counts of the geolocations near the middle intersection have to be combined. However, the geolocations at the neighbouring intersections nearby must not be combined during the analysis.

(c) Map view of Figure 2.6a. Since the bottom geolocation is within 8 meters of the dangerous intersection, the accident counts for both geolocations are combined. If a cyclist would cross the intersection, the analysis will now show consistent results when the cyclist GNSS trace is linked to either geolocation, as both geolocations now share their accident counts.

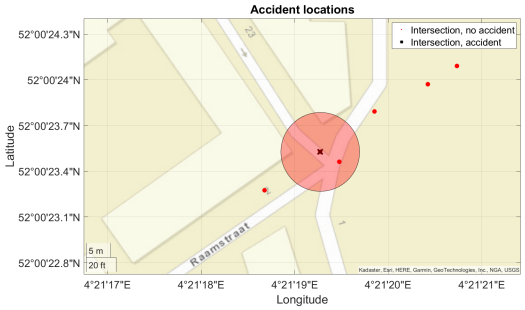

(d) Map view of Figure 2.6b. The accident counts of the two geolocations in close proximity at the middle intersection are combined. The geolocations of the neighbouring intersections fall outside the 8 m radius and are not combined. When a cyclist crosses the middle intersection, the analysis will now show consistent results when the cyclist GNSS trace is linked to either geolocation, as both geolocations now share their accident counts.

Figure 2.6: Examples of how the accident counts of geolocations of intersections that are extremely close to each other are combined.

Linking cyclist traces to intersections

After processing the accident dataset, the cycling data must be coupled with individual intersections. The first step is to determine which intersections were crossed during each cycling trip. For every run of the experiment, any intersection that was not within ten metres of any geolocation of the positional data is excluded from the analysis. A visual representation of this exclusion criterion can be seen in Figure 2.7. This exclusion will make the next step of the analysis faster and more accurate.

(a) Intersections before exclusion based on proximity to the cyclist GNSS trace.

(b) Intersections after exclusion based on proximity to the cyclist GNSS trace.

Figure 2.7: Excluding intersections that were not within 10 meters of any GNSS geolocation of the cyclist trace.

The next step is to assign parts of the cyclist's GNSS trace to specific intersections. This is achieved by assigning each geolocation of the GNSS trace to the closest intersection for that geolocation. The closest intersection for a specific cyclist geolocation is defined by the intersection with the lowest Euclidean distance for that geolocation. By repeating this for every geolocation of the GNSS trace of the cyclist, every geolocation of the cyclist trip will be attached to a specific intersection (see Figure 2.8).

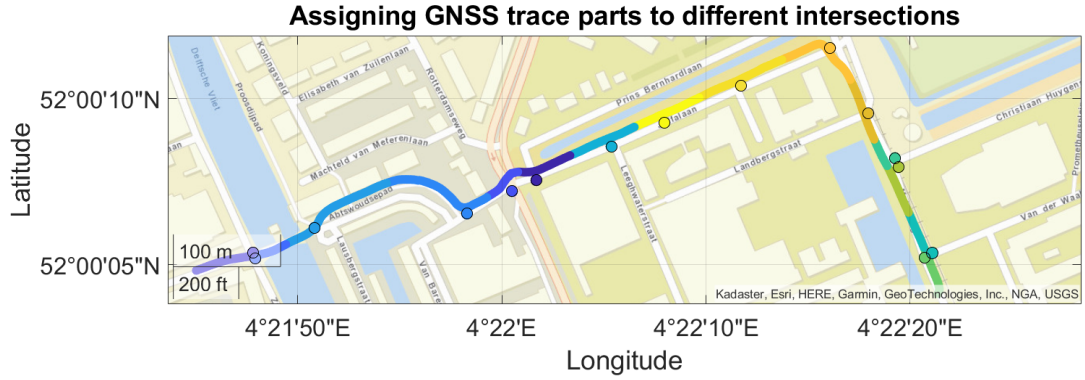

Figure 2.8: Separating parts of the GNSS trace based on proximity to intersections. Each different color of the GNSS trace corresponds to a different intersection. Intersection geolocations are shown as colored circles with a black perimeter.

Since it is likely that there is a difference in the behaviour of cyclists when they approach an intersection compared to when they exit an intersection, it is important to distinguish these two parts in the GNSS traces. Each part of the GNSS trace assigned to an intersection is separated into these two parts by determining the point in the GNSS trace that is closest to the intersection to which the GNSS trace is bound. The first part of the GNSS trace up to this point is the approach part, and the part of

the GNSS trace from this point to the end of the trace is the exit part.

An additional check is performed on both parts to ensure that they correctly indicate an approach or exit from the intersection. This is done by looking at the median of the difference between the heading of the GNSS trace and the direction to the intersection. If this difference is less than 90 degrees, that part should be labelled as an approach part. If this difference is greater than 90 degrees, that part should be labelled as an exit part. If this check does not match the initial label of the GNSS part, that part will be excluded from the analysis. A visual representation of the result of this process can be seen in Figure 2.9.

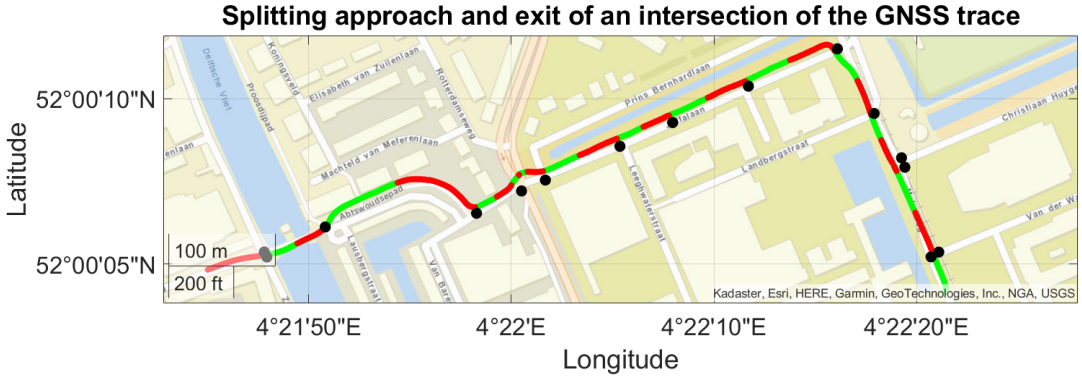

Figure 2.9: Defining exit (red traces) and approach (green traces) parts by considering the difference between the heading of the cyclist and the location of the intersection. Intersections are shown as black dots.

Several assumptions have been made with regard to further analysis of the GNSS traces.

- **Binary classification of intersections as safe or dangerous** Most of the intersections in Delft had zero accidents (4,763 intersections) or one accident (260 intersections) recorded in the traffic accident dataset. Since intersections with two or more accidents logged are comparatively rare (116 intersections), it has been decided to make a binary split in the danger level of intersections. Intersections with zero accidents assigned are labelled safe and intersections with one or more accidents assigned are labelled dangerous. This decision was necessary due to the limited accident data in Delft. Other cities, such as The Hague and Amsterdam, show higher accident counts at intersections (likely due to higher traffic). The binary split in the danger level could be set at a higher accident count in these cities.
- **Limit analysis to approaches** It can be argued that the exit parts of the GNSS traces (see Figure 2.9) correspond to cyclists who are cycling away from that intersection and are therefore no longer influenced by the situation at that intersection. Additionally, the designated exit parts of the GNSS trace may be influenced by another intersection on the path of the cyclist. With these arguments in mind, the approach parts of the GNSS traces are likely to be more interesting than the exit parts. Therefore, the analysis will be limited to intersection approaches and the exit parts of the GNSS traces will not be included in the analysis.
- **Limit analysis to approaches exceeding 35 m** By limiting the analysis to approaches of 35 m or longer, shorter approaches or errors in intersection linking are avoided. Then, the traces of all approaches are cut so that only the last 35 m of each approach is kept and analysed. This means that the analysis will only analyse approaches of a length of 35 m.

Cycling data analysis

The timestamps of the data from the GNSS antenna and the IMU sensor are based on timestamps from GNSS data (the IMU sensor also captures GNSS data at a rate of 1 Hz). Therefore, these sensors can be synchronised according to the timestamps of the GNSS data from both sensors. The power pedal data was collected by a cycling app, which unfortunately did not record timestamps based on GNSS data and instead simply recorded duration. However, the cycling app data did record positional data. The synchronisation of the cycling app data was achieved by synchronising the positional data of the GNSS antenna and the cycling app. Specifically, both datasets are searched for the first timestamp of the positional data that is closest to the first crossed intersection in both datasets. The duration data of the cycling app is then timeshifted by the timestamp of the GNSS antenna timestamp at that specific timestamp. Details of the raw data can be found in Table 2.2. The raw data is then processed into several metrics for every GNSS trace part assigned to an intersection approach. This means that each intersection approach is assigned a single value for each metric in Table 2.3. These metrics are then studied to determine the correlation with the risk level of intersections. An example of an intersection approach with the associated raw data and the calculated metrics for that approach can be found in Appendix D.

Table 2.2: Details of raw data.

Data source	Data type	Frequency
GNSS sensor	GNSS position (Latitude, Longitude, Timestamp)	10 Hz
GNSS sensor	Speed	10 Hz
Phone IMU	GNSS position (Latitude, Longitude, Timestamp)	100 Hz
Phone IMU	Accelerometer	100 Hz
Phone IMU	Gyroscope	100 Hz
Phone cycling app	GNSS position (Latitude, Longitude)	1 Hz
Phone cycling app	Speed	1 Hz
Phone cycling app	Power & Cadence	1 Hz

Table 2.3: Metrics processed from raw data

Metric name	Explanation
Stopped at intersection	Cyclist stood still at intersection
GNSS acc mean	Mean acceleration based on speed measured by GNSS sensor
GNSS acc p85	85th percentile of absolute acceleration based on speed measured by GNSS sensor
GNSS acc p85 pos	85th percentile of acceleration based on speed measured by GNSS sensor
GNSS acc p15 neg	15th percentile of deceleration based on speed measured by GNSS sensor
Accelerometer Forward mean	Mean forward acceleration of IMU
Accelerometer Forward deviation	Standard deviation of forward acceleration of IMU
Accelerometer Forward p85 pos	85th percentile of forward acceleration of IMU
Accelerometer Forward p15 neg	15th percentile of forward deceleration of IMU
Accelerometer Forward max	Maximum forward acceleration recorded
Accelerometer Forward min	Maximum forward deceleration recorded
Accelerometer Lateral mean	Mean lateral acceleration of IMU
Accelerometer Lateral deviation	Standard deviation of lateral acceleration of IMU
Accelerometer Lateral abs max	Maximum absolute lateral acceleration of IMU
Accelerometer Total mean	Mean absolute total acceleration of IMU
Accelerometer Total deviation	Standard deviation of absolute total acceleration of IMU
Accelerometer Total max	Maximum absolute total acceleration of IMU
Gyro Yaw mean	Mean yaw angular velocity
Gyro Yaw deviation	Standard deviation of yaw angular velocity
Gyro Yaw displacement rate	Mean absolute yaw angular velocity
Gyro Yaw abs max	Maximum absolute yaw angular velocity
Gyro Roll mean	Mean roll angular velocity
Gyro Roll deviation	Standard deviation of roll angular velocity
Gyro Roll displacement rate	Mean absolute roll angular velocity
Gyro Roll abs max	Maximum absolute roll angular velocity
Gyro Total mean	Mean total absolute angular velocity
Gyro Total deviation	Standard deviation of total absolute angular velocity
Gyro Total abs max	Maximum total absolute angular velocity
Approach speed	Average speed during the first half second of the intersection approach
Intersection speed	Average speed during the last half second of the intersection approach
Accelerometer Hard acceleration	1 if forward acceleration exceeds 3.3 m/s^2, else 0
Accelerometer Hard deceleration	1 if forward acceleration goes below -3.3 m/s^2, else 0
Gyro Yaw Hard swerve	1 if absolute yaw angular velocity exceeds 0.5 rad/s, else 0
Gyro Roll Hard swerve	1 if absolute roll angular velocity exceeds 0.5 rad/s, else 0
Cadence mean	Mean cadence of the cyclist, measured by power pedals
Cadence deviation	Standard deviation of cadence of the cyclist, measured by power pedals
Power mean	Mean power input of the cyclist, measured by power pedals
Power deviation	Standard deviation of power input of the cyclist, measured by power pedals
Time not pedalling	Time the cyclist does not pedal, measured by power pedals

2.2. Results

The data analysis approach creates a dataset consisting of n intersection approaches, where each single intersection approach is associated with m metrics (these can be found in Table 2.3) and is labelled as an approach to a safe or dangerous intersection. This results in a dataset of size $m \times n$. This section will be divided into two parts. The first part (2.2.1) will investigate the statistical significance of each metric by investigating the hypothesis that the probability distribution of the metric is different in approaches to safe intersections compared to approaches to dangerous intersections. In addition, the effect size of each metric will be investigated. The second part (2.2.2) will describe how the data can be used in a classification model that can predict whether an intersection is safe or dangerous by analysing the metrics of a single approach.

2.2.1. Overall metrics statistics

With an approach limit of 35 m, the processed dataset contains n = 576 intersection approaches. Of these approaches, 374 (64,9%) approaches were located at a safe intersection and 202 (35,1%) approaches were located at a dangerous intersection. Each metric is analysed for statistical significance with two significance tests. The first test is the one-way analysis of variance (ANOVA) test (which assumes normality), and the second test is the nonparametric Kruskal-Willis rank sum test (which does not assume normality). Furthermore, the metrics are also analysed for effect size with two tests similar to the significance tests. The first effect size metric is Cohen's d (which assumes normality). The second effect size metric is the common-language effect size, which can be calculated from the Kruskal-Willis test result (which does not assume normality).

The effect sizes of a metric are calculated as follows. A metric γ (e.g., average cadence during the intersection approach) is divided into two sets according to the intersection labels; γ_{safe} and $\gamma_{\text{dangerous}}$. The Cohen's distance is calculated by analysing the difference between the means of the two distributions, divided by the pooled standard deviation:

$$d = \left| \frac{\overline{\gamma}_{\text{safe}} - \overline{\gamma}_{\text{dangerous}}}{SD} \right| \tag{2.1}$$

The pooled standard deviation (SD) is calculated as follows:

$$SD = \sqrt{\frac{(n_{\text{safe}} - 1)\sigma_{\text{safe}} + (n_{\text{dangerous}} - 1)\sigma_{\text{dangerous}}}{n_{\text{safe}} + n_{\text{dangerous}} - 2}} \tag{2.2}$$

With n_{safe} and $n_{\text{dangerous}}$ as the number of safe and dangerous intersection approaches and σ_{safe} and $\sigma_{\text{dangerous}}$ as the standard deviation of γ_{safe} and $\gamma_{\text{dangerous}}$. The Cohen's distance can be a value of zero to infinity. The following ranges are often used for the interpretation of the metric: 0.2 is a small effect size, 0.5 is a medium effect size, and 0.8 is a large effect size.

The common-language effect size is calculated by determining the probability that a random value of one distribution exceeds a random value of the other distribution. First, the values of γ_{safe} and $\gamma_{\text{dangerous}}$ are grouped and ordered from low to high. Then, for each value of γ_{safe}, count the number of $\gamma_{\text{dangerous}}$ values that are lower than that particular value. Add the counts together to obtain the statistic U_{safe}. The common-language effect size for γ_{safe} is then calculated as follows:

$$d_{\text{KW,safe}} = \frac{U_{\text{safe}}}{n_{\text{safe}} n_{\text{dangerous}}} \tag{2.3}$$

To obtain the overall common-language effect size, repeat the previous calculation for the $U_{\text{dangerous}}$ statistic (number of values of γ_{safe} that every value of $\gamma_{\text{dangerous}}$ exceeds) and take the maximum value between the two.

$$d_{KW} = \max(d_{\text{KW,safe}}, d_{\text{KW,dangerous}}) \tag{2.4}$$

d_{KW} is a value between 0.50 and 1.00 and indicates the probability that a random value of one distribution is higher or lower (depending on which distribution has a higher mean) than a random value of the other distribution. A value close to 0.50 indicates a very small effect size, and a value closer to 1.00 indicates a very high effect size.

The results of the significance tests and the effect size metrics can be found in Table 2.4. It shows

that some metrics, such as cadence standard deviation and mean power output, show statistical significance in both ANOVA and Kruskal-Willis analyses (p-values <0.05) and also show a large effect size (Cohen's d >0.80). Regarding the standard deviation of cyclist cadence, cyclists tend to have a larger deviation in their cadence at dangerous intersections, for example. A detailed look at the distribution of the cadence standard deviation metric can be seen in Figure 2.10.

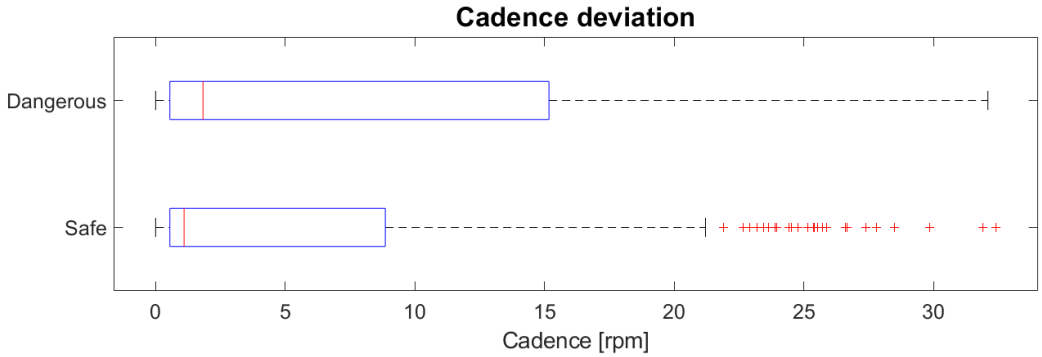

Figure 2.10: Box plot of the cadence standard deviation metric. It can be seen that cyclists are less consistent in their cadence at dangerous intersections. The correlation of this metric mean that this metric can therefore be used to identify dangerous intersections.

Box plots of all metrics can be found in Appendix E. The box plots can be used together with Table 2.4 to better understand how statistical significance and a large effect are represented in the actual distribution of a specific metric.

Table 2.4: Statistical significance tests and effect size metrics for each metric

Metric name	ANOVA P-value	Cohen's d	Kruskal-Willis P-value	KW distance
Stopped at intersection	0.057	0.072	0.058	0.515
GNSS acc mean**	0.005	0.090	0.002	0.579
GNSS acc p85	0.117	0.153	0.006	0.569
GNSS acc p85 pos	0.658	0.055	0.108	0.541
GNSS acc p15 neg	0.717	0.044	0.080	0.544
Accelerometer Forward mean	0.423	0.026	0.583	0.514
Accelerometer Forward deviation	0.068	0.102	0.342	0.524
Accelerometer Forward p85 pos	0.510	0.043	0.944	0.502
Accelerometer Forward p15 neg	0.545	0.039	0.935	0.502
Accelerometer Forward max**¤	0.000	0.521	0.006	0.570
Accelerometer Forward min	0.010	0.316	0.112	0.541
Accelerometer Lateral mean**	0.005	0.119	0.001	0.584
Accelerometer Lateral deviation	0.258	0.048	0.114	0.541
Accelerometer Lateral max	0.102	0.151	0.014	0.563
Accelerometer Total mean	0.688	0.026	0.861	0.505
Accelerometer Total deviation*	0.000	0.267	0.014	0.563
Accelerometer Total max	0.428	0.065	0.775	0.507
Gyro Yaw mean	0.155	0.010	0.173	0.535
Gyro Yaw deviation	0.091	0.029	0.096	0.543
Gyro Yaw displacement rate	0.206	0.019	0.260	0.529
Gyro Yaw abs max*	0.007	0.085	0.018	0.561
Gyro Roll mean	0.339	0.006	0.501	0.517
Gyro Roll deviation	0.800	0.004	0.742	0.508
Gyro Roll displacement rate	0.851	0.003	0.916	0.503
Gyro Roll abs max	0.649	0.012	0.549	0.515
Gyro Total mean*	0.014	0.055	0.027	0.557
Gyro Total deviation**	0.000	0.085	0.004	0.574
Gyro Total max**	0.000	0.160	0.003	0.576
Approach speed	0.252	0.184	0.801	0.506
Intersection speed*¤	0.002	0.551	0.038	0.552
Accelerometer hard acceleration	0.123	0.095	0.123	0.533
Accelerometer hard brake	0.176	0.083	0.176	0.529
Gyro hard yaw swerve*	0.014	0.110	0.014	0.527
Gyro hard roll swerve	0.829	0.006	0.830	0.501
Cadence mean*¤	0.008	1.044	0.015	0.561
Cadence deviation**¤	0.002	0.806	0.001	0.580
Power mean*¤	0.007	1.677	0.015	0.562
Power deviation**¤	0.005	0.954	0.006	0.569
Time not pedalling	0.635	0.142	0.018	0.537

*: ANOVA and KW p values <0.05, **: ANOVA and KW p values <0.01, ¤: Cohen's d >0.50,

2.2.2. Classification model

In order to predict whether an intersection is safe or dangerous, a classification model is trained on the dataset. The classification model analyses the metrics of a single approach to an intersection and will then classify the intersection as safe or dangerous (binary classification) based on that single approach. Creating a classification model requires a training and testing dataset. The training set is used to determine the model parameters, the testing set is then used to test the model. The training and testing set were created based on the routes that were cycled by the cyclists. The training set consisted of all intersection approaches that were made during the identical routes of the cyclists, see Figure 2.4a. The test set consisted of all approaches made during the random routes of the cyclists, see Figure 2.4b. This ensures that the classification model is tested with approaches at intersections that have not been seen by the model before. The training set with identical cycling routes contains 384 (66,7%) intersection approaches. The testing set with random cycling routes contains 192 (33,3%) intersection approaches.

A cubic support-vector machine (SVM) model has been chosen as the classification model. A SVM model looks for the best hyperplane of dimension $m - 1$ for its binary classification on a dataset with binary labels (safe vs. dangerous in this case) and m metrics/features. The cubic variant of the SVM model uses a so-called ”kernel-trick” to transform the data to a higher-dimensional space (using a third-degree polynomial kernel function), with the expectation that the accuracy of the model is better when a separating hyperplane is determined after the kernel-trick transformation. The accuracy of the model during training and testing can be seen in Figure 2.11.

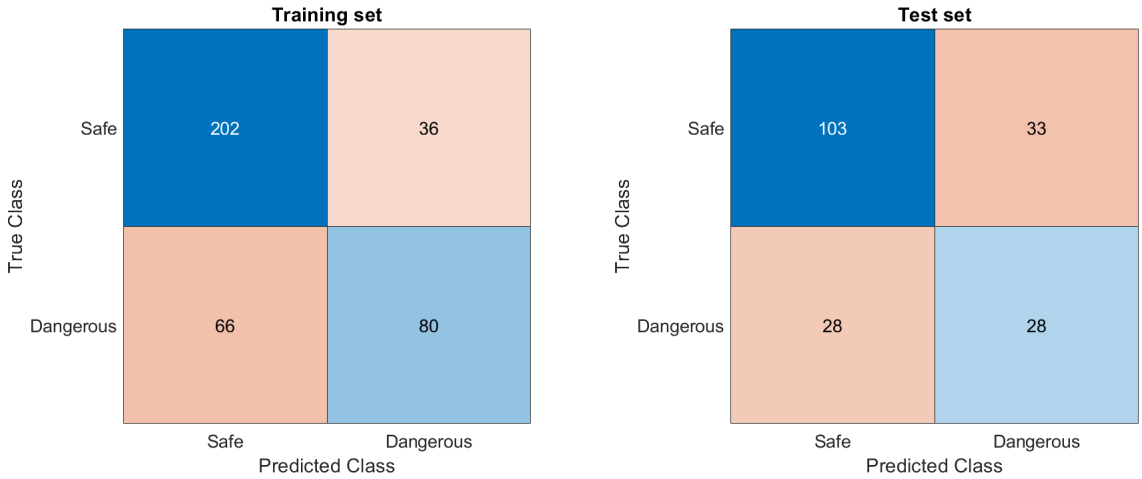

(a) Confusion matrix of the model's prediction performance on the training set. Accuracy during training was 73,4%.

(b) Confusion matrix of the model's prediction performance on the test set. Accuracy during testing was 68,2%.

Figure 2.11: Confusion matrices of the trained SVM classification model on the training set (identical routes) and test set (random routes). Note that the ”true” label indicates an approach to a ”dangerous intersection” and a ”false” label indicates an approach to a ”safe intersection”. The South East tile indicates the amount of approaches correctly classified as a ”dangerous intersection” by the model, for example. The South West tile indicates the amount of approaches incorrectly classified as a ”safe intersection” by the model.

The accuracy of the classification model has to be compared with the accuracy of a random weighted guess with weights equal to the proportion of the amount of safe and dangerous intersection approaches in the training set, to ensure that the model is not making purely random guesses on the data. The accuracy of such a weighted guess can be considered to be a baseline accuracy; if the model cannot perform better than a random guess, then the model has no value.

The training set contains 146 dangerous intersection approaches (38,0%) and 238 safe intersection approaches (62,0%). A random guess with the same proportions would result in an accuracy of $0.38^2 + 0.62^2$ or 52,9%. The accuracy of the model on the training set had a higher accuracy of 74,2%. The test set contains 56 dangerous intersection approaches (29,2%) and 136 safe intersection approaches (71,8%). A random guess with these proportions would result in an accuracy of 60,1%. The accuracy of the model on the test set was higher, with an accuracy of 68,2%.

The model's performance can be further evaluated by analysing the Receiver Operating Characteristic (ROC) curve; see Figure 2.12. These figures show the relationship between the true positive rate, also known as Specificity (calculated as $\frac{TP}{TP+FN}$) and the false positive rate, also known as Sensitivity (calculated as $\frac{FP}{TN+FP}$) for different classification parameters. The definition of these parameters can be seen in Table 2.5. A classification model can use different classification thresholds; however, each threshold carries different false positive rates. Some thresholds correctly identify more dangerous intersections, but in the process also incorrectly classify more safe intersections as dangerous compared to other classification thresholds. The ROC curves show the performance of the classification model at all classification thresholds at different false positive rates.

Table 2.5: Model accuracy parameters

Variable	Value
TP	Intersection predicted as dangerous, intersection was dangerous
TN	Intersection predicted as safe, intersection was safe
FP	Intersection predicted as dangerous, intersection was safe
FN	Intersection predicted as safe, intersection was dangerous

The True Positive rate and False Positive rate of a random guess are always the same. They could both decrease/increase when the weights of the random guess are adjusted, but they will always remain equal to each other. The ROC curve of a random guess plots the True Positive vs False Positive rate for all guessing weights and will therefore be a straight line from (0,0) to (1,1). The Area Under Curve (AUC) of the random guess is 0.5. The performance of the model can be further investigated by comparing the ROC curves and AUC scores of the classification model with the random guess model. These can be seen in Figure 2.12. The ROC curves of the training and testing set are considerably different and better than the ROC curve of a random guess. With AUC scores of 0.76 and 0.67 respectively, it can be safely concluded that the classification model performs better than a random guess. The classification model is always able to correctly identify more dangerous intersections for a certain false positive rate than a random guessing algorithm that guesses 'dangerous' at a proportion identical to the same false positive rate.

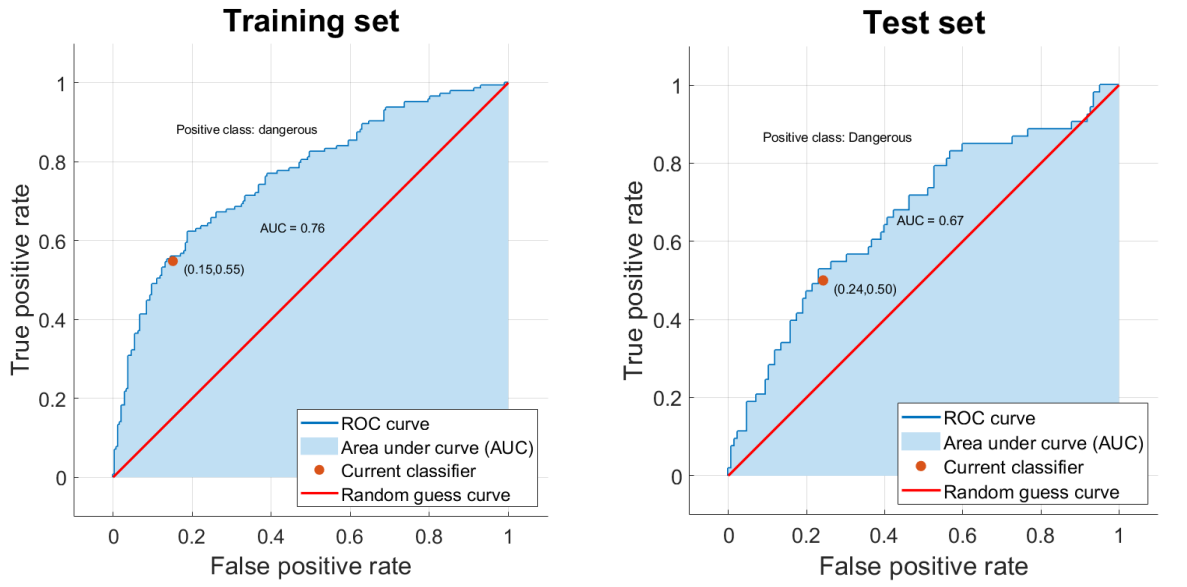

(a) ROC curve of the training set, compared to the ROC curve of a random guess.

(b) ROC curve of the test set, compared to the ROC curve of a random guess.

Figure 2.12: ROC curves (Receiver Operating Characteristic) of the trained SVM classification model on the training set (identical routes) and test set (random routes). The positive class corresponds to a "dangerous" label classification of an intersection approach.

2.3. Discussion

The findings show that capturing cycling data in conjunction with GNSS position data is a tool that can be used to predict intersection cycling risk. The metrics showing the highest correlation with intersection cycling risk were mean cadence, cadence devation, mean power output, and deviation of power output, each showing a large effect size (Cohen's d > 0.80) and large statistical significance (p-values < 0.02). Cyclists had a lower cadence and power output and a higher deviation in their cadence and power output at dangerous intersections. Interestingly, these effects were not seen as clearly in the accelerometer data, although they should be directly related to the power and cadence data. The only statistically significant metrics for the accelerometer data were the maximum forward acceleration, the mean lateral acceleration, and the deviation in absolute total acceleration. These accelerometer metrics had effect sizes considerably lower than the cadence and power metrics, with values of 0.52, 0.12 and 0.27 respectively. The same notion holds for the metrics that were gathered from the gyroscope data; some metrics showed statistical significance but had relatively small effect sizes. This shows that the metrics from the power and cadence data are the most important to collect for the prediction of intersection cycling risk.

The classification model performs better than a random guess, with an accuracy of 68,2% on the testing dataset compared to the accuracy of a random guess with the same proportions, which would have an accuracy of 60,1%. Moreover, the model correctly identifies 50% of dangerous intersections in the test dataset, with a false positive rate of 24%. A random guess with a false positive rate of 24% would result in correct identification of dangerous intersections only 24% of the time. Note that in this study, false positive results (intersection classified as dangerous, intersection was safe) are weighed equally as false negative results during training. False negative results could be weighed more heavily than false positive results, which would push the model to classify approaches as dangerous more frequently. The performance of the model could be improved by addressing the limitations of the approach of this study. These limitations are the small sample size of the dataset, the method of classifying intersections, the lack of integration of prior data, and the lack of integration of other posterior data.

The dataset of the natural cycling experiment is of high granularity, but is lacking in the total volume of cycling trips. This is in stark contrast to the approach of similar studies, such as the study of Strauss et al., (2017) [22], where a large volume of low-granularity data is used. The low-volume, high-granularity approach of this study is a limitation; for example, none of the experiment participants stated that they were actually involved in a potentially dangerous situation during the experiment. Such situations might introduce large and easily detectable braking or swerving behaviour in the IMU data. The current approach is based on the detection of changes in cyclist behaviour at dangerous intersections. For example, an intersection with poor sight lines could result in a slower approach to that intersection. In other words, this work relies on cyclists changing their behaviour to dangerous intersections even when there is no dangerous event, and does not depend on the detection of actual dangerous events. With a larger dataset, the focus of the intersection risk estimation model can instead be shifted towards the detection of these dangerous events, which could result in a more accurate classification model. If the current approach is kept (not focussing on detection of dangerous events), a higher volume dataset could still result in a more accurate classification model. Since many metrics did not show statistical significance, a high-volume dataset containing only the important metrics (for example, a dataset with positional data, power output metrics, and cadence metrics) could suffice to create a better model than the model in this study.

Another limitation caused by the small size of the dataset lies in the approach of the intersection risk classification model. Each intersection approach is analysed separately in the current approach. For example, if there were ten separate intersection approaches at the same intersection in the dataset, they would all be analysed separately with the current model approach. This means that that intersection would receive ten safety classifications, one for each approach in the dataset. A better method would be to group the data and metrics of all approaches at that intersection and analyse them simultaneously. In the current data set, most intersections on random routes were only approached a single time, which does not allow for such a method. However, if more data is available, the focus of the model could be shifted towards analysing aggregate metrics and data for each intersection, instead of analysing every single intersection approach separately. This approach goes hand in hand with the previous suggestion of using dangerous event detection, as the frequency of these events could be counted and included in the aggregate metrics for each intersection.

The model could be further improved by integrating prior data (such as characteristics of the built environment) into the model. For example, adding information about the type of intersection (3- or 4-legged, priority or not, roundabout, signalised, etc.) could increase the accuracy of the model, as it is extremely likely that the type of intersection has an influence on cyclist behaviour, and therefore also on cycling data. Other types of prior information could also be included, such as cyclist separation, car speed limit, number of car lanes, and sight lines. In addition to prior data, posterior data (such as traffic counts) could also be integrated into the model.

Storing and sending raw data from the bicycle to another database would be inconvenient and might not be possible with the current system limitations in Gazelle e-bikes. Currently, the sensor modules on Gazelle e-bikes can record and send data with a maximum frequency of once every three seconds. This means that a practical implementation of this system relies on analysing metrics at fixed GNSS positions, rather than carefully constructing the metrics based on raw data, as was done in this study. In a practical scenario, the IoT module on the e-bike would calculate the metrics locally in three-second intervals and send them to Gazelle. The available data would then consist of metrics attached to a single location, which are recorded and processed at intervals of 3 seconds, as can be seen in Figure 2.13.

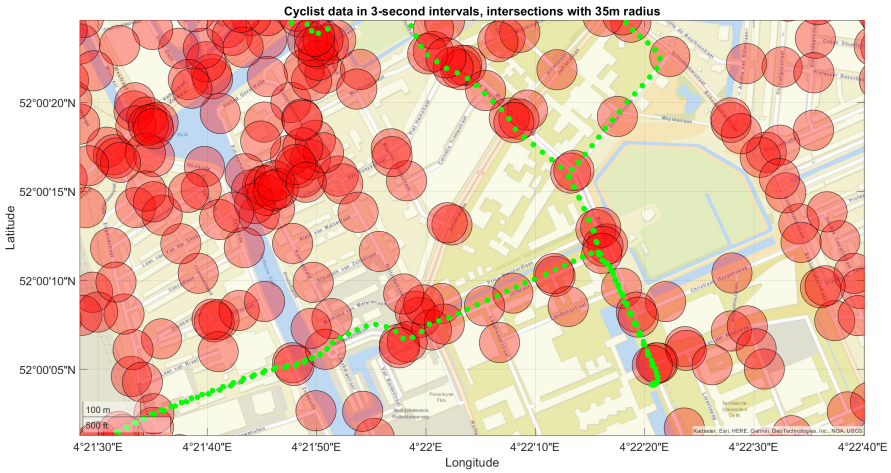

Figure 2.13: Recording cycling data and position at three-second intervals (green dots). The data can be coupled to the closest intersection that is also within 35 m of the position. The circles show a radius of 35 m around each nearby intersection geolocation. The metrics could be calculated locally (by the IoT module on the bicycle) and sent to Gazelle for storage and analysis.

A practical approach would have to attach the metrics to intersections based on a single location. This differs from the approach of this study, as this study calculated cyclist metrics by carefully splitting the raw cycling data into intersection approach parts. In a practical scenario, these approaches cannot be identified, as the data analysis must now rely on metrics attached to a single location. This can be achieved by associating the calculated metrics with the intersection that is closest to the recorded GNSS position and also within 35 m. This approach goes hand in hand with the suggestion to change the approach of the model to analysis of aggregate intersection statistics.

3

Investigating e-bike speed limitation with geofencing

3.1. Methods

The answer to the second research sub-question (see 1.5) depends on the specific implementation of geofencing for an e-bike speed limiter. Implementing a geofencing-based speed-limiting technology for e-bikes raises some challenges, which are mainly caused by bicycle dynamics. The two main challenges to address are *"How should the speed limiter act when the e-bike is in a geofence to lower the speed of the cyclist?"* and *"How big should the geofence be to effectively slow down the cyclist?"*.

The first question is relatively simple to answer. There are two main mechanisms that can be used to slow down a cyclist; you can stop or limit the assistance of the motor, or you can engage the brakes in addition to the previous option. The latter option will slow down a cyclist very quickly but can result in dangerous situations, as unexpected braking can result in instability (owing to large speed changes) or unexpected behaviour for surrounding traffic. It is more reasonable to use the former option, as this slows the cyclist down in a gradual way and allows the cyclist to retain more control.

Limiting cyclist speed by merely turning off the motor assistance does come with a disadvantage, as it is difficult to determine when the motor should stop assisting to ensure that the cyclist is sufficiently slowed by the time they actually enter the low-speed area. One can imagine that the geofence needs to be larger than the actual specific area where the cyclist needs to ride at a slower target speed. The difference in size between the geofence and the low-speed area will from now on be referred to as the ”buffer zone”. This study will investigate the minimum required size of this buffer zone that still effectively slows e-bike cyclists to a certain speed (for example, 15 km/h or 20 km/h) by cutting the assistance of the e-bike motor.

3.1.1. Simulation model

To investigate the minimum size of the buffer zone, a simulation was carried out. In this simulation, a large number of cyclists (different in weight and power output) approaching a geofence are simulated. This geofence is placed at an intersection, where the geofence represents the aforementioned ”buffer zone” and the intersection the low-speed area. Before the cyclists enter the geofence, the motor assistance of the e-bike will work normally. Once they enter the buffer zone (shown as the yellow zone in Figure 3.1, the motor assistance of the e-bike will stop, gradually slowing down the cyclist. Then it is determined whether they were sufficiently slowed down by looking at their speed when they reached the actual low-speed zone (shown as the red zone in Figure 3.1). In addition to the different weights and power output of the cyclists, multiple environmental scenarios will be simulated. These scenarios will change the parameters of the relative wind speed and the level of incline of the road. This will result in ideal buffer zone sizes for, for example, a flat and windless environment, an environment with a decline but strong headwind, an environment with an incline but strong tailwind, and everything in between.

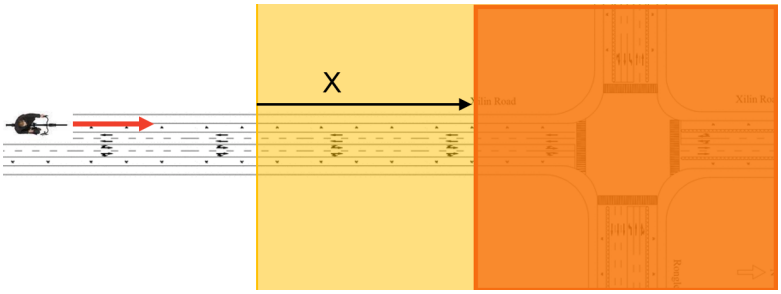

Figure 3.1: Visualisation of a cyclist approaching an intersection. The simulation will determine the minimal distance X needed to slow a cyclist down to the safe speed before they enter the true low-speed zone (red zone).

The simulation model is a simple 2D time marching model of the most important forces acting on a cyclist. The forces considered in the simulation model can be seen in Figure 3.2. By calculating the forces acting on the cyclist at a specific time step, the position and velocity of the cyclist at the next time step can be approximated. The definitions of all simulation variables can be seen in Table 3.1.

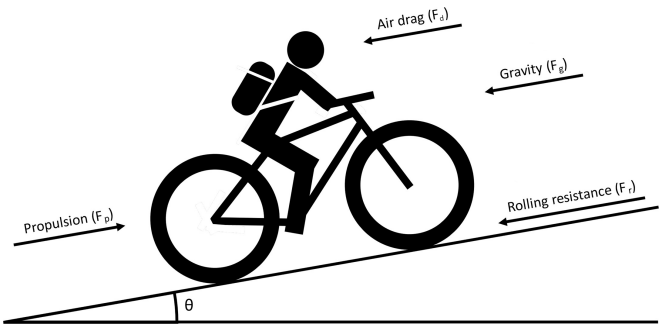

Figure 3.2: Schematic of the forces simulated in the model, this figure has been edited from [26].

The acting forces are calculated as follows:

$$F_p = \frac{P_{\text{cyclist}}}{v_{\text{cyclist}}} \ , \ F_{\text{motor}} = \frac{P_{\text{motor}}}{v_{\text{cyclist}}} \tag{3.1}$$

$$F_d = \frac{C_d \ A \ \rho_{\text{air}} \ (v_{\text{cyclist}} + v_{\text{wind}})^2}{2} \tag{3.2}$$

$$F_g = m \ g \ \sin\theta \tag{3.3}$$

$$F_r = C_{\text{roll}} \ m \ g \ \cos\theta \tag{3.4}$$

$$F_{\text{total}} = \mu(F_p + F_{\text{motor}}) - F_d - F_g - F_r \tag{3.5}$$

Table 3.1: Definitions of simulation variables

Variable	Definition
v_{cyclist}	Speed of the cyclist
x_{cyclist}	Position of the cyclist
P_{cyclist}	Power output of the cyclist
P_{motor}	Power output of the motor
μ	Drive train efficiency
m	Combined mass of the cyclist and bicycle
F_p	Propelling force of the cyclist
F_{motor}	Propelling force of the motor
F_d	Aerodynamic drag force
F_g	Gravitational force
F_r	Roll resistance force
F_{total}	Total propelling force
v_{wind}	Wind speed (global perspective, i.e. independent of cyclist speed)
C_dA	Aerodynamic drag coefficient
C_r	Roll resistance coefficient

The result of equation 3.5 can then be used to make a linear approximation of the velocity and position of the cyclist at the next time step.

$$v_{\text{cyclist}}(t+\delta) = v_{\text{cyclist}}(t) + \delta\frac{F_{\text{total}}}{m} \tag{3.6}$$

$$x_{\text{cyclist}}(t+\delta) = x_{\text{cyclist}}(t) + \delta\frac{v_{\text{cyclist}}(t+\delta) + v_{\text{cyclist}}(t)}{2} \tag{3.7}$$

The model keeps some parameters fixed for all environments and cyclists, these can be seen in Table 3.2. Drag and roll coefficients have been collected from the literature, [27] (see European upright commuter). The motor assistance power limit has been provided by Gazelle and is a common limit of motor output in e-bikes. Drive train efficiency is estimated to be around 97%, which has also been collected from the literature, [28].

The changing variables between the cyclists and environments can be seen in Table 3.3. The mass of the bicycle-cyclist system (m) is modelled as a flat weight (corresponding to the weight of the e-bike, which is the same as the weight of the e-bike used in the natural cycling experiment) added on top of a uniform distribution (corresponding to the weight of the cyclist). This uniform distribution is based on a rough and simple estimate of the weight distribution of cyclists in the Netherlands, corresponding to a range of 40 kg around the mean weight of all adults in the Netherlands (with a slight increase in the mean from 77.8 kg to 80 kg to account for clothes and other carried items by the cyclist) [29]. The distribution of the power output of the cyclists is based on the distribution of the power output of the participants during the cycling experiment when they were cycling steadily and were not approaching an intersection. Two types of e-bikes have been simulated, the regular e-bike and the speed-pedelec.

Table 3.2: Fixed variables in the simulation

Variable	Value
g	9.81 m/s^2
ρ	1.2 kg/m^3
δ	0.1 s
C_{roll}	0.006
C_dA	0.612
P_{motor}	350 W
μ	97%

Table 3.3: Changing variables in the simulation

Variable	Value
m	$28 + U[60, 100]$ kg
P_{cyclist}	$U[40, 90]$ W
θ	$[-2, 2]$ degrees, in steps of 0.5 degree
v_{wind}	$[-4, 4]$ m/s, in steps of 0.1 m/s

It is important to note that several key assumptions have been made regarding the simulation configuration. These result in a (slight) overestimation of the speed of the cyclist when they enter the true low-speed zone and, therefore, result in an overestimation of the minimum effective geofence size.

- **Motor assistance behaviour** The simulation assumes that the motor always provides a constant power output, which is set to the maximum power that the motor could theoretically provide. The only difference between speed-pedelecs and e-bikes in this simulation is the internal speed limit of the bicycle. For regular e-bikes, the motor will gradually stop providing assistance if the speed exceeds 25 km/h. For speed-pedelecs, this limit is set to 45km/h. In reality, the power provided by the motor always depends on the power input of the cyclist, which should always result in a lower power output of the motor than the maximum it could provide.
- **Cyclist power input** The simulation assumes that the power output of the cyclist does not change when approaching the intersection / true zone. In reality, this behaviour might change depending on where the true low-speed zone is located. For example, cyclists approaching an intersection may stop pedaling before reaching the intersection, lowering their average power input before entering the low-speed zone. This behaviour would then result in a lower minimal effective geofence size. On the contrary, cyclists could increase their power output once they notice that motor assistance is reduced, resulting in a larger minimal effective geofence size.
- **Straight path in the buffer zone** The simulation simulates a cyclist moving in a 2D environment (backward/forward and up/down if the road is inclined/declined). This approach has two caveats. First, the cyclist travels along the shortest path possible to the true low-speed zone. In reality, the road in the buffer zone may contain some curvature, resulting in an increase in the distance travelled in the buffer zone. Second, the cyclists themselves are simulated to ride perfectly straight along the path of the road. In reality, cyclists do not travel straight and, for example, could increase their distance travelled due to some weaving behaviour.

3.1.2. Simulation data analysis

The result of a single simulated cyclist approaching the intersection on a speed-pedelec with a buffer zone size of 200 m can be seen in Figure 3.3. It can be seen that this cyclist would cycle around 16 km/h if not assisted by the motor (indicated by the blue line). If they were assisted by the motor of the speed-pedelec, they would be cycling at a higher speed. If the motor stops assisting the cyclist 200 m before the intersection/true zone, the cyclist would have a speed of around 18 km/h when they enter the true zone, which is well below the target speed of 25 km/h.

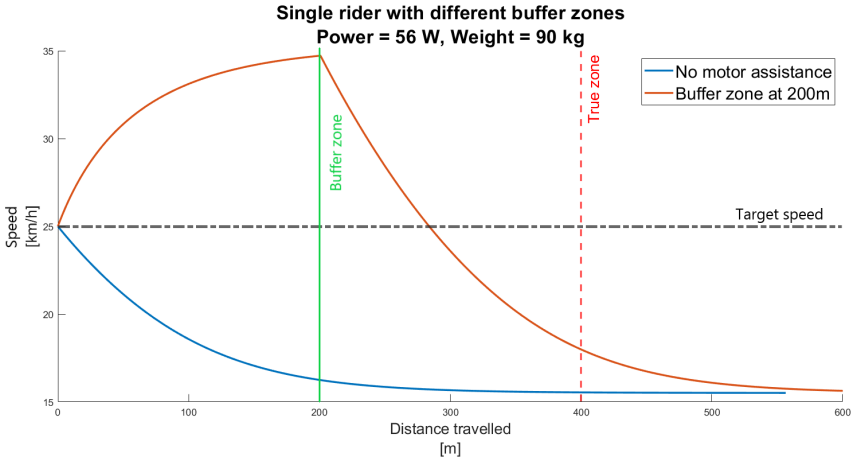

Figure 3.3: A single cyclist that is simulated to be riding towards the intersection. The cyclist is riding on a speed-pedelec, which is continuously outputting 350 W. The cyclist starts at the target speed, as if they had just been limited by a previous geofence. Two scenarios are shown, one where the motor is not assisting at all, the other where the motor stops working 200 m before the intersection. The goal is to determine whether the cyclist is slowed down to below the target speed (25 km/h in this scenario) at the intersection (shown by the ”true zone” line in the figure). The cyclist is cycling slower than the target speed when they enter the true zone in this scenario, so a buffer zone of 200 m is deemed to be effective in this specific scenario for this particular cyclist.

Repeating this simulation for each cyclist (each with different weight and power output) gives an indication of the effectiveness of a single buffer zone size. The speed profile of each cyclist during their approach can be seen in Figure 3.4. Of particular interest in this figure is the difference in effectiveness of a buffer zone placed at 150 m before the true zone and one placed 80 m before the true zone.

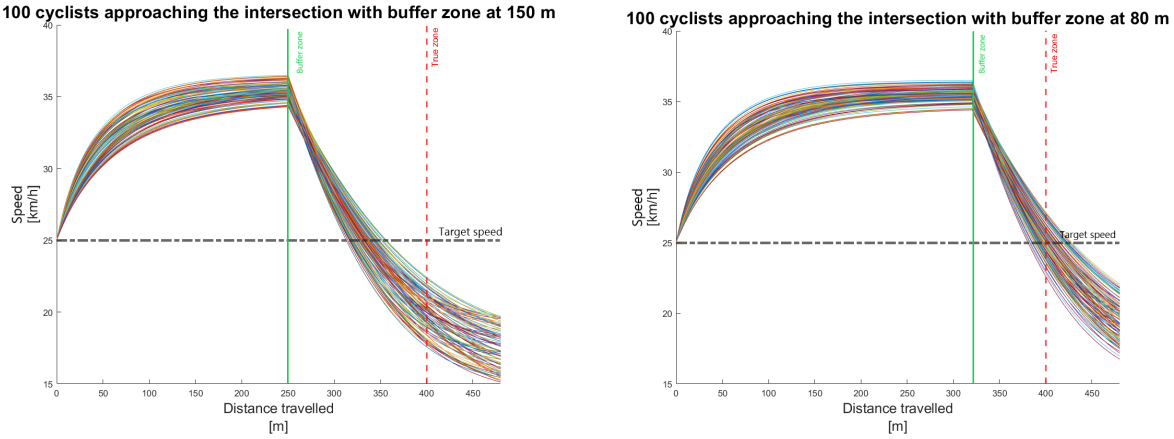

(a) Buffer zone placed at 150m before the intersection. All cyclists were slowed down to below the target speed when they reached the true zone.

(b) Buffer zone placed at 80m before the intersection. Not all cyclists (about sixty percent) were slowed down to below the target speed when they reached the true zone.

Figure 3.4: Simulating a hundred cyclists approaching an intersection with different buffer zones. Not all buffer zone sizes are effective at slowing down the cyclists to below the target speed.

The proportion of cyclists cycling below the target speed when they reach the true zone is the effectiveness of that buffer zone size. A visualisation of this can be seen in Figure 3.5. From this figure, it can be concluded that buffer zones smaller than 60 m will not be effective in limiting the speed of cyclists to the target speed. Also, buffer zones larger than 110 m will not provide additional effectiveness in limiting the speed to the target speed.

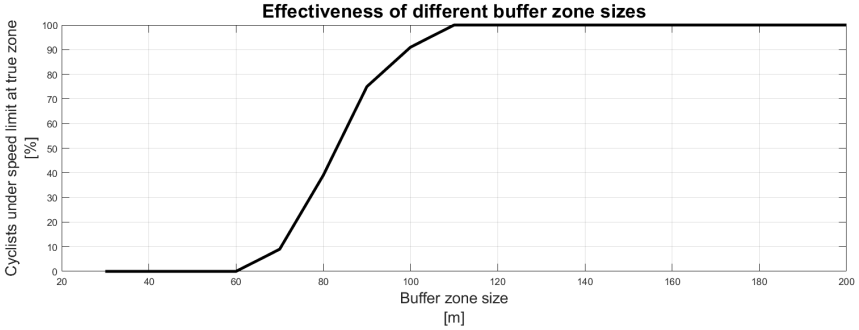

Figure 3.5: Simulation repeated for different buffer zone sizes. The line shows the proportion of cyclists that are cycling below the target speed when they reach the intersection/true zone for different buffer zone sizes.

Note that the validity of this figure is limited to the environmental parameters of the simulated scenario. In this case, the simulation assumes a road incline of zero degrees, a wind speed of 0 m/s, with cyclists riding on a speed-pedelec (instead of a regular e-bike) and a target speed of 25 km/h. To get a picture of how the effectiveness of different buffer zone sizes changes for different environments, this simulation is repeated for different wind speeds, incline levels, type of bicycle (e-bikes or speed-pedelec), and target speeds.

3.2. Results

The result of the simulation for a regular e-bike with a target speed of 20 km/h in the true zone can be seen in Figure 3.6 and Figure 3.7. These figures show the proportion of cyclists that were slowed down to a speed below the target speed when they entered the true zone for a specific buffer zone size and wind speed or incline level. For example, a buffer zone size of 100 m with a wind speed of 0 m/s and an incline level of 0 degrees slows down around 80% of the e-bike cyclists to below 20 km/h when they enter the true zone. However, a buffer zone size of 100 m is completely ineffective when the incline level is decreased to a -1 degree decline, as none of the cyclists are slowed down to below the target speed.

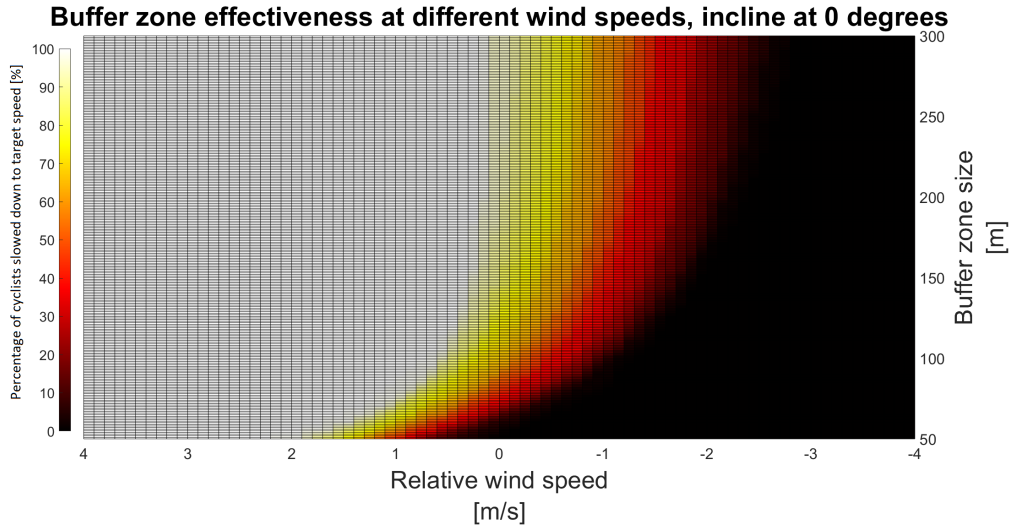

Figure 3.6: Effectiveness of different buffer zone sizes for varying wind speeds with incline set at zero degrees. Negative wind speeds indicate tail winds, positive wind speeds indicate head winds. The color bar on the left shows the proportion of cyclists that were slowed down to the target speed when they entered the true zone.

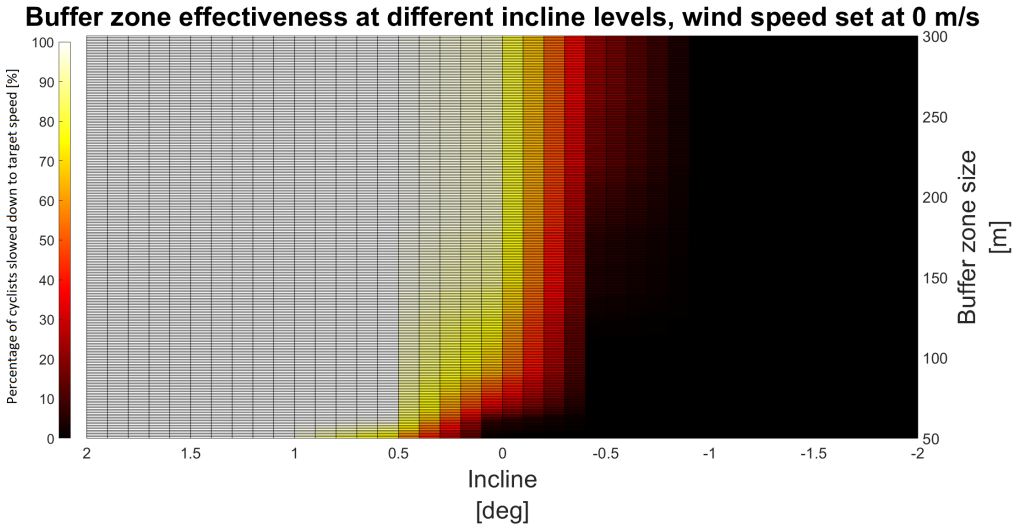

Figure 3.7: Effectiveness of different buffer zone sizes for varying incline levels with relative wind speed set at zero. A negative incline indicates a downward slope of the road, a positive incline indicates an upward slope of the road. The color bar on the left shows the proportion of cyclists that were slowed down to the target speed when they entered the true zone. Note the lower resolution of this figure compared to Figure 3.6. This is caused by the lower amount of investigated incline levels (see Table 3.3).

In order to visualise the combined effect of the wind speed level and incline level on the effectiveness of the buffer zone sizes in a single figure, a threshold was established for the minimal effective buffer zone size. The minimal effective buffer zone size is determined to be the smallest size at which the buffer zone limits at least 50 % of cyclists to the target speed when entering the true zone. For example, the minimal effective buffer zone size for a relative wind speed of -1 m/s and an incline level of 0 degrees is around 160m, as can be seen in Figure 3.6.

The minimal effective buffer zone size can be determined for each combination of different wind speeds and incline levels. The result of this can be seen in Figure 3.8, where the minimal effective buffer zone size is plotted for an e-bike with a target speed of 20 km/h. The line plots denote the minimal effective buffer zone size (x-axis) for a specific wind speed (y-axis) and incline level (number above the line).

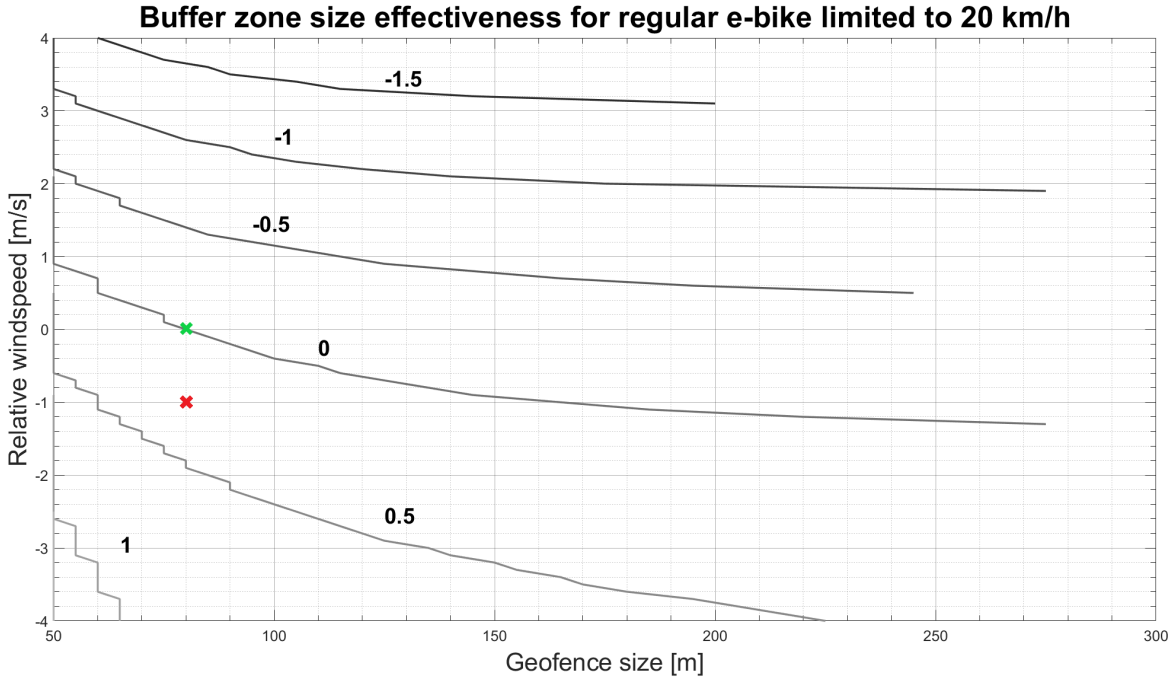

Figure 3.8: Minimal effective buffer zone size for varying incline levels and relative wind speeds. The cyclists are cycling on a regular e-bike and the target speed for the true zone is set to 20 km/h. The plots show the minimal effective buffer zones for a specific road incline and wind speed. For example, a flat road with a wind speed of 0 m/s requires a buffer zone of at least 80 m (green cross in the figure). If a point (a buffer zone size and wind speed) is **above** the line plot for the incline of the road, the buffer zone size meets the required minimum size. For example, a buffer zone size of 80 m and wind speed of -1 m/s (red cross in the figure) will not be effective at a flat road, since the point lies beneath the plot for a 0 degree road. However, it will be effective at a road with a positive incline of 0.5 degrees, as the point lies above the line plot for a 0.5 degree road.

Note the effect that a single degree difference in the road incline level or a 1 m/s wind speed difference has on the minimal effective buffer zone size. For example, a buffer zone of 70 m is effective enough at an incline level of one degree, even with a 4 m/s tailwind. However, even a buffer zone of 300 m is not effective with a 4 m/s tailwind when the incline level is changed to a flat 0 degree road. Note that for this scenario, the lines for a -2° decline, 1.5° incline and 2° incline level are not visible. This is due to the fact that there is no effective buffer zone size for a road with a -2° decline, even with a 4 m/s headwind. In contrast, the lowest buffer zone size evaluated (which is 50m) was 100 % effective on a road with a 1.5° incline and 2° incline level for all simulated wind speeds (even a tailwind of 4 m/s). For other scenarios, these incline levels will be visible in the figures.

In Figure 3.9, the target speed of the regular e-bike has been changed from 20 km/h to 15 km/h. Several insights can be gained by comparing Figure 3.8 and 3.9. For example, the line for the minimal effective buffer zone size for a flat, 0 degree incline road moves up along the y-axis. This means that a (stronger) headwind is needed in order to get the same effectiveness for a specific buffer zone size (e.g., a buffer zone size of 80 m is effective at a wind speed of 0 m/s with a target speed of 20 km/h; however, a buffer zone size of 80 m is only effective with a headwind of 2.6 m/s when you lower the target speed to 15 km/h).

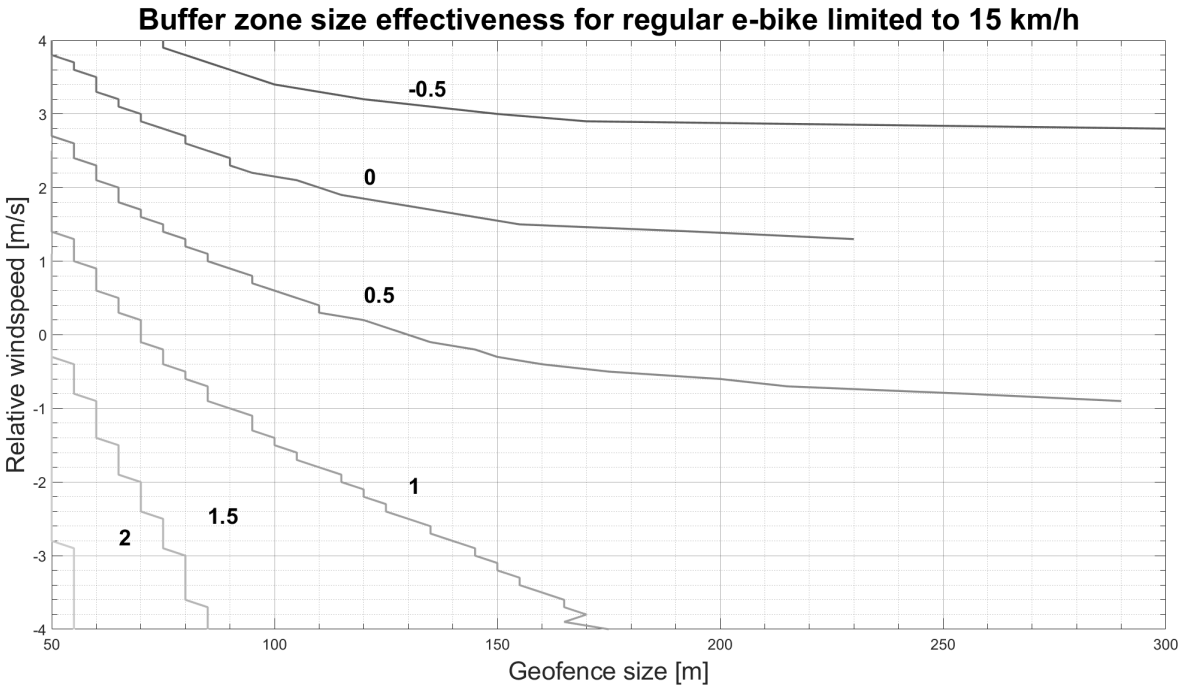

Figure 3.9: Minimal effective buffer zone size for varying incline levels and relative wind speeds. The cyclists are cycling on a regular e-bike and the target speed for the true zone is set to 15 km/h.

The results of the simulation scenarios for a speed-pedelec can be seen in Figures 3.10, 3.11 and 3.12. These figures show the results of simulations focused on different target speeds for a speed-pedelec. Similar insights to the example of the regular e-bike can be gained in these figures. For example, a buffer zone size of 85 m is effective for all target speeds in a flat and windless environment for speed-pedelecs. When the incline level is changed to a -0.5° decline, the 85m buffer zone is no longer effective for a target speed of 25 km/h (but it is still effective for the other target speeds).

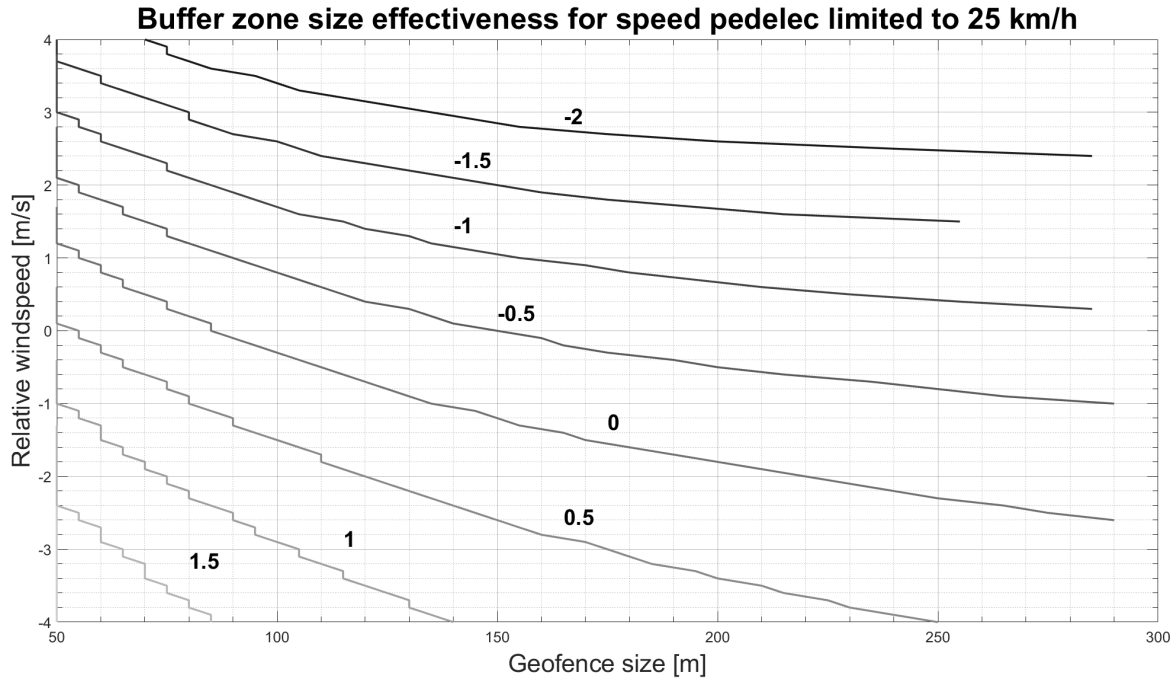

Figure 3.10: Minimal effective buffer zone size for varying incline levels and relative wind speeds. The cyclists are cycling on a speed-pedelec and the target speed is set to 25 km/h.

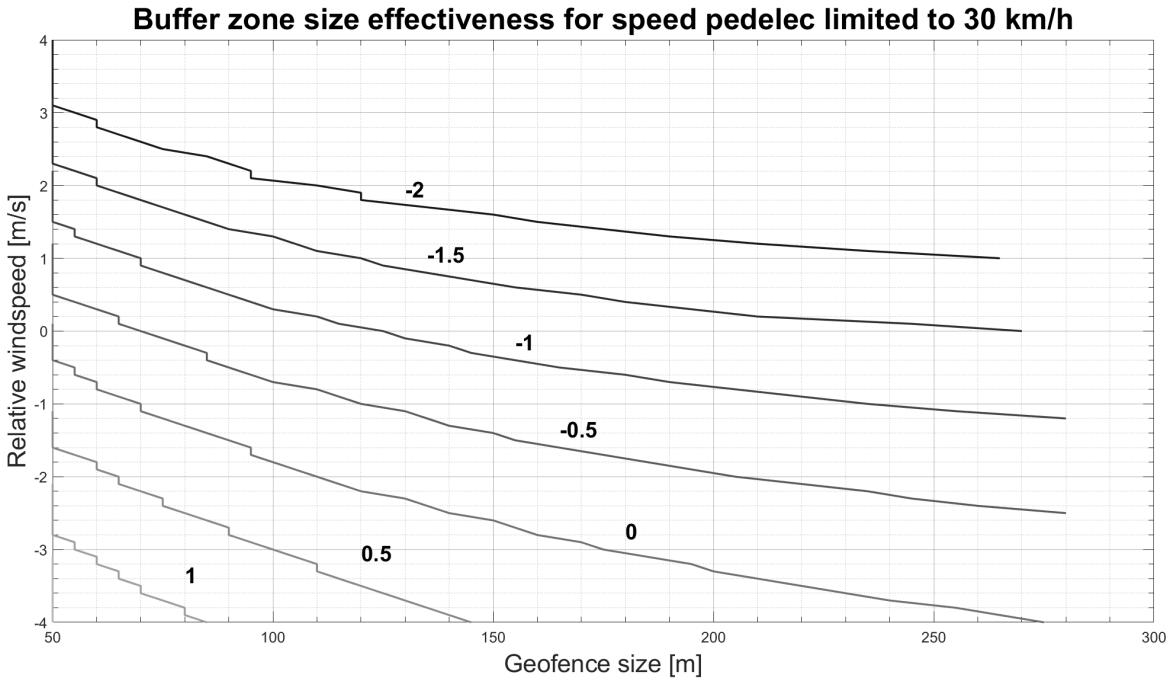

Figure 3.11: Minimal effective buffer zone size for varying incline levels and relative wind speeds. The cyclists are cycling on a speed-pedelec and the target speed is set to 30 km/h.

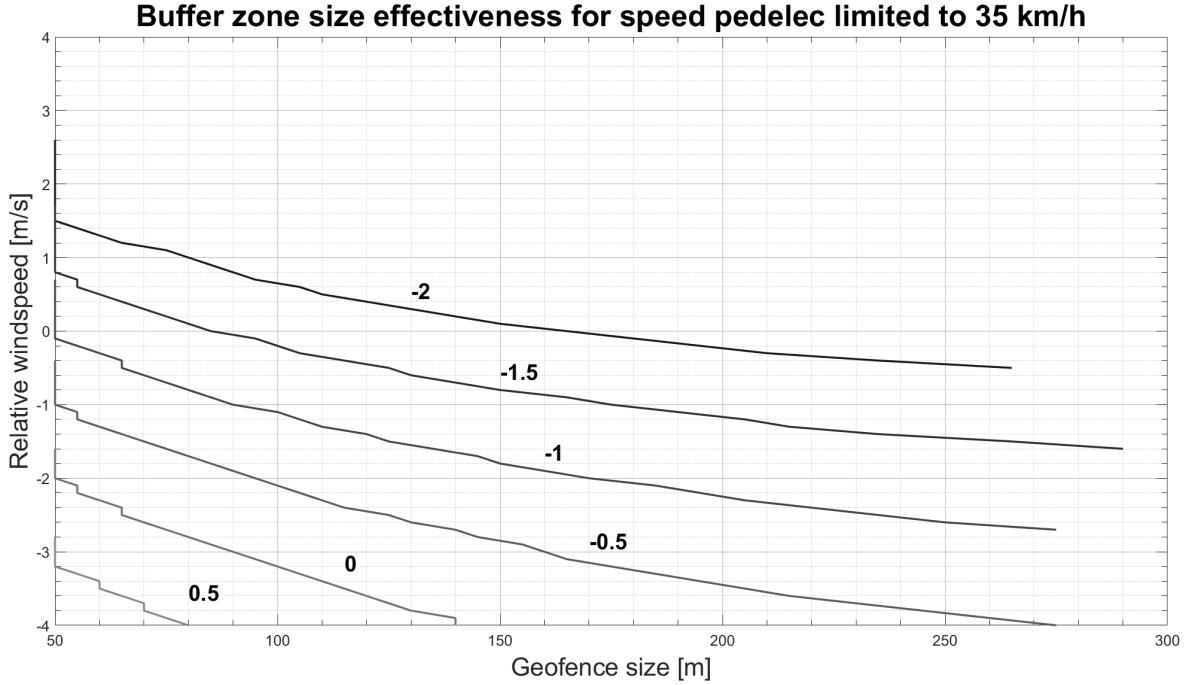

Figure 3.12: Minimal effective buffer zone size for varying incline levels and relative wind speeds. The cyclists are cycling on a speed-pedelec and the target speed is set to 35 km/h.

3.3. Simulation validation

A validation experiment has been conducted to investigate the validity of the simulation model. The aim of this experiment is to investigate whether the model simulates a similar speed over time profile compared to real-life data, employing the same time marching model as the simulation, with the power measured by the power pedals as the power input in the model. In this validation experiment, a setup similar to the setup shown in Figure 2.2 is used. However, the only data collected in the validation experiment is speed data and power data from the phone/cycling app to make sure that the data is retrieved at the same intervals. Since it is difficult to measure the motor assistance power, the e-bike motor is turned off during the experiment. This means that the power measured by the power pedals should be the only driving force in the validation experiment.

The experiment was carried out on a flat road on a windless day, with wind speeds around 1 bft. The experiment was carried out on the campus of TU Delft; see Figure 3.13. The experiment was carried out with one participant, the responsible researcher for this study. The weight of the researcher was recorded, and it was assumed that the environment was flat and windless in the simulation. The variables entered in the simulation can be seen in Table 3.4, all other variables are identical to those shown in Table 3.2. Note the lower weight of the bicycle (23 kg) compared to the original simulation setup, which is due to the absence of the e-bike battery during the experiment.

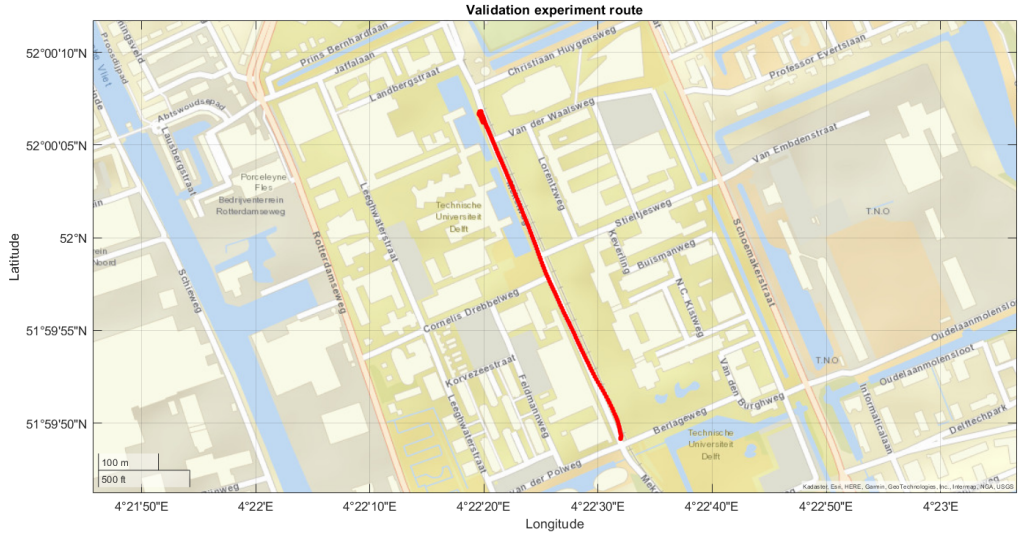

Figure 3.13: GPS trace of the first run of the validation experiment

The validation experiment was divided into four runs. The first run goes from south to north, where the researcher tries to maintain a constant power output similar to what they would output when they cycled during their commute. The second run is identical to the first run, but instead goes from north to south. The third run is a mix between normal cycling power output (similar to the previous runs) and more intense cycling, going from south to north. The fourth run is identical to the third, but again goes in the opposite direction.

Table 3.4: Variables of the validation experiment

Variable	Value
m	$23 + 80$ kg
θ	0 degrees
v_{wind}	0 m/s

The purpose of the validation experiment was to determine whether the simulation model simulates cycling data similar to data measured in a real environment. In particular, the speed over time and acceleration profile of the simulation should be similar to those from real-life measurements. The speed and

acceleration profiles of the validation experiment can be seen in Figure 3.14 and Figure 3.15. Since the simulation values are calculated at a higher frequency compared to the measured values (10 Hz versus 1 Hz), the simulation values have to be resampled to the same frequency as the measured values to calculate the error values. This is done by taking the average values of the ten closest simulated data points. The error rates in Table 3.5 are determined by calculating the mean absolute error (MAE) and the mean absolute percent error (MAPE) of the simulation prediction, which are calculated as follows.

$$\text{MAE} = \frac{\sum_{i=1}^{n} \mid v_{\text{simulated}}(i) - v_{\text{measured}}(i) \mid}{n} \tag{3.8}$$

$$\sigma_{\text{MAE}} = \frac{\sum_{i=1}^{n} (\mid v_{\text{simulated}}(i) - v_{\text{measured}}(i) \mid - \text{MAE})^2}{n-1} \tag{3.9}$$

$$\text{MAPE} = \frac{\sum_{i=1}^{n} \mid \frac{v_{\text{simulated}}(i) - v_{\text{measured}}(i)}{v_{\text{measured}}(i)} \times 100\% \mid}{n} \tag{3.10}$$

$$\sigma_{\text{MAPE}} = \frac{\sum_{i=1}^{n} (\mid \frac{v_{\text{simulated}}(i) - v_{\text{measured}}(i)}{v_{\text{measured}}(i)} \times 100\% \mid - \text{MAPE})^2}{n-1} \tag{3.11}$$

Table 3.5: Error values of the validation simulation

Run	Speed MAE	Speed MAPE	Acceleration MAE	Acceleration MAPE
1	0.352 ± 0.194 m/s	9.25 ± 5.20 %	0.026 ± 0.019 m/s^2	68.6 ± 46.7 %
2	0.548 ± 0.196 m/s	14.22 ± 6.66 %	0.017 ± 0.011 m/s^2	98.8 ± 79.1 %
3	0.295 ± 0.182 m/s	6.86 ± 4.38 %	0.021 ± 0.018 m/s^2	54.9 ± 44.5 %
4	0.602 ± 0.238 m/s	14.21 ± 5.08 %	0.022 ± 0.017 m/s^2	68.9 ± 60.1 %

The simulation speed profile is closer to the real-life speed profile during runs 1 and 3. Even though the environmental circumstances during that were quite windless with wind speeds at around 1 bft, the difference in error of the simulated speeds between different runs is still most likely caused by the change of direction (and thus relative wind speed) between the runs.

The acceleration profiles of the simulation have a more consistent similarity to the real-world environment between each run. Of particular importance are the acceleration profiles during the freewheeling portions of the runs and during the power changes in runs 3 and 4. Both the timing and the amplitude of the simulated acceleration pattern closely follow the real-life data.

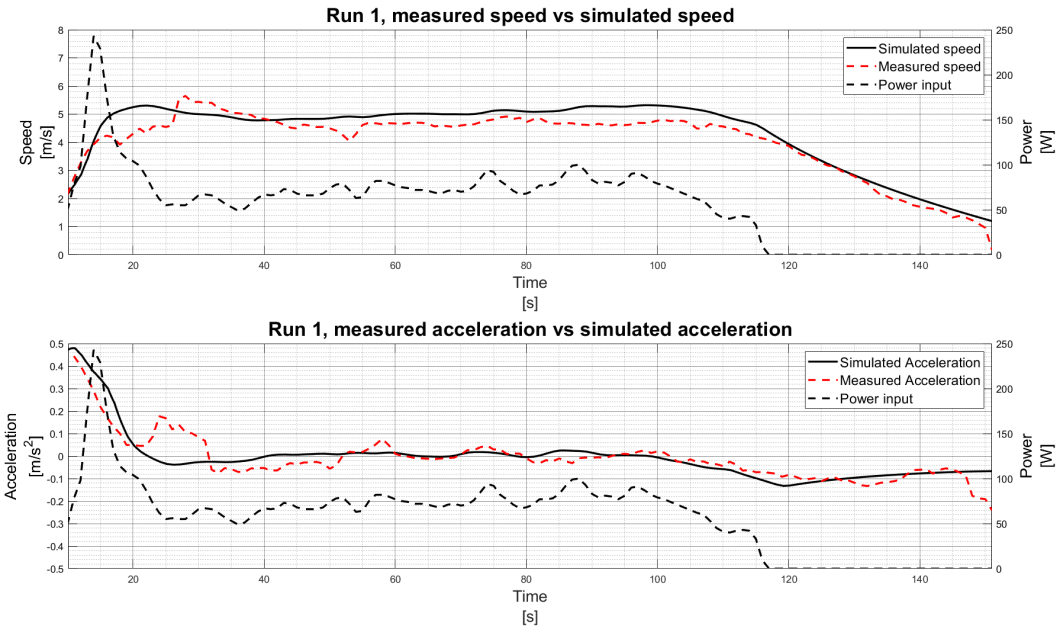

(a) First run, steady cycling to freewheeling, from south to north

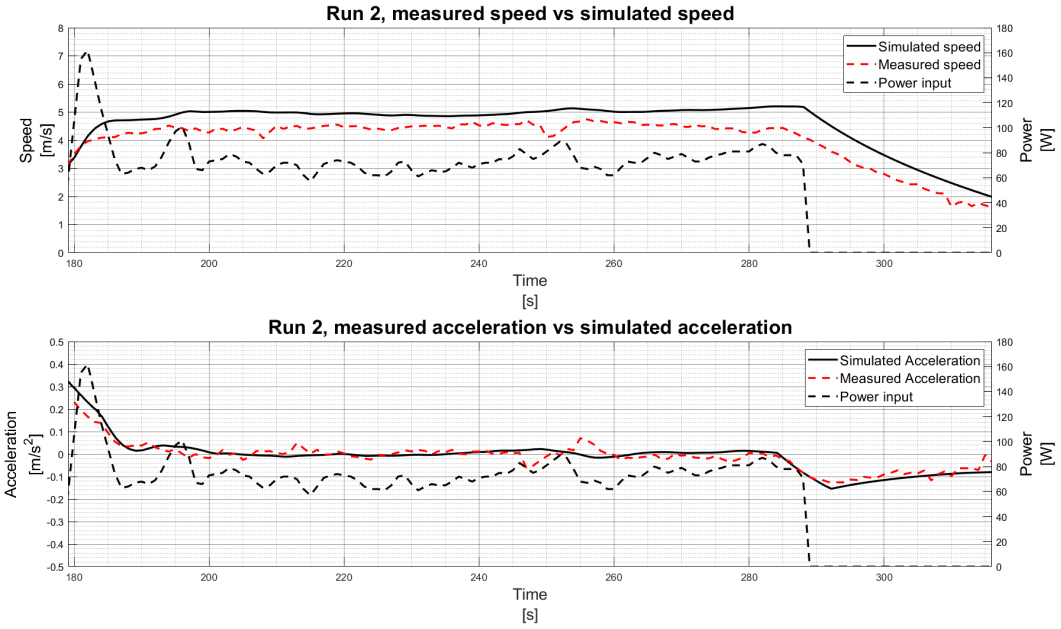

(b) Second run, steady cycling to freewheeling, from north to south

Figure 3.14: Results of runs 1 and 2 of the validation experiment. The top figures show the measured speed over time and the power input as measured by the cycling app, at a frequency of 1 Hz. In addition, the simulation results are plotted, which are simulated with a frequency of 0,1 Hz. The bottom figures show the acceleration over time, calculated by taking the first order derivative of the measured/simulated speed. The acceleration is smoothed with a moving average window of eight seconds.

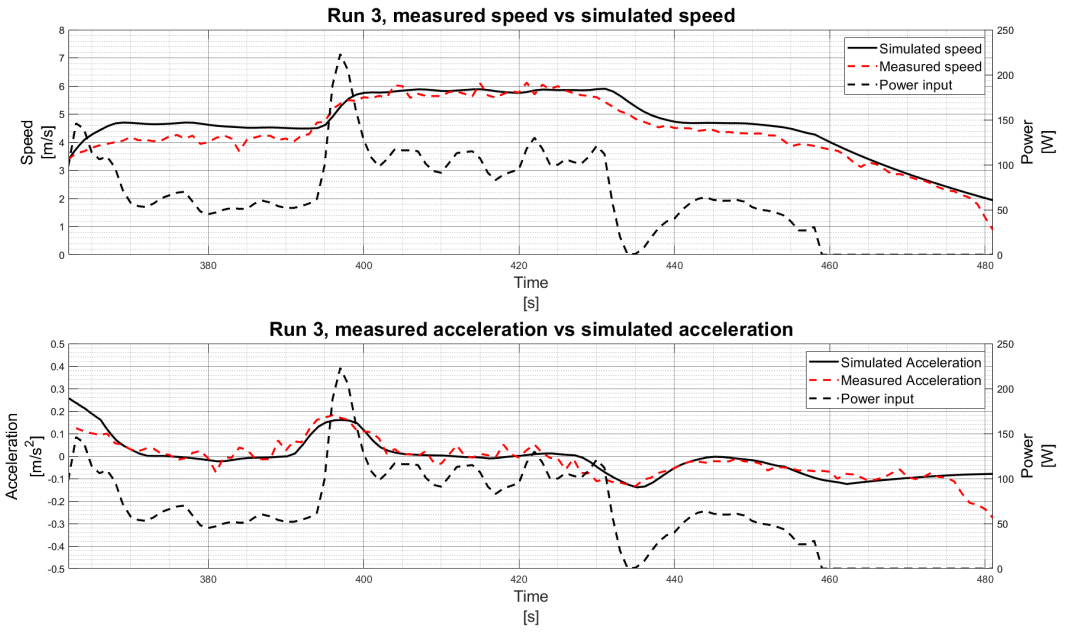

(a) Third run, steady cycling to hard cycling to steady to freewheeling, from south to north

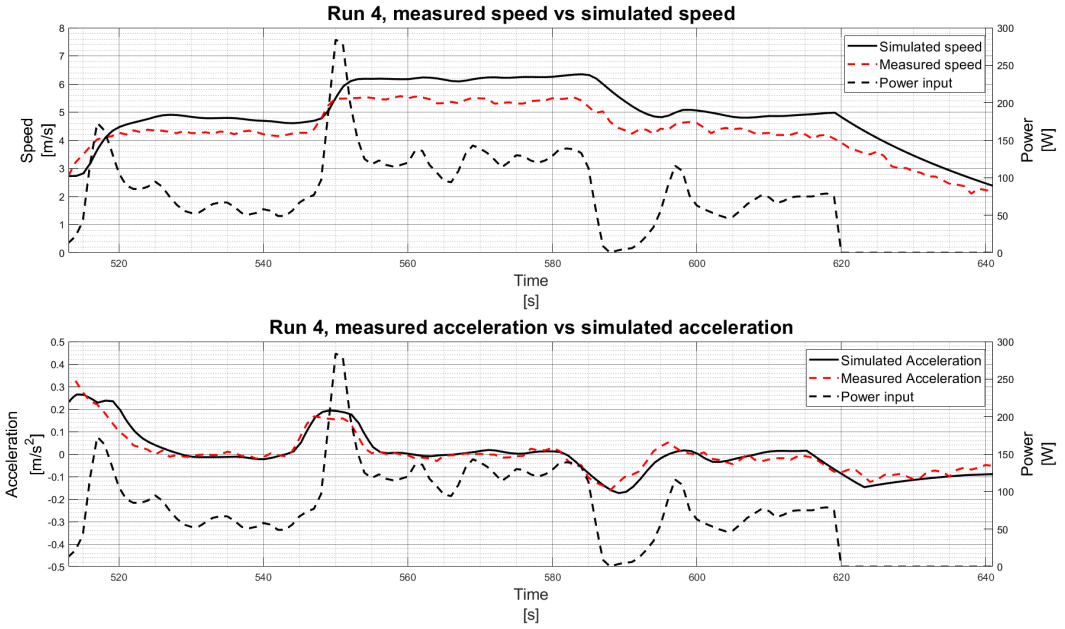

(b) Fourth run, steady cycling to hard cycling to steady to freewheeling, from north to south

Figure 3.15: Results of runs 3 and 4 of the validation experiment. The top figures show the measured speed over time and the power input as measured by the cycling app, at a frequency of 1 Hz. In addition, the simulation results are plotted, which are simulated with a frequency of 0,1 Hz. The bottom figures show the acceleration over time, calculated by taking the first order derivative of the measured/simulated speed. The acceleration is smoothed with a moving average window of eight seconds.

3.4. Discussion

The findings show that the minimal effective buffer zone size is highly dependent on the slope of the road and the relative wind speed. The lower the target speed, the more sensitive the minimal effective buffer zone size is to these changes. Note that the current approach in the geofence simulation assumes a worst-case scenario due to the assumptions made (cyclists cycling at a constant power, motor at maximum power output). A realistic minimal effective buffer zone size could be smaller if these assumptions were not made.
With the current approach, using geofencing for a speed limiter that simply turns off the motor assistance inside the geofence is not viable to implement on the scale of individual intersections. For example, a buffer zone size of 170 m is needed to effectively limit cyclists on a flat road while allowing for a slight tailwind of 1,0 m/s (see Figure 3.8, 0 degree line). To give a visual representation of the sheer size of such a geofence, Figure 3.16 shows what it looks like when geofences of 170 m are placed at intersections with many accidents (two or more). Many safe intersections and road parts are affected by geofences of this size.

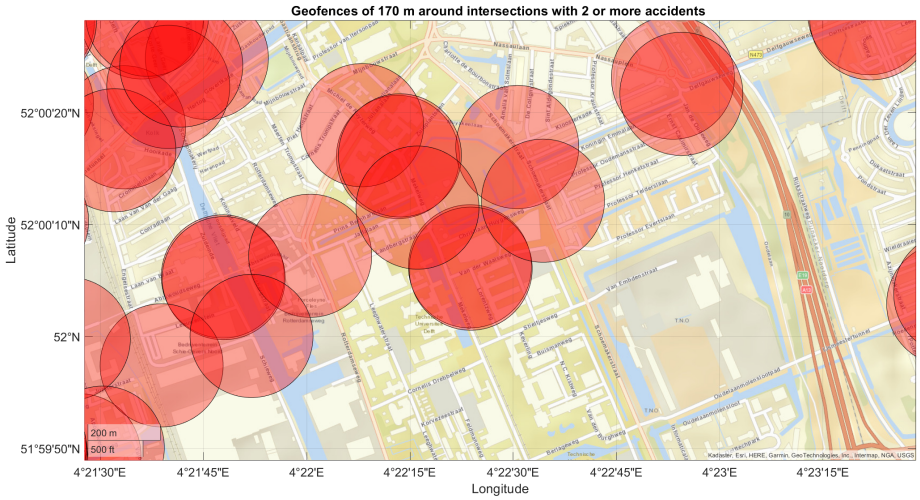

Figure 3.16: A visual representation of geofences of 170 m centered around intersections with two or more accidents logged in the accident dataset. Note the large amount of safe intersections that are also affected by the geofences.

This shows that the use of geofencing to limit the speed of regular e-bikes at specific dangerous intersections in cities is not viable, as the geofence must be extremely large to effectively limit the speed of the cyclist. The only instance where it is viable to do so is in rural areas, where the density of intersections is much lower. An option to decrease the size of the required size of a geofence is to employ braking in the speed limitation behaviour when the cyclist enters the geofence. However, as mentioned above, this could result in loss of control for the cyclist. Furthermore, unexpected braking could also actually result in more dangerous situations, defeating the main purpose of speed limitation.

Speed limitation with geofences for speed-pedelecs is more viable, when the target speed is set to a relatively high speed. For example, limiting speed-pedelecs to a target speed of 30 km/h with the same conditions as before (flat road, geofence must be effective with a tailwind of 1,0 m/s) can be achieved with a geofence of 70 m. Unfortunately, the use-case of limiting the speed of speed-pedelecs on the scale of intersections is more difficult, as they must drive on the same road part as mopeds and share most of the same legislation. Limiting the speed of a speed-pedelec to 30km/h when they drive on the same road as cars with a normal speed limit of 50 km/h could again result in more dangerous situations.

The main practical implementation of the geofence simulation findings can be found in the implementation of larger geofences. For example, a geofence that spans a whole neighbourhood has to be increased in size by the minimal effective buffer zone size for the desired target speed. The main problem of applying geofences to individual intersections (overlapping geofences) does not apply in this case, since there will only be a single buffer zone around the neighbourhood geofence.

4

Conclusions and recommendations

4.1. Conclusions

This study investigated the potential for estimation of the safety of cyclists at intersections based on natural cycling data, with the aim of identifying dangerous intersections in order to implement geofences at these intersections to locally limit the speed of e-bikes. One main research question and two sub-questions have been formulated to show the viability of this aim.

Sub-question 1: *Is there a significant correlation in certain metrics of bicycle data at accident-prone intersections and can this be used to detect dangerous intersections?*

Cycling data was collected with a natural cycling experiment and combined with a detailed open access traffic accident dataset. Several metrics were calculated from the cycling data (power output, IMU data, and GNSS position) and coupled to intersections. Data from some metrics, such as average power output, cadence deviation, and maximum forward acceleration, show a significant difference during the approach of dangerous intersections compared to safe intersections. The metrics based on power and cadence data showed the highest statistical significance (p-values <0.02) and effect size (Cohen's d > 0.80). All metrics were used by a classification model to predict whether an intersection is safe or dangerous according to the metrics of a single intersection approach, which had an accuracy of 68,2%, a specificity of 50,0%, and a sensitivity of 24,2%. Therefore, certain cycling data metrics show statistical significance at accident-prone intersections, and cycling data can be used to detect dangerous intersections. The performance of the prediction model can be improved by collecting more cycling data, integrating other types of data into the model, changing the approach of the model to summarised metrics at intersections, or changing the approach to dangerous event detection.

Sub-question 2: *What is the smallest area of a geofence that still effectively enforces a low speed on an e-bike cyclist?*

A simulation of e-bike cyclists approaching a geofenced low-speed area was carried out. By varying the geofence size, the wind speed, the level of incline, and the target speed of the cyclist, the minimal effective geofence size was determined. The minimal effective size ranges from 50 to 300 + m, and is extremely dependent on all parameters. Limiting a regular e-bike (that is already limited to 25 km/h) to 20km/h requires a geofence of at least 170 m to account for a slight tailwind (1 m/s). Limiting a regular e-bike to 15 km/h is not feasible, as the power output of the cyclist already exceeds the power needed to cycle faster than 15 km/h. Limiting speed-pedelecs to 25 km/h, 30 km/h, and 35 km/h requires geofences of at least 85 m, 70 m, and 50 m respectively.

Main research question: Can e-bike cycling data be utilised to identify dangerous intersections and enforce low-speed areas for e-bike cyclists?

Cycling data can be used to identify dangerous intersections by collecting certain metrics, based primarily on power and cadence. Enforcing a lower speed at these intersections through the use of local geofencing is not feasible, as the geofences have to be extremely large (170+ m for a speed limit of 20 km/h on a regular e-bike) to account for slight tailwinds or decline levels. Large geofences

would affect other intersections near the dangerous intersection, defeating the purpose of localised geofencing. However, geofencing can be used on a larger scale, for example, on the scale of whole neighbourhoods.

4.2. Future recommendations

Several opportunities for future research work were found.

Intersection prediction approach

The model could be improved by changing the analysis approach from predicting intersection risk based on a single intersection approach to predicting intersection risk based on summarised statistics from all approaches at a intersection. This improvement would result from the fact that this approach combines data from multiple approaches into one single safety estimate, rather than estimating intersection safety for each approach separately. Furthermore, such an approach would also have to be used in a realistic implementation, where only processed metrics are saved and analysed (instead of raw data).

Adding additional information to the classification model

By introducing additional metrics to the model such as the characteristics of the built environment, the type of intersection, or other traffic data, the model could make better predictions. Furthermore, insights could be gained on the difference in cycling behaviour at different types of intersections.

Dangerous event detection

It should be possible to identify potentially dangerous situations by analysing IMU data (for example, by detecting heavy decelerations or large swerves). Currently, there is little to no research available investigating how these situations can be detected. If dangerous events can be identified in IMU data, they can also be coupled with intersections, which could be an extremely important metric in the risk estimation model.

Speed limitation through forced braking

Although it seems intuitive to assume that speed limitation through forced braking seems dangerous, this has not yet been actually proved. If research shows that forced braking does not result in dangerous situations, speed limitation through geofencing at specific intersections suddenly becomes feasible again, as the minimal effective geofence size is severely reduced if forced braking can be employed.

References

[1] CBS. *Twee derde 55-plussers heeft gewone fiets, 4 op de 10 elektrische fiets*. https://www.cbs.nl/nl-nl/longread/statistische-trends/2020/verkeersmobiliteit-van-55-plussers-2018-2019/2-resultaten. [accessed: 22.9.2021].

[2] Christopher R. Cherry et al. "Dynamics of electric bike ownership and use in Kunming, China". In: *Transport Policy* 45 (2016), pp. 127–135. ISSN: 0967070X. DOI: 10.1016/j.tranpol.2015.09.007.

[3] Angelika Wolf and Sebastian Seebauer. "Technology adoption of electric bicycles: A survey among early adopters". In: *Transportation Research Part A: Policy and Practice* 69 (2014), pp. 196–211. ISSN: 09658564. DOI: 10.1016/j.tra.2014.08.007.

[4] BOVAG. *E-BIKE DOMINEERT FIETSVERKOPEN IN 2021*. https://www.bovag.nl/nieuws/leveringsproblemen-drukten-fietsverkoop-in-2021. [accessed: 21.4.2022].

[5] Fleet Mobility. *KIM: E-bike vervangt auto in woon-werkverkeer*. https://fleet-mobility.nl/mobility/mobiliteitsoplossingen/21215-kim-e-bike-vervangt-auto-in-woon-werkverkeer. [accessed: 22.9.2021].

[6] CBS. *Verkeersdoden 2021*. https://www.cbs.nl/nl-nl/maatwerk/2022/15/verkeersdoden-2021. [accessed: 22.4.2022].

[7] Univé. *E-BIKE ONDERZOEK Wat vindt Nederland van de E-bike?* https://www.unive.nl/binaries/content/assets/pdfs/actueel/unive-e-bike-personderzoek-2018-rapport.pdf. [accessed: 21.4.2022].

[8] D. Baschera et al. "Incidence and Severity of Head Injury due to E-Bike Accidents Compared to Normal Bicycle Accidents". In: *J Neurol Surg A Cent Eur Neurosurg* 78.S 01 (2017), O19. ISSN: 2193-6315 DOI - 10.1055/s-0037-1603842.

[9] *Verkeersongevallen - Bestand geRegistreerde Ongevallen Nederland*. Dataset. 2022. URL: https://data.overheid.nl/dataset/a516ffaf-fbcc-44bc-88cb-fca799c5cd29.

[10] B. C. Langford, J. Chen, and C. R. Cherry. "Risky riding: Naturalistic methods comparing safety behavior from conventional bicycle riders and electric bike riders". In: *Accid Anal Prev* 82 (2015), pp. 220–6. ISSN: 1879-2057 (Electronic) 0001-4575 (Linking). DOI: 10.1016/j.aap.2015.05.016. URL: https://www.ncbi.nlm.nih.gov/pubmed/26093098.

[11] Marco Dozza, Julia Werneke, and Michael Mackenzie. "E-BikeSAFE: A naturalistic cycling study to understand how electrical bicycles change cycling behaviour and influence safety". In: *Proceedings of the International Cycling Safety Conference*.

[12] Divera Twisk et al. "Preliminary results from a field experiment on e-bike safety: speed choice and mental workload for middle-aged and elderly cyclists". In: *Proceedings of the International Cycling Safety Conference 2013, ICSC2013*. Acquire Publishing BV, pp. 1–15.

[13] Tibor Petzoldt et al. "Traffic conflicts and their contextual factors when riding conventional vs. electric bicycles". In: *Transportation Research Part F: Traffic Psychology and Behaviour* 46 (2017), pp. 477–490. ISSN: 13698478. DOI: 10.1016/j.trf.2016.06.010.

[14] T. Petzoldt et al. "Drivers' gap acceptance in front of approaching bicycles – Effects of bicycle speed and bicycle type". In: *Safety Science* 92 (2017), pp. 283–289. ISSN: 09257535. DOI: 10.1016/j.ssci.2015.07.021.

[15] D. S. Pawar and G. R. Patil. "Pedestrian temporal and spatial gap acceptance at mid-block street crossing in developing world". In: *J Safety Res* 52 (2015), pp. 39–46. ISSN: 1879-1247 (Electronic) 0022-4375 (Linking). DOI: 10.1016/j.jsr.2014.12.006. URL: https://www.ncbi.nlm.nih.gov/pubmed/25662881.

[16] Marco Dozza, Giulio Francesco Bianchi Piccinini, and Julia Werneke. “Using naturalistic data to assess e-cyclist behavior”. In: *Transportation Research Part F: Traffic Psychology and Behaviour* 41 (2016), pp. 217–226. ISSN: 13698478. DOI: 10.1016/j.trf.2015.04.003.

[17] FORD MEDIA CENTER. *FORD TRIALS GEOFENCING TECH THAT COULD AUTOMATICALLY REDUCE THE SPEED OF VEHICLES TO IMPROVE SAFETY FOR ALL*. https://media.ford.com/content/fordmedia/feu/en/news/2022/05/24/ford-pro-trials-connected-tech-that-could-automatically-reduce-t.html. [accessed: 15.7.2022].

[18] David L Harkey et al. *Development of the bicycle compatibility index: A level of service concept, final report*. Report. United States. Federal Highway Administration, 1998.

[19] Alex Sorton and Thomas Walsh. “Bicycle stress level as a tool to evaluate urban and suburban bicycle compatibility”. In: *Transportation Research Record* (1994), pp. 17–17. ISSN: 0361-1981.

[20] Ulf Brüde and Jörgen Larsson. “Models for predicting accidents at junctions where pedestrians and cyclists are involved. How well do they fit?” In: *Accident Analysis Prevention* 25.5 (1993), pp. 499–509. ISSN: 00014575. DOI: 10.1016/0001-4575(93)90001-d.

[21] Cláudia Machado et al. “Characterization of Black Spot Zones for Vulnerable Road Users in São Paulo (Brazil) and Rome (Italy)”. In: *ISPRS International Journal of Geo-Information* 4.2 (2015), pp. 858–882. ISSN: 2220-9964. DOI: 10.3390/ijgi4020858.

[22] J. Strauss et al. “Cyclist deceleration rate as surrogate safety measure in Montreal using smartphone GPS data”. In: *Accid Anal Prev* 99.Pt A (2017), pp. 287–296. ISSN: 1879-2057 (Electronic) 0001-4575 (Linking). DOI: 10.1016/j.aap.2016.11.019. URL: https://www.ncbi.nlm.nih.gov/pubmed/27992762.

[23] Quan Yuan et al. “What factors impact injury severity of vehicle to electric bike crashes in China?” In: *Advances in Mechanical Engineering* 9.8 (2017). ISSN: 1687-8140 1687-8140. DOI: 10.1177/1687814017700546.

[24] Seyed Amir H Zahabi et al. “Estimating potential effect of speed limits, built environment, and other factors on severity of pedestrian and cyclist injuries in crashes”. In: *Transportation research record* 2247.1 (2011), pp. 81–90. ISSN: 0361-1981.

[25] Michael Klobucar and Jon D Fricker. “Feasibility study for bicycle safety: Data assessment and network evaluation”. In: *Joint Transportation Research Program* (2007), p. 249.

[26] Mathis Dahl Fenre and Alex Klein-Paste. “Bicycle rolling resistance under winter conditions”. In: *Cold Regions Science and Technology* 187 (2021). ISSN: 0165232X. DOI: 10.1016/j.coldregions.2021.103282.

[27] Albert C. Gross, Chester R. Kyle, and Douglas J. Malewicki. “The Aerodynamics of Human-powered Land Vehicles”. In: *Scientific American* 249.6 (1983), pp. 142–153. ISSN: 00368733, 19467087. URL: http://www.jstor.org.tudelft.idm.oclc.org/stable/24969056.

[28] Elizabeth A Casteel and Mark Archibald. “A Study on the Efficiency of Bicycle Hub Gears”. In: *ASME International Mechanical Engineering Congress and Exposition*. Vol. 56420. American Society of Mechanical Engineers, V013T14A044. ISBN: 0791856429.

[29] CBS. *Lengte en gewicht van personen, ondergewicht en overgewicht; vanaf 1981*. https://opendata.cbs.nl/statline/#/CBS/nl/dataset/81565NED/table?dl=8566. [accessed: 19.7.2022].

[30] Anton Umek and Anton Kos. “Validation of smartphone gyroscopes for mobile biofeedback applications”. In: *Personal and Ubiquitous Computing* 20.5 (2016), pp. 657–666. ISSN: 1617-4909 1617-4917. DOI: 10.1007/s00779-016-0946-4.

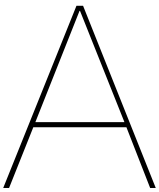

Ethics proposal

I. Applicant Information

PROJECT TITLE:	**Spatial accident risk estimation for speed-controlled e-bikes**
Research period: *Over what period of time will this specific part of the research take place*	**03/2022-09/2022**
Faculty:	**Mechanical, Maritime and Materials Engineering**
Department:	**BioMechanical Engineering**
Type of the research project: *(Bachelor's, Master's, DreamTeam, PhD, PostDoc, Senior Researcher, Organisational etc.)*	**Master project**
Funder of research: *(EU, NWO, TUD, other – in which case please elaborate)*	**-**
Name of Corresponding Researcher: *(If different from the Responsible Researcher)*	**Daniël Landré**
E-mail Corresponding Researcher: *(If different from the Responsible Researcher)*	**d.landre@student.tudelft.nl**
Position of Corresponding Researcher: *(Masters, DreamTeam, PhD, PostDoc, Assistant/ Associate/ Full Professor)*	**MSc student**
Name of Responsible Researcher: ***Note:*** *all student work must have a named Responsible Researcher to approve, sign and submit this application*	**Jason Moore**
E-mail of Responsible Researcher: *Please ensure that an institutional email address (**no Gmail, Yahoo, etc.**) is used for all project documentation/ communications including Informed Consent materials*	**j.k.moore@tudelft.nl**
Position of Responsible Researcher : *(PhD, PostDoc, Associate/ Assistant/ Full Professor)*	**Assistant Professor**

II. Research Overview

NOTE: *You can find more guidance on completing this checklist here*

a) Please summarise your research very briefly (100-200 words)

What are you looking into, who is involved, how many participants there will be, how they will be recruited and what are they expected to do?

Add your text here – (please avoid jargon and abbrevations)
The aim of the project is to create a basis for the potential of a speed-controlled e-bike. The focus lies on where the speed control should act, based on maximising safety for the e-bike cyclist. Open-access data is used from the Dutch government for the accident analysis and a naturalistic cycling experiment will be performed for GPS data. The aim is to compare accurate GPS traces from a differential GPS sensor to inaccurate GPS data from a mobile phone provided by the researcher. The expected result will be that a difference in deceleration patterns at accident-heavy intersections compared to safe intersections is visible in the accurate GPS data, but not in the inaccurate data.

This will provide insight on a minimum viable sensor setup that's needed for a speed-controlled e-bike that's able to identify dangerous intersections based on GPS information from the GPS sensor on the e-bike.

Around ten healthy young adults (between 20-30 years old, recruited using personal contacts) will be asked to ride specific pre-determined routes throughout Delft on a sensor-equipped e-bike for a duration of 1 hour. The GPS (and kinematic data) data of their trips during the experiment will be saved and analysed. Participants will be asked to cycle according to safety margins and to respect traffic rules, traffic lights and other road-users. This will not arise any extra risk with respect to everyday urban cycling experience.

b) **If your application is an additional project** related to an existing approved HREC submission, please provide a brief explanation including the existing relevant HREC submission number/s.

Add your text here – (please avoid jargon and abbrevations)
-

c) **If your application is a simple extension of, or amendment to,** an existing approved HREC submission, you can simply submit an HREC Amendment Form as a submission through LabServant.

III. Risk Assessment and Mitigation Plan

NOTE: *You can find more guidance on completing this checklist here*

Please complete the following table in full for all points to which your answer is "yes". Bear in mind that the vast majority of projects involving human participants as Research Subjects also involve the collection of **Personally Identifiable Information (PII)** and/or **Personally Identifiable Research Data (PIRD)** which may pose potential risks to participants as detailed in Section G: Data Processing and Privacy below.

To ensure alighment between your risk assessment, data management and what you agree with your Research Subjects you can use the last two columns in the table below to refer to specific points in your Data Management Plan (DMP) and Informed Consent Form (ICF) – **but this is not compulsory**.

It's worth noting that **you're much more likely to need to resubmit your application if you neglect to identify potential risks**, than if you identify a potential risk and demonstrate how you will mitigate it. If necessary, the HREC will always work with you and colleagues in the Privacy Team and Data Management Services to see how, if at all possible, your research can be conducted.

			If YES please complete the Risk Assessment and Mitigation Plan columns below.		*Please provide the relevant reference #*	
ISSUE	**Yes**	**No**	**RISK ASSESSMENT – what risks could arise?** *Please ensure that you list ALL of the actual risks that could potentially arise – do not simply state whether you consider any such risks are important!*	**MITIGATION PLAN – what mitigating steps will you take?** *Please ensure that you summarise what actual mitigation measures you will take for each potential risk identified – do not simply state that you will e.g. comply with regulations.*	**DMP**	**ICF**
A: Partners and collaboration						
1. Will the research be carried out in collaboration with additional organisational partners such as: • One or more collaborating research and/or commercial organisations • Either a research, or a work experience internship provider[1] *[1] If yes, please include the graduation agreement in this application*	**x**					
2. Is this research dependent on a Data Transfer or Processing Agreement with a collaborating partner or third party supplier? *If yes please provide a copy of the signed DTA/DPA*		**x**				
3. Has this research been approved by another (external) research ethics committee (e.g.: HREC and/or MREC/METC)? *If yes, please provide a copy of the approval (if possible) and summarise any key points in your Risk Management section below*		**x**				
B: Location						

			If YES please complete the Risk Assessment and Mitigation Plan columns below.		*Please provide the relevant reference #*	
ISSUE	**Yes**	**No**	**RISK ASSESSMENT – what risks could arise?** *Please ensure that you list ALL of the actual risks that could potentially arise – do not simply state whether you consider any such risks are important!*	**MITIGATION PLAN – what mitigating steps will you take?** *Please ensure that you summarise what actual mitigation measures you will take for each potential risk identified – do not simply state that you will e.g. comply with regulations.*	**DMP**	**ICF**
4. Will the research take place in a country or countries, other than the Netherlands, within the EU?		**x**				
5. Will the research take place in a country or countries outside the EU?		**x**				
6. Will the research take place in a place/region or of higher risk – including known dangerous locations (in any country) or locations with non-democratic regimes?		**x**				
C: Participants						
7. Will the study involve participants who **may** be vulnerable and possibly (legally) unable to give informed consent? (e.g., children below the legal age for giving consent, people with learning difficulties, people living in care or nursing homes,).		**x**				
8. Will the study involve participants who **may** be vulnerable under specific circumstances and in specific contexts, such as victims and witnesses of violence, including domestic violence; sex workers; members of minority groups, refugees, irregular migrants or dissidents?		**x**				
9. Are the participants, outside the context of the research, in a dependent or subordinate position to the investigator (such as own children, own students or employees of either TU Delft and/or a collaborating partner organisation)? *It is essential that you safeguard against possible adverse consequences of this situation (such as allowing a student's failure to participate to your satisfaction to affect your evaluation of their coursework).*		**x**				
10. Is there a high possibility of re-identification for your participants? (e.g., do they have a very specialist job of which there are only a small number in a given country, are they members of a small community, or employees from a partner company collaborating in the research? Or are they one of only a handful of (expert) participants in the study?		**x**				
D: Recruiting Participants						
11. Will your participants be recruited through your own, professional, channels such as conference attendance lists, or through specific network/s such as self-help groups		**X**				
12. Will the participants be recruited or accessed in the longer term by a (legal or customary) gatekeeper? (e.g., an adult professional working with children; a community leader or family member who has this customary role – within or outside the EU; the data producer of a long-term cohort study)		**x**				

			If YES please complete the Risk Assessment and Mitigation Plan columns below.		*Please provide the relevant reference #*	
ISSUE	**Yes**	**No**	**RISK ASSESSMENT – what risks could arise?** *Please ensure that you list ALL of the actual risks that could potentially arise – do not simply state whether you consider any such risks are important!*	**MITIGATION PLAN – what mitigating steps will you take?** *Please ensure that you summarise what actual mitigation measures you will take for each potential risk identified – do not simply state that you will e.g. comply with regulations.*	**DMP**	**ICF**
13. Will you be recruiting your participants through a crowd-sourcing service and/or involve a third party data-gathering service, such as a survey platform?		x				
14. Will you be offering any financial, or other, remuneration to participants, and might this induce or bias participation?		x				
E: Subject Matter *Research related to medical questions/health may require special attention. See also the website of the CCMO before contacting the HREC.*						
15. Will your research involve any of the following: • Medical research and/or clinical trials • Invasive sampling and/or medical imaging • Medical and *In Vitro Diagnostic Medical* Devices Research		x				
16. Will drugs, placebos, or other substances (e.g., drinks, foods, food or drink constituents, dietary supplements) be administered to the study participants? *If yes see here to determine whether medical ethical approval is required*		x				
17. Will blood or tissue samples be obtained from participants? *If yes see here to determine whether medical ethical approval is required*		x				
18. Does the study risk causing psychological stress or anxiety beyond that normally encountered by the participants in their life outside research?		x				
19. Will the study involve discussion of personal sensitive data which could put participants at increased legal, financial, reputational, security or other risk? (e.g., financial data, location data, data relating to children or other vulnerable groups) *Definitions of sensitive personal data, and special cases are provided on the TUD Privacy Team website.*		x				
20. Will the study involve disclosing commercially or professionally sensitive, or confidential information? (e.g., relating to decision-making processes or business strategies which might, for example, be of interest to competitors)		x				
21. Has your study been identified by the TU Delft Privacy Team as requiring a Data Processing Impact Assessment (DPIA)? *If yes please attach the advice/ approval from the Privacy Team to this application*		x				
22. Does your research investigate causes or areas of conflict? *If yes please confirm that your fieldwork has been discussed with the appropriate safety/security advisors and approved by your Department/Faculty.*		x				

			If YES please complete the Risk Assessment and Mitigation Plan columns below.		*Please provide the relevant reference #*	
ISSUE	**Yes**	**No**	**RISK ASSESSMENT – what risks could arise?** *Please ensure that you list ALL of the actual risks that could potentially arise – do not simply state whether you consider any such risks are important!*	**MITIGATION PLAN – what mitigating steps will you take?** *Please ensure that you summarise what actual mitigation measures you will take for each potential risk identified – do not simply state that you will e.g. comply with regulations.*	**DMP**	**ICF**
23. Does your research involve observing illegal activities or data processed or provided by authorities responsible for preventing, investigating, detecting or prosecuting criminal offences *If so please confirm that your work has been discussed with the appropriate legal advisors and approved by your Department/Faculty.*		**x**				
F: Research Methods						
24. Will it be necessary for participants to take part in the study without their knowledge and consent at the time? (e.g., covert observation of people in non-public places).		**x**				
25. Will the study involve actively deceiving the participants? (For example, will participants be deliberately falsely informed, will information be withheld from them or will they be misled in such a way that they are likely to object or show unease when debriefed about the study).		**x**				
26. Is pain or more than mild discomfort likely to result from the study? And/or could your research activity cause an accident involving (non-) participants?		**x**				
27. Will the experiment involve the use of devices that are not 'CE' certified? *Only, if 'yes': continue with the following questions:*		**x**				
• Was the device built in-house?						
• Was it inspected by a safety expert at TU Delft? *If yes, please provide a signed device report*						
• If it was not built in-house and not CE-certified, was it inspected by some other, qualified authority in safety and approved? *If yes, please provide records of the inspection*						
28. Will your research involve face-to-face encounters with your participants and if so how will you assess and address Covid considerations?	**x**		**A potential risk could arise in breaking government regulations regarding keeping distance during the experiment briefing.**	**Every part of the experiment (including briefing and post-experiment discussion) will take place outdoors. Distance regulations are often indoors-only. Should there also be a distance regulation outside, the experiment briefing and post-discussion will take place on fixed seats, measured to be 1,5m apart.**		
29. Will your research involve **either:** a) "big data", combined datasets, new data-gathering or new data-merging techniques which might lead to re-identification of your participants **and/or** b) artificial intelligence or algorithm training where, for example biased datasets could lead to biased outcomes?		**x**				
G: Data Processing and Privacy						

			If YES please complete the Risk Assessment and Mitigation Plan columns below.		*Please provide the relevant reference #*	
ISSUE	**Yes**	**No**	**RISK ASSESSMENT – what risks could arise?** *Please ensure that you list ALL of the actual risks that could potentially arise – do not simply state whether you consider any such risks are important!*	**MITIGATION PLAN – what mitigating steps will you take?** *Please ensure that you summarise what actual mitigation measures you will take for each potential risk identified – do not simply state that you will e.g. comply with regulations.*	**DMP**	**ICF**
30. Will the research involve collecting, processing and/or storing any directly identifiable PII (Personally Identifiable Information) including name or email address that will be used for administrative purposes only? (eg: obtaining Informed Consent or disbursing remuneration)	**x**		**The informed consent form will contain the names and signatures of the participants.**	**The signed forms will be kept in a locked cabinet in the office of the supervisor. After the project deadline, the signed forms will be destroyed immediately.**		
31. Will the research involve collecting, processing and/or storing any directly or indirectly identifiable PIRD (Personally Identifiable Research Data) including videos, pictures, IP address, gender, age etc and **what other Personal Research Data** (including personal or professional views) will you be collecting?	**x**		**I'll be saving the following data of the participants: Weight, Age bracket (e.g., 20-30 years old) and Gender. Their names will be fully anonymised in the dataset (for example: "Participant 1"). These parameters alone have been deemed to be insignificant enough to not require a DPIA by the privacy team.**	**The names of the participants will be fully anonymised. The only personal information saved to the dataset will be weight, age bracket and gender. The participants will be informed of this in the informed constent form.**		
32. Will this research involve collecting data from the internet, social media and/or publicly available datasets which have been originally contributed by human participants		**x**			**10,19**	
33. Will your research findings be published in one or more forms in the public domain, as e.g., Masters thesis, journal publication, conference presentation or wider public dissemination?	**x**		**Research findings will be recorded in a Masters thesis.**			
34. Will your research data be archived for re-use and/or teaching in an open, private or semi-open archive?	**x**		**Research dataset will be published to the 4TU repository.**		**22-25**	

B

Informed consent form

Informed consent form

WHAT IS THIS STUDY ABOUT?

The aim of this master thesis project is to create a basis for the potential of a speed-controlled e-bike. The focus lies on where such a speed control should act, based on maximising safety for the e-bike cyclist.

This experiment will try to identify differences in e-bike cyclist deceleration distributions at intersections or road parts where accidents happened in the past compared to places where no accidents occurred. This will be achieved by comparing accurate GPS cycling traces from a high-quality on-board GPS module to inaccurate GPS data from a mobile phone. Kinematic (IMU) data will also be recorded with the sensors on the mobile phone.

The expected result will be that a difference in deceleration patterns at accident-prone places compared to safer places is visible in the accurate GPS data, but not in the inaccurate data. This gives the researcher information on what accuracy is needed on on-board cycling GPS systems for accurate spatial safety estimation.

WHAT DOES PARTICIPATION TO THE EXPERIMENT INVOLVE?

The experiment will take place in Delft. Each participant will be asked to ride specific cycling routes throughout Delft on a sensor-equipped e-bike provided by the researcher. You'll be shown where to ride by the on-board navigation system. You'll be asked to ride just like you do on your own bicycle. The experiment will be performed during commuting times (17:00-18:00 on workdays), during which it is expected to be busy on the roads. You will be asked to cycle according to safety margins and to respect traffic rules, traffic lights and other road-users. This will not result in any extra risk with respect to everyday urban cycling experience. The experiment will last approximately 1 hour, with one five-minute break during the duration of the experiment.

WHAT ARE THE RISKS AND BENEFITS ASSOCIATED WITH THIS EXPERIMENT?

The risks associated with this experiment are the ones arising from cycling in an urban environment in everyday life. You are expected to ride in a manner which is not different from your normal cycling behaviour. You will not directly benefit from participating in this study.

IS IT POSSIBLE TO WITHDRAW?

It is possible to withdrawal from the study at any time. If you decide to withdraw, the personal data collected with questionnaire and sensors will be destroyed.
At any time, the participant has the right to request access to and rectification or erasure of personal data.

WHAT WILL HAPPEN TO MY INFORMATION?

Personal contact information such as name and surname will be kept confidential and will not be saved in any repository.
The information relevant to the research collected through the questionnaire (age, gender, weight) and the cycling data (GPS traces and inertial measurements) will be collected and safely stored in SURFdrive for 10 years or more, in accordance with the TU Delft Research Data Framework Policy.

No one outside the research group will have access to data before publication of the thesis report. The recorded GPS traces will be only of the experiment route, it is not monitoring the real transportation habits of the person, so it is not possible to connect it to the rider.
Upon analysis and publication, the anonymized data will be stored on a public repository (4TU Research Data) and made available open access for other researchers to analyse.

Contacts

Research student:
Daniël Landré d.landre@student.tudelft.nl

Supervisor:
Jason Moore j.k.moore@tudelft.nl

PLEASE TICK THE APPROPRIATE BOXES	Yes	No
A: GENERAL AGREEMENT – RESEARCH GOALS, PARTICPANT TASKS AND VOLUNTARY PARTICIPATION		
1. I have read and understood the study information dated [*14/06/2022*], or it has been read to me. I have been able to ask questions about the study and my questions have been answered to my satisfaction.	☐	☐
2. I consent voluntarily to be a participant in this study and understand that I can refuse to answer questions and I can withdraw from the study at any time, without having to give a reason.	☐	☐
3. I understand that taking part in the study involves me, as a participant, being weighted and riding several routes through Delft during commuting times on a sensor-equipped e-bike.	☐	☐
B: POTENTIAL RISKS OF PARTICIPATING (INCLUDING DATA PROTECTION)		
4. I understand that taking part in the study involves the following risks: • Physical discomfort/fatigue due to physical activity	☐	☐
C: RESEARCH PUBLICATION, DISSEMINATION AND APPLICATION		
12. I understand that after the research study, the data I provide will be used for a master thesis project.	☐	☐
13. I understand that personal information collected about me that could identify me (limited to age bracket, gender and weight) will be recorded and saved to the published dataset.	☐	☐
D: (LONGTERM) DATA STORAGE, ACCESS AND REUSE		
16. I give permission for the cycling data and personal data (age bracket, gender, weight) that I provide to be archived in the TU Delft repository after publication of the thesis document, so it can be used for future research and learning.	☐	☐
17. I understand that access to this repository is open.	☐	☐

Signatures

_____	_____	_____
Name of participant	Signature	Date

I have accurately read out the information sheet to the potential participant and, to the best of my ability, ensured that the participant understands to what they are freely consenting.

_____	_____	_____
Researcher name	Signature	Date

C

Experiment Protocol

Step by Step plan

Intro						Welcome participant
						Read through consent form and sign form
						Record Weight, Age Bracket and Gender & experience
						Take bicycle & participant outside 3ME
Sensor setup						Configure IMU phone
						Start Wahoo fitness app
						Start Wahoo workout
						Connect USB-C piski power input
						Check GPS antenna connection
						Check USB drive (Red light)
						Check position fix (solid yellow light)
Experiment start						Put on backpack
						Set assistance level to Medium/Normal
						Determine random destination
						Give instructions for random destination & ride
						Tap screen of IMU phone
						Give instructions for Route 1 & ride
						Tap screen of IMU phone
						Give instructions for Route 2 & ride
Experiment end						Switch off IMU stream
						End Wahoo workout
						Remove USB
						Remove power
Post-Processing						Upload Wahoo file to drive
						Import into golden cheetah & export raw data
						Change first timestamp into unix timestamp
						Use SBP2report on .sbp file from GNSS sensor
						(optional) combine raw .csv files into one file
						Rename all files into the appropriate format & move to folder

IMU phone setup

					GPS position
					Linear Acceleration
					Gravity
					Include in stream
					Fastest sensor frequency
					SD stream
					Run in Background
					Switch Stream on

D

Raw cycling data example

This appendix entry shows the raw data of a single intersection approach that was identified in the cycling dataset. The metrics used in the prediction model are calculated from the data shown. The data from the smartphone is rotated according to the orientation of the smartphone, i.e., rotating the reference frame of the smartphone IMU to the global reference frame (see Figure D.1a). This is done by calculating the rotation matrix between the gravity data of the smartphone and the direction of gravity in the global reference frame. Then, the accelerometer data and gyroscope data are rotated according to this rotation matrix [1]. The result of this rotation can be seen in Figure D.6 and D.8.

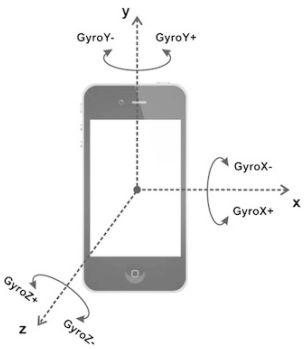

(a) Smartphone IMU orientation, [30]

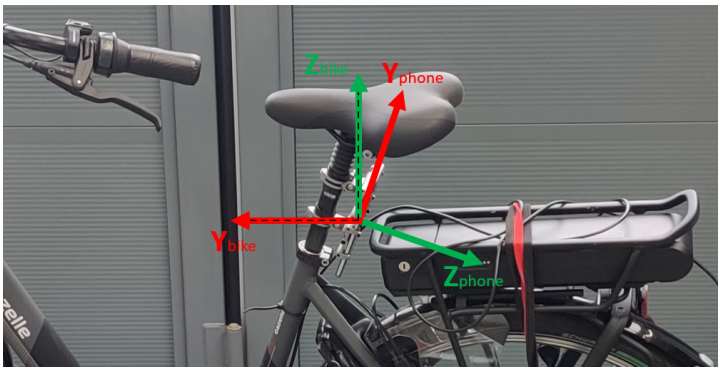

(b) The smartphone orientation and global (bike) reference frame

Figure D.1: The smartphone orientation is rotated to the global (bike) reference frame by considering the orientation of the gravity vector in the data and rotating the gravity data it until it is pointing upwards. The gyroscope and accelerometer data are then rotated with the same rotation. The x-axis is pointing into the picture frame, i.e., to the right of the cyclist.

[1] Special thanks to user "Kuba hasn't forgotten Monica" on Mathematics Stack Exchange for a detailed guide on the transformation and alignment of two 3D vectors. *[Kuba hasn't forgotten Monica (https://math.stackexchange.com/users/76513/kuba-hasnt-forgotten-monica), "Calculate Rotation Matrix to align Vector A to Vector B in 3d?", URL (version: 2018-09-12): https://math.stackexchange.com/q/897677]*

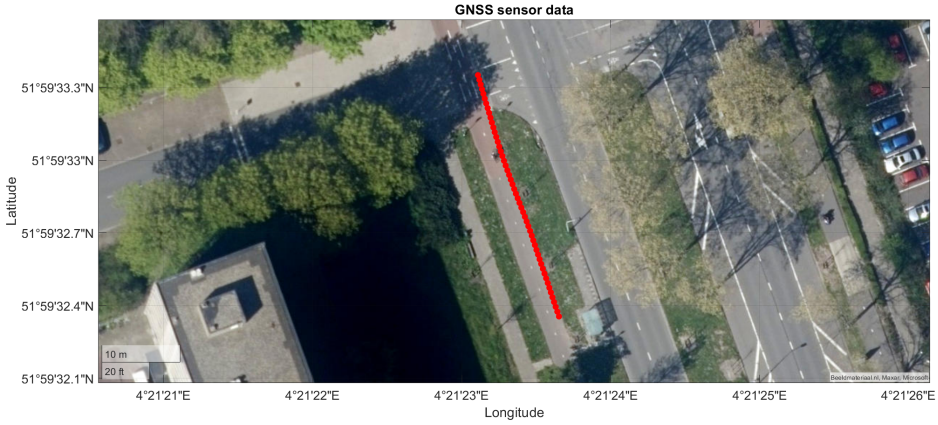

Figure D.2: GNSS trace that has been assigned to an intersection, cut and analysed. The cyclist is cycling from north to south.

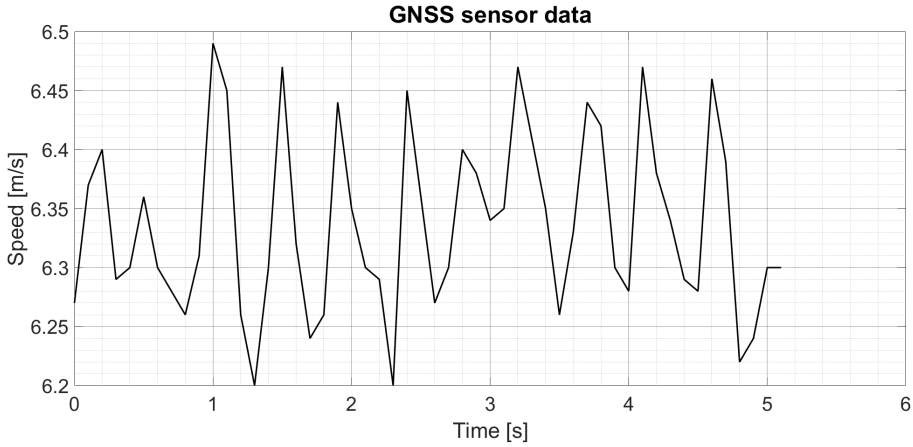

Figure D.3: Speed calculated by considering the euclidean distance between the GNSS positions

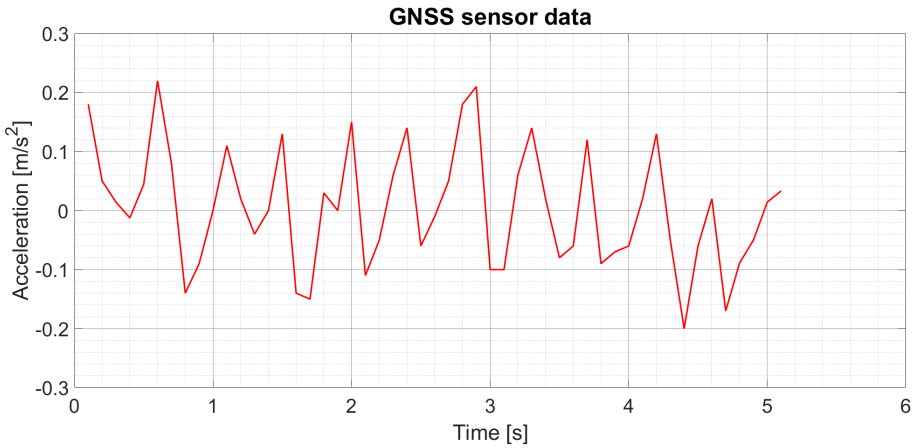

Figure D.4: Acceleration calculated by considering the euclidean distance between the GNSS positions

The raw accelerometer data is rotated to the global reference frame shown in D.1a. The lateral direction is defined as the x-axis in the global reference frame (with the positive direction in the right direction). The longitudinal direction is defined as the y-axis in the global reference frame (with the positive direction in the forward direction).

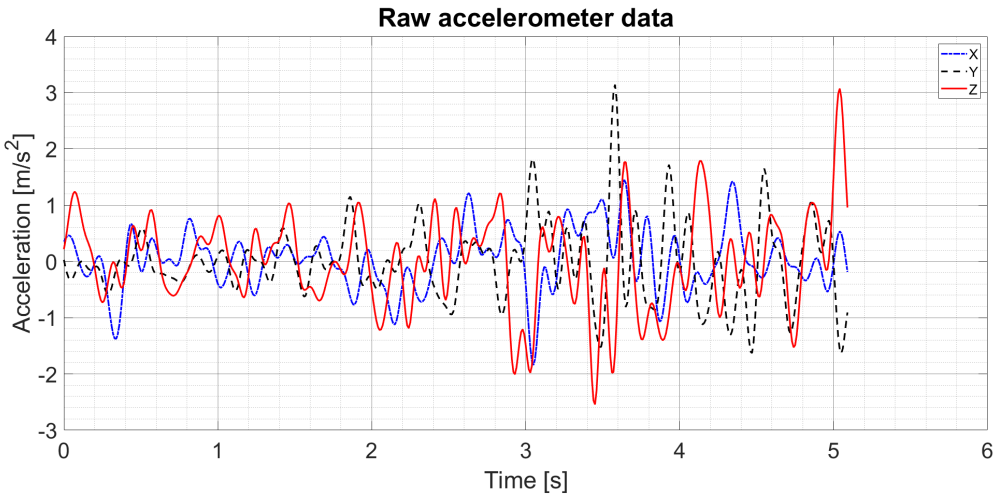

Figure D.5: Three axis accelerometer data. This data has been low-pass filtered with a cut-off frequency of 5 Hz, in order to get rid of noise.

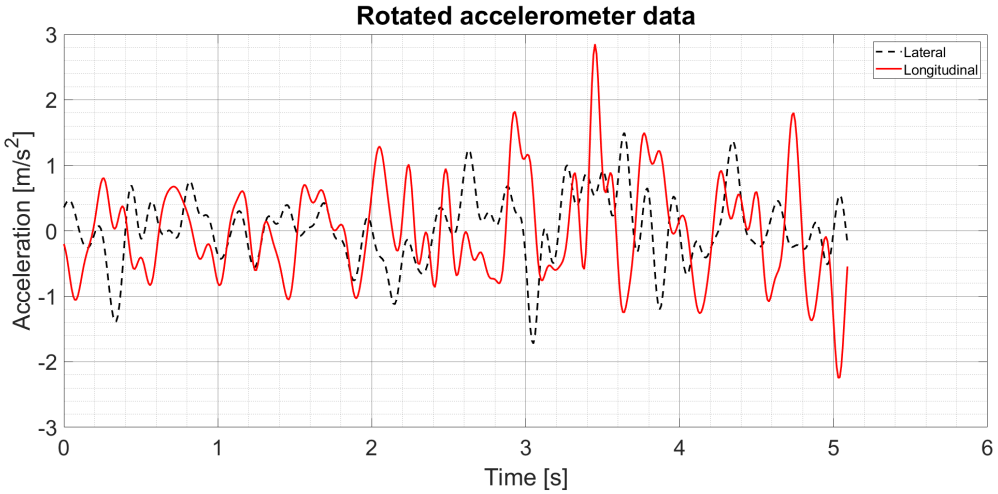

Figure D.6: Three axis accelerometer data rotated to obtain forwards/longitudinal acceleration (from the cyclist's perspective) and sideways/lateral acceleration.

The raw accelerometer data is rotated to the global reference frame shown in D.1a. The yaw direction is defined as the rotation around the z-axis in the global reference frame (with the positive rotation in the left direction). The roll direction is defined as the rotation around the y-axis in the global reference frame (with the positive direction in the right direction).

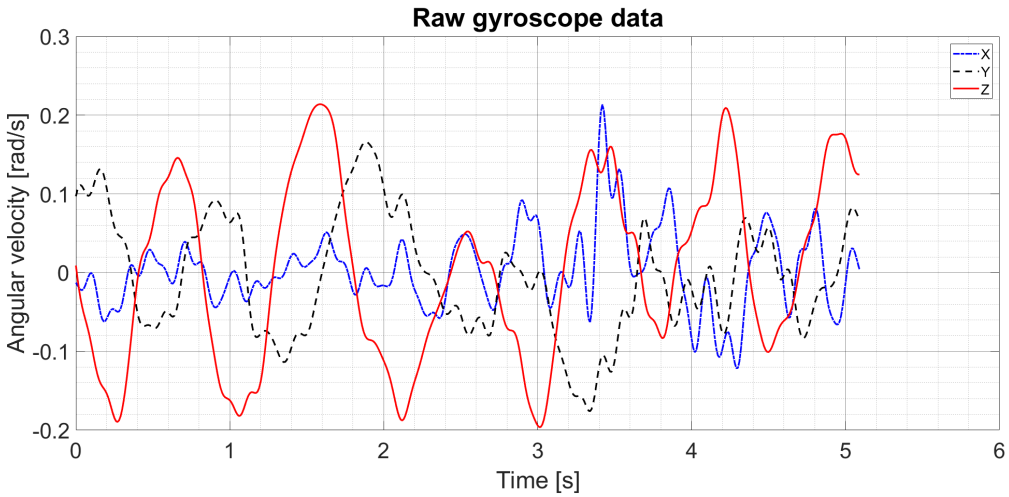

Figure D.7: Three axis gyroscope data. This data has been band-pass filtered with a low-pass cut-off frequency of 5 Hz and a high-pass cut-off frequency, in order to get rid of noise and normal curvature of the road.

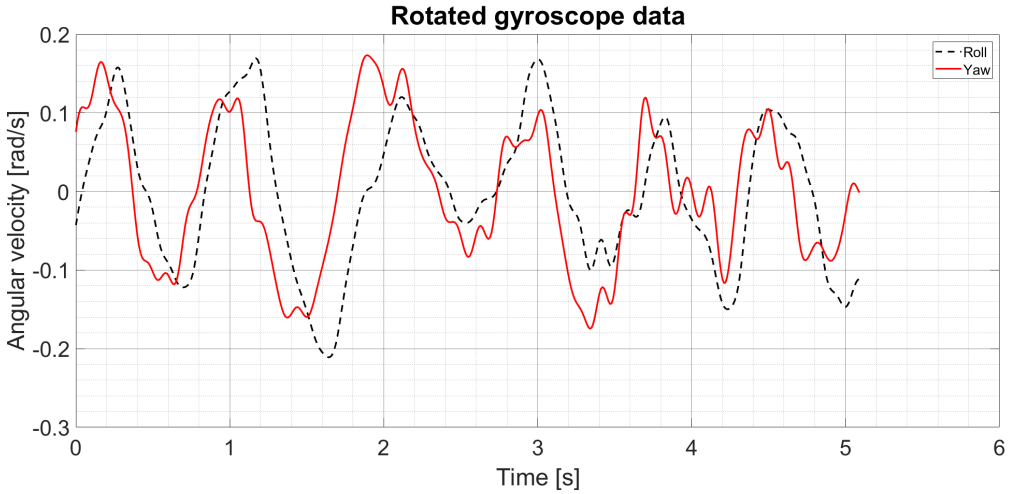

Figure D.8: Three axis gyroscope data transformed to roll and yaw angular velocities (from the cyclist's perspective).

Table D.1: Raw cycling app data

Time [s]	Cadence [rev/s]	Speed [m/s]	Power [W]
0.2	67	6.26	91
1.2	67	6.27	86
2.2	67	6.29	81
3.2	67	6.41	81
4.2	68	6.28	87

Table D.2: Metrics processed from analysed raw data

Metric	Value
Stopped at intersection	0
GNSS acc mean	0.006 m/s^2
GNSS acc p85	1.08 m/s^2
GNSS acc p85 pos	1.80 m/s^2
GNSS acc p15 neg	-1.12 m/s^2
Accelerometer Forward mean	0.003 m/s^2
Accelerometer Forward deviation	0.765 m/s^2
Accelerometer Forward p85 pos	1.150 m/s^2
Accelerometer Forward p15 neg	-0.990 m/s^2
Accelerometer Forward max	2.850 m/s^2
Accelerometer Forward min	-2.244 m/s^2
Accelerometer Lateral mean	0.038 m/s^2
Accelerometer Lateral deviation	0.518 m/s^2
Accelerometer Lateral abs max	1.721 m/s^2
Accelerometer Total mean	1.031 m/s^2
Accelerometer Total deviation	0.610 m/s^2
Accelerometer Total max	3.601 m/s^2
Gyro Yaw mean	0.0035 rad/s
Gyro Yaw deviation	0.120 rad/s
Gyro Yaw rotation rate	0.100 rad/s
Gyro Yaw abs max	0.306 rad/s
Gyro Roll mean	-0.0015 rad/s
Gyro Roll deviation	0.112 rad/s
Gyro Roll rotation rate	0.092 rad/s
Gyro Roll abs max	0.256 rad/s
Gyro Total mean	0.156 rad/s
Gyro Total deviation	0.066 rad/s
Gyro Total max	0.323 rad/s
Approach speed	6.33 m/s
Intersection speed	6.29 m/s
Accelerometer Hard acceleration	0
Accelerometer Hard deceleration	0
Gyro Yaw Hard swerve	0
Gyro Roll Hard swerve	0
Cadence mean	67 rpm
Cadence deviation	1 rpm
Power mean	85 W
Power deviation	4.27 W
Time not pedalling	0 s

E

Natural cycling experiment metrics distributions

This appendix entry shows the distributions of all metrics gathered from the natural cycling experiment data. Figures E.1-E.7 and Table E.1 can be used together with Table 2.4 to get a better picture of how the effect sizes are represented in the actual distributions of the metrics.

Table E.1: Percentages of the threshold metrics for approaches at safe and dangerous intersections

Metric	Safe	Dangerous
Stopped at intersection	2.4 %	5.5 %
Accelerometer hard acceleration	35.2 %	41.8 %
Accelerometer hard brake	33.5 %	39.3 %
Gyro hard yaw swerve	4.8 %	10.2 %
Gyro hard roll swerve	0.8 %	1.0 %

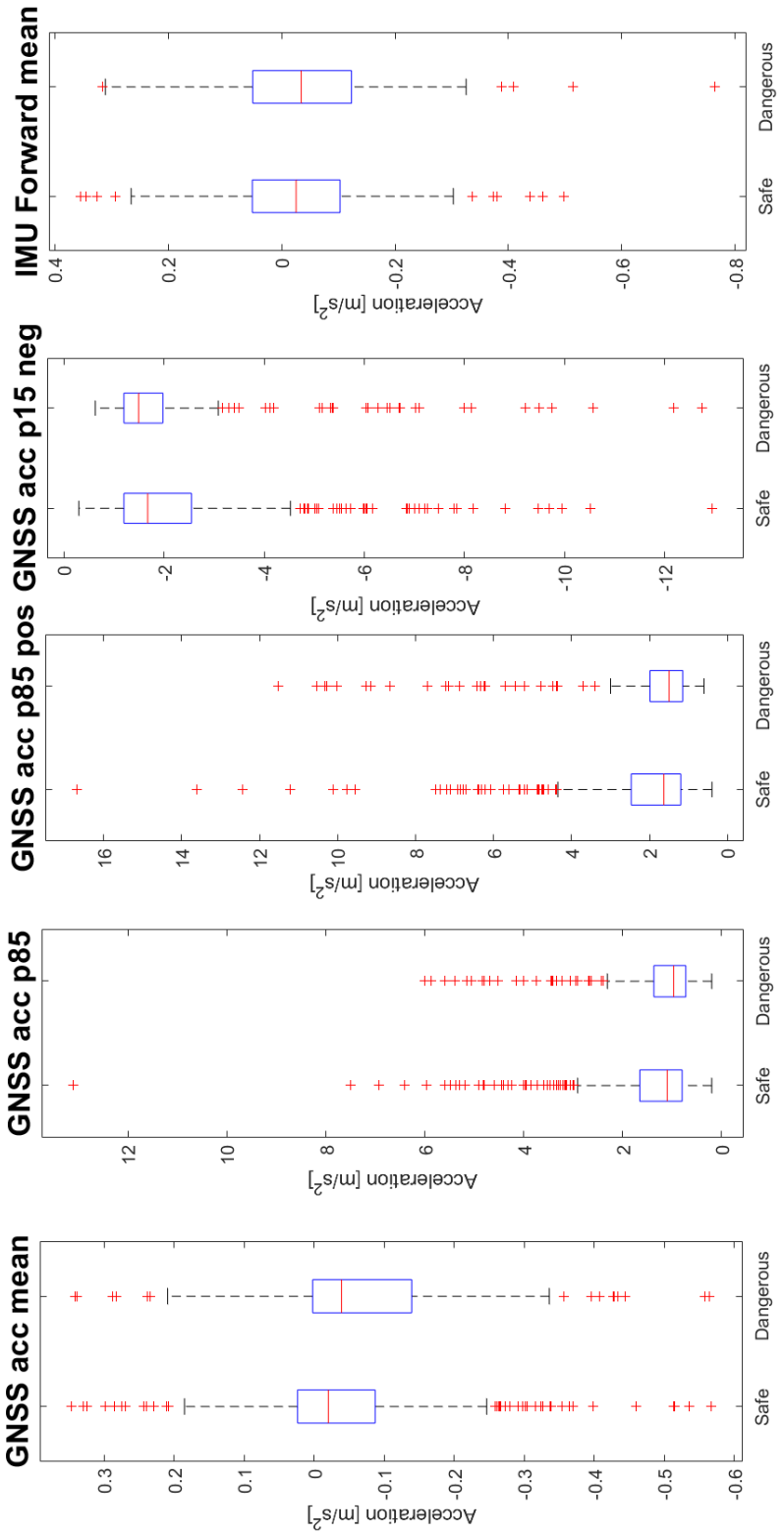

Figure E.1: Box plots of a) Mean acceleration as determined by the GNSS sensor, b) 85th percentile of GNSS acceleration, c) 85th percentile of positive values of the GNSS acceleration, d) 15th percentile of negative values of the GNSS acceleration, e) Mean forward acceleration measured by the IMU accelerometer.

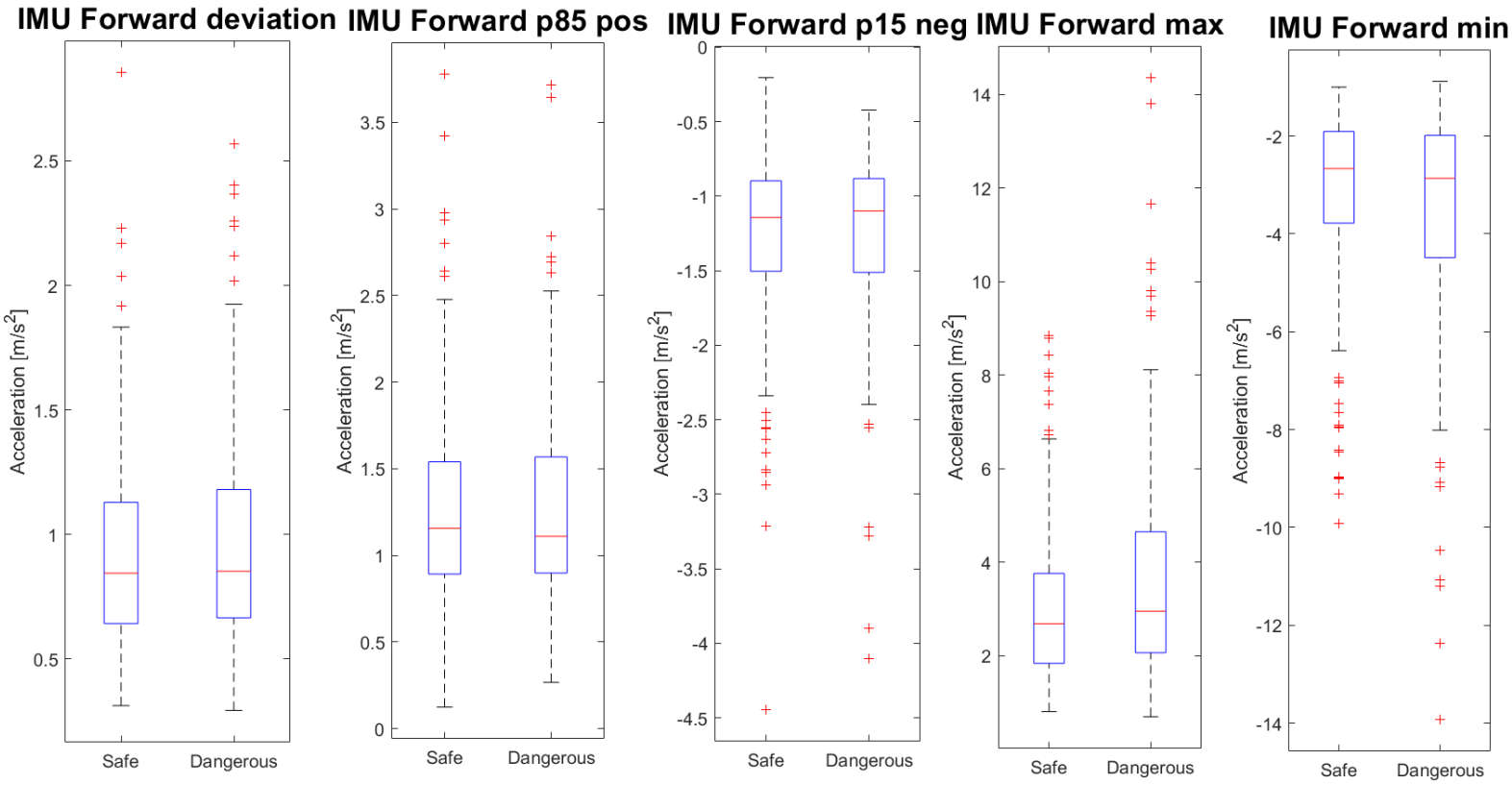

Figure E.2: Box plots of a) Standard deviation of forward acceleration as measured by the IMU accelerometer, b) 85th percentile of positive values of forward acceleration as measured by the IMU accelerometer, c) 15th percentile of negative values of forward acceleration as measured by the IMU accelerometer, d) Maximum value of forward acceleration as measured by the IMU accelerometer, e) Minimum value of forward acceleration as measured by the IMU accelerometer.

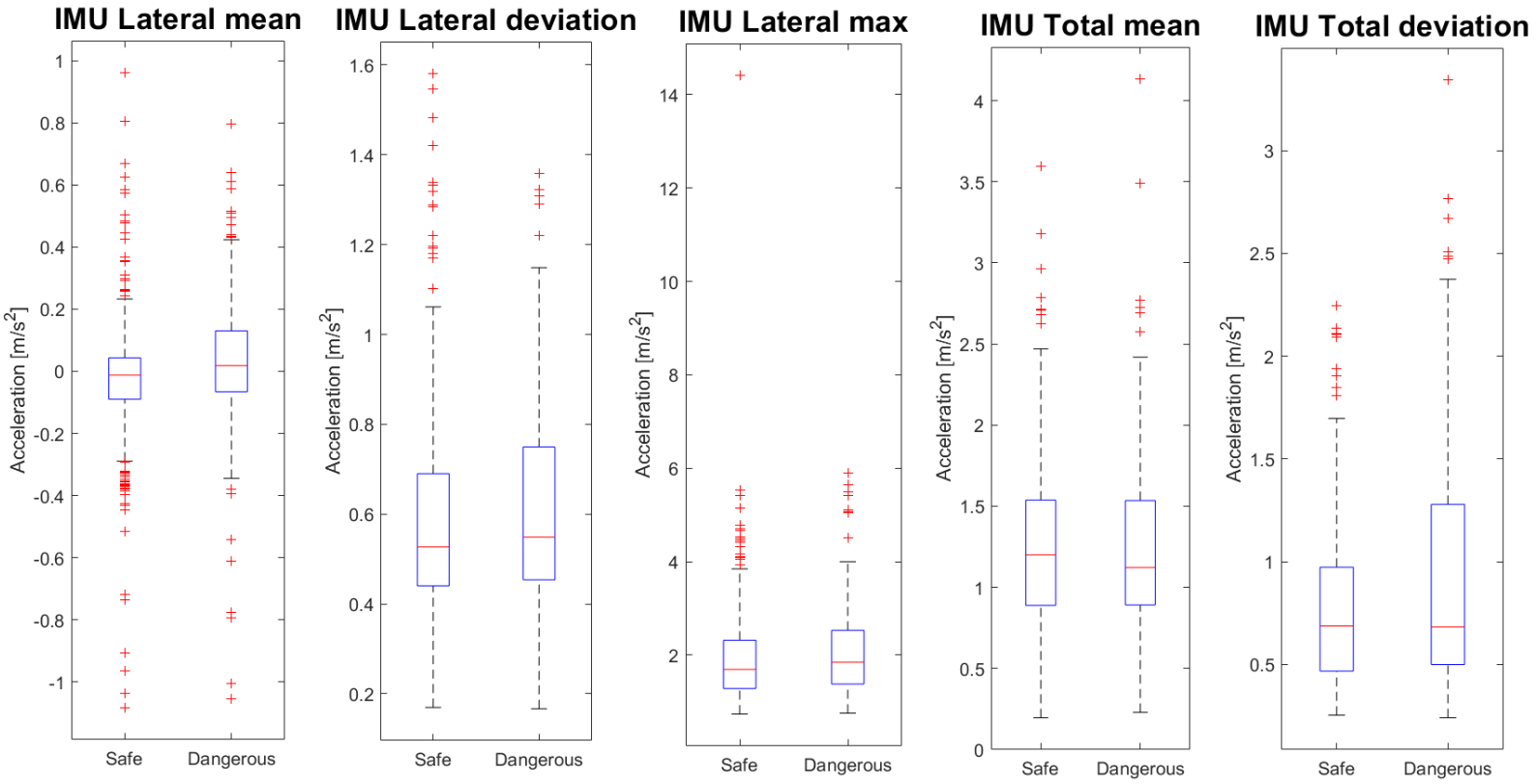

Figure E.3: Box plots of a) Mean lateral acceleration measured by the IMU accelerometer, b) Standard deviation of lateral acceleration as measured by the IMU accelerometer, c) Maximum absolute value of lateral acceleration as measured by the IMU accelerometer, d) Mean total acceleration as measured by the IMU accelerometer, e) Standard deviation of total acceleration as measured by the IMU accelerometer.

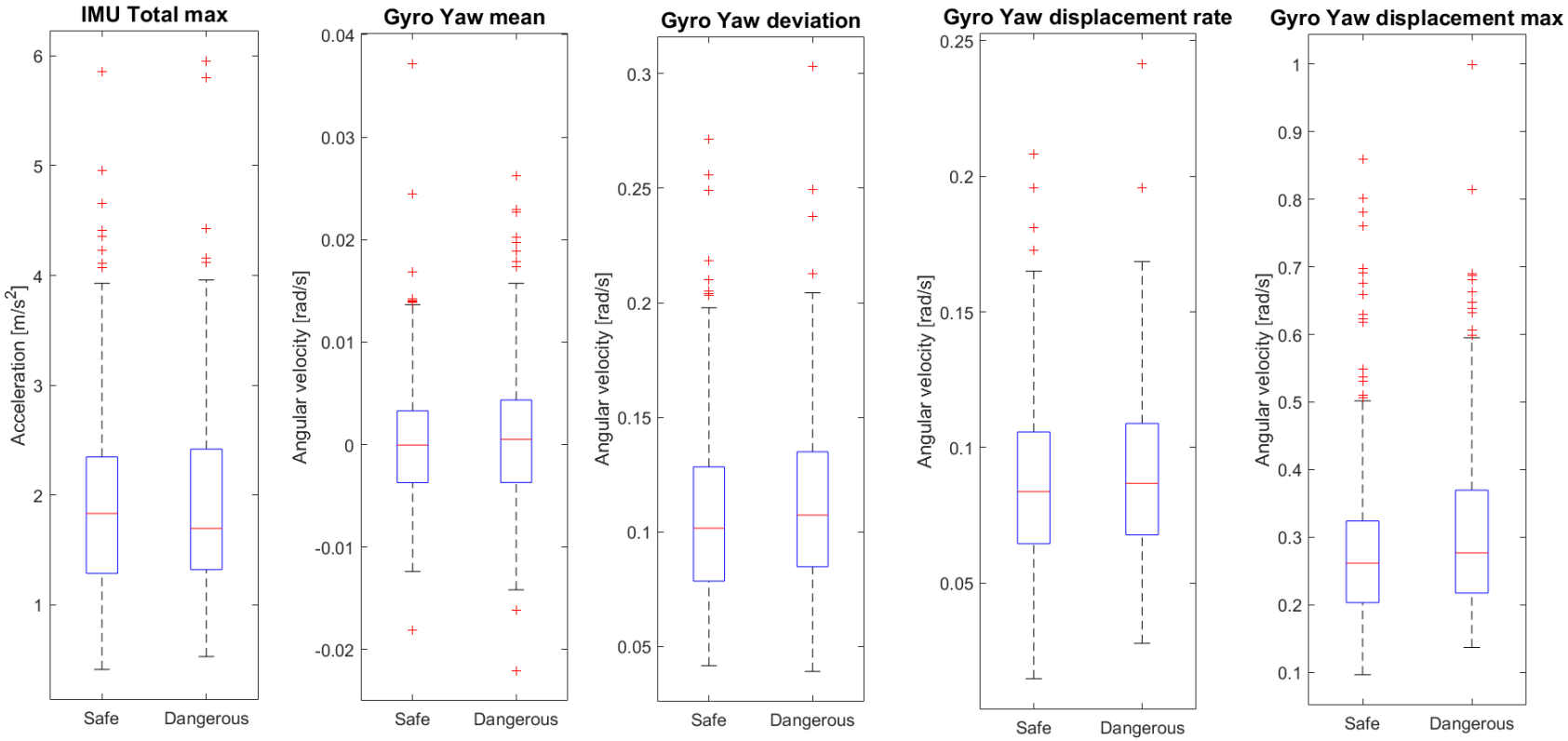

Figure E.4: Box plots of a) Maximum value of total acceleration as measured by the IMU accelerometer, b) Mean yaw angular velocity as measured by the IMU gyroscope, c) Standard deviation of yaw angular velocity as measured by the IMU gyroscope, d) Displacement rate (or mean absolute value) of yaw angular velocity as measured by the IMU gyroscope, e) Displacement max (or maximum absolute value) of yaw angular velocity as measured by the IMU gyroscope.

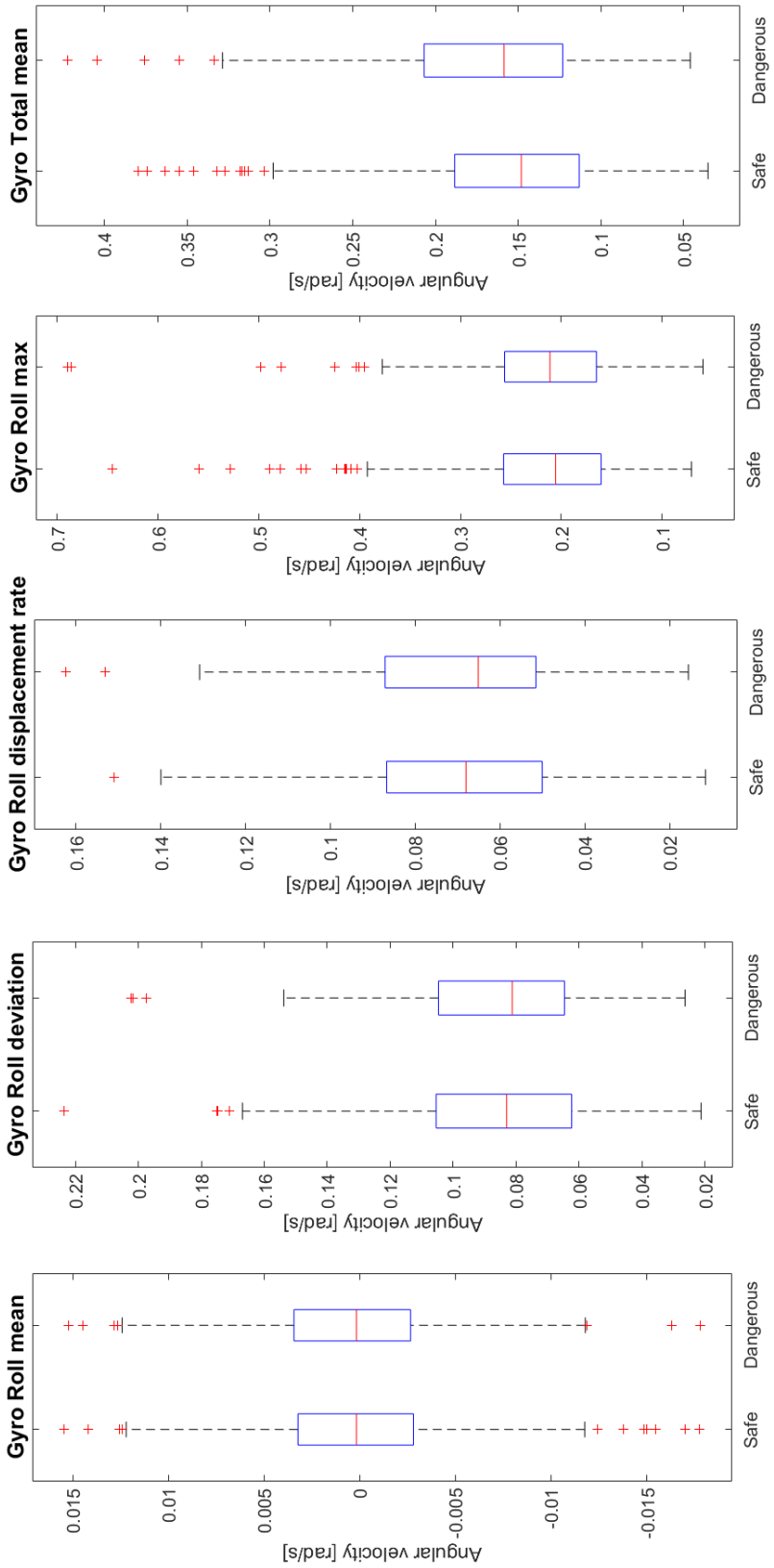

Figure E.5: Box plots of a) Mean roll angular velocity as measured by the IMU gyroscope, b) Standard deviation of roll angular velocity as measured by the IMU gyroscope, c) Displacement rate (or mean absolute value) of roll angular velocity as measured by the IMU gyroscope, d) Displacement max (or maximum absolute value) of roll angular velocity as measured by the IMU gyroscope, e) Mean total angular velocity as measured by the IMU gyroscope.

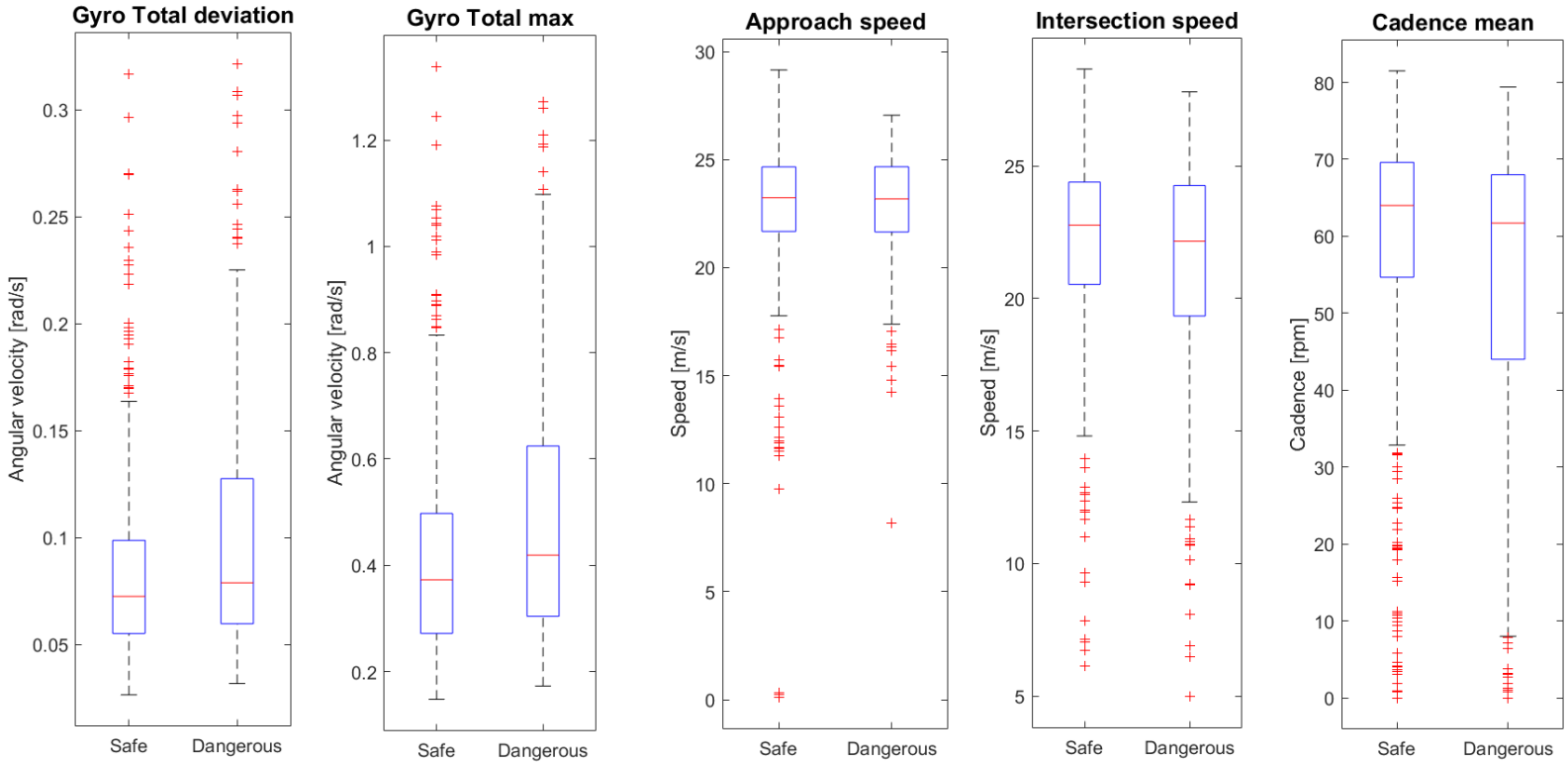

Figure E.6: Box plots of a) Standard deviation of total angular velocity as measured by the IMU gyroscope, b) Maximum value of total angular velocity as measured by the IMU gyroscope, c) Approach speed (speed during first half second of the 35m approach), d) Intersection speed (speed during last half second of the 35m approach), e) Mean cadence.

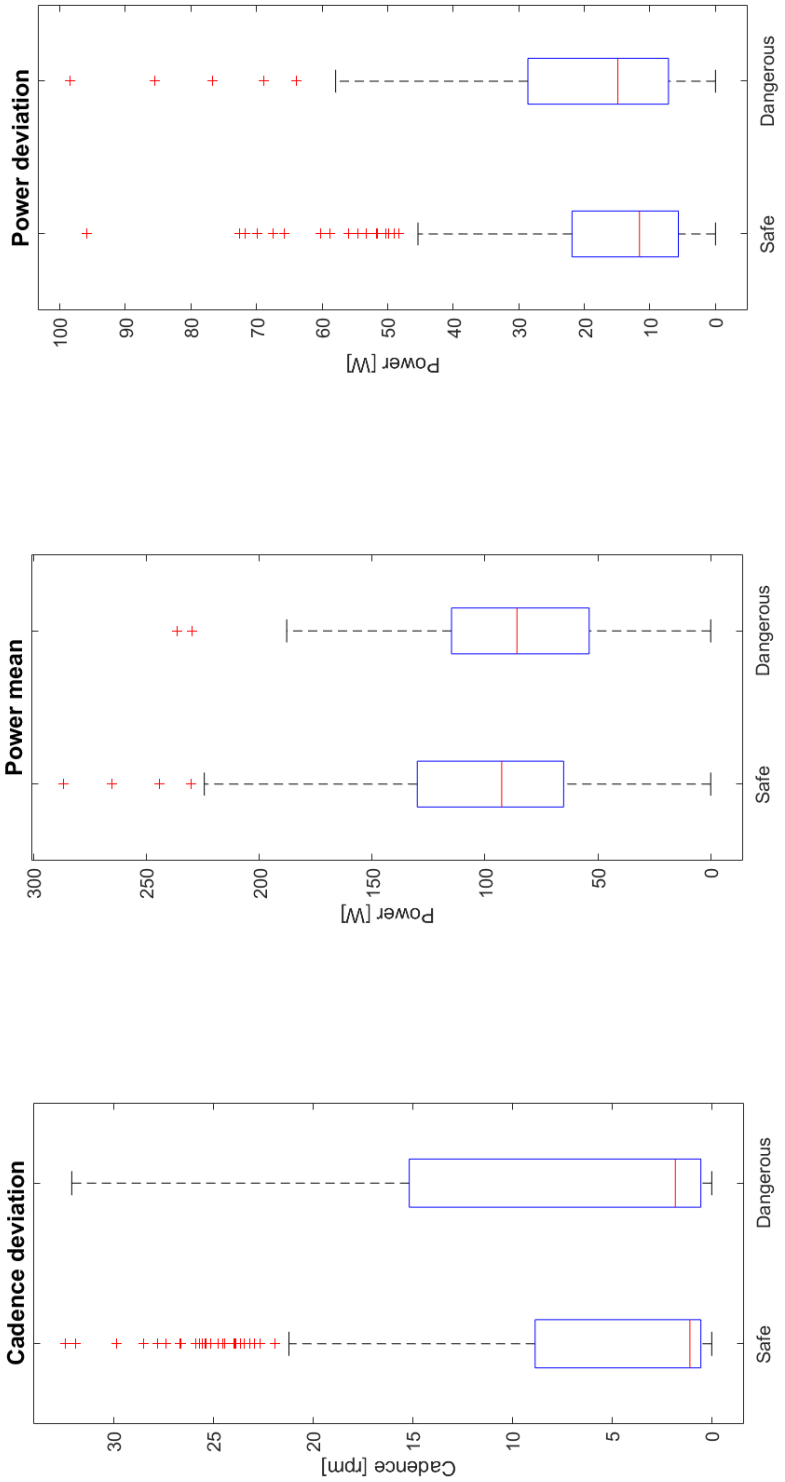

Figure E.7: Box plots of a) Standard deviation of cadence, b) Mean power output of the cyclist, c) Standard deviation of power output of the cyclist.